2012

Conserved and Novel Properties of Clathrin-Mediated Endocytosis in Dictyostelium Discoideum

Laura Macro

CONSERVED AND NOVEL PROPERTIES OF CLATHRIN-MEDIATED ENDOCYTOSIS IN *DICTYOSTELIUM DISCOIDEUM*

A Thesis Presented to the Faculty of

The Rockefeller University

in Partial Fulfillment of the Requirements for

the degree of Doctor of Philosophy

by

Laura Macro

June 2012

CONSERVED AND NOVEL PROPERTIES OF CLATHRIN-MEDIATED ENDOCYTOSIS IN *DICTYOSTELIUM DISCOIDEUM*

Laura Macro, Ph.D.

The Rockefeller University 2012

The protein clathrin mediates one of the major pathways of endocytosis from the extracellular milieu and plasma membrane. Clathrin functions with a network of interacting accessory proteins, one of which is the adaptor complex AP-2, to co-ordinate vesicle formation. Disruption of genes involved in clathrin-mediated endocytosis causes embryonic lethality in multicellular animals suggesting that clathrin-mediated endocytosis is a fundamental cellular process. However, loss of clathrin-mediated endocytosis genes in single cell eukaryotes, such as *S.cerevisiae* (yeast), does not cause lethality, suggesting that clathrin may convey specific advantages for multicellularity. Furthermore, the spatiotemporal dynamics and requirements for individual components of the clathrin-mediated endocytic pathway differ between yeast and mammals. I therefore sought to study the components of clathrin-mediated endocytosis in another unicellular system, the organism *Dictyostelium*, which diverged early from the lineage leading to yeast and mammals. *Dictyostelium* offers a unique advantage as upon starvation it transitions from a unicellular to multicellular state. In this thesis I studied clathrin-mediated endocytosis in the unicellular growth phase of *Dictyostelium* and identified a heterotetrameric AP-2 complex in *Dictyostelium* that is homologous to that

present in mammalian cells. Analysis of this pathway at a high spatial and temporal resolution shows the high degree of similarity in the kinetics of internalization of individual clathrin-coated vesicles between *Dictyostelium* and mammalian cells. These similarities support the conclusion that the formation of clathrin-coated vesicles is homologous between *Dictyostelium* and mammals and, thus, these features likely evolved early. I also found a role for clathrin-mediated endocytosis in maintenance and biogenesis of the contractile vacuole in *Dictyostelium*. Contractile vacuoles are specialized organelles found in some single celled organisms that allow cells to osmoregulate by collecting and removing excess water from the cytoplasm; they are not found in yeast or animals. I found that that the contractile vacuole protein, dajumin-GFP, is trafficked via the cell membrane and is a cargo that is internalized by clathrin-mediated endocytosis in *Dictyostelium.* Internalization of dajumin-GFP is via a clathrin-dependent, AP-2 independent mechanism and is distinct from other endocytic mechanisms. These results suggest the role of clathrin in protein sorting also evolved early, while dependence on specific components of the clathrin-mediated endocytic pathway, may have evolved later, as demonstrated by internalization independent of AP-2 function. In *Dictyostelium*, clathrin is known to be required for the formation of multicellular structures. Since it is possible to visualize the transition from a unicellular state to multicellularity, *Dictyostelium* is now uniquely positioned to study the dynamics of clathrin-mediated endocytosis during multicellular development.

`

For Wol, Flop, Gog & CPB

Acknowledgements

Firstly, I would like to thank my advisor Dr. Sandy Simon for his mentorship throughout my time at Rockefeller. His support, kindness, generosity and encouragement were much appreciated. He taught me what it means to be a scientist and allowed me to be truly independent.

I would also like to thank the members of my committee Dr. Shai Shaham and Dr. Elaine Fuchs for their insight and helpful advice throughout the years. They both were not only generous with their time, but shared with me their expertise and allowed me into their labs to use equipment.

I would also like to thank Dr. Theresa O'Halloran for travelling to New York to be my external committee member. She has also been kind enough to share a variety of reagents with me over the course of this project.

I would like to thank the past and present members of the Simon Lab for providing a friendly and stimulating work environment. A special acknowledgement goes to Dr. Jyoti Jaiswal who guided me through those first few tricky years of graduate school and introduced me to the world of *Dictyostelium*. He spent many hours helping me design and critique experiments and encouraged me when I felt like giving up. Thanks also go to Dr. Marina Fix, who was always there with answers to all my questions, and to Dr. Alexa Mattheyses for making TIR1 the awesome microscope it is today. I am certain I would not have been able to do my experiments without it. She also taught me the value of careful image analysis and encouraged me to publish my work. I would also like to mention Dr. Dan Johnson, for helping me with various microscope problems, and Dr.

Joshua Rappoport who encouraged me to join the Simon Lab. Thanks also go to Marcello Im for his help with many things over the years.

A huge thanks goes to Claire Atkinson, not only for reading this thesis and giving me feedback, but for all her advice, companionship and friendship throughout our time in the Simon Lab together.

I would also like to thank the Rockefeller BioImaging Resource Center and the Proteomics Resource Center, and their staff for their assistance with many parts of this thesis.

I am also grateful to Dr. Sid Strickland and the Rockefeller Dean's Office staff for their support during my time here. I would particularly like to thank Dr. Emily Harms for allowing me to be involved in the SURF program.

I would also like to acknowledge the Rockefeller Women & Science Program and the Boehringer Ingelheim Fonds for funding.

Thanks go to Dr. Annette Muller-Taubenberger for sharing reagents and technical advice with me. I would also like to thank the Dicty Stock Center and Dictybase. This resource has been invaluable to me and they have provided me with many reagents over the years.

I would like to thank my friends, especially my fellow RU classmates, who were always willing to listen and provided support and advice. A huge thanks goes to my family for always supporting me whatever it is I do, and finally to David for being a superstar.

Table of Contents

List Of Figures

List Of Tables

List Of Abbreviations

CHC – clathrin heavy chain

CLC – clathrin light chain

EGFR – epidermal growth factor receptor

ENTH – epsin N-terminal homology

EPI – epifluorescence or wide-field

ER – endoplasmic reticulum

GFP – green fluorescent protein

GPCR – G-protein coupled receptor

KS – Kolmogorov-Smirnoff

LDLR – low density lipoprotein receptor

NHS – N-hydroxysulfosuccinimide

NtAv – neutravidin

$PI(4,5)P_2$ – phosphatidylinositol-4,5-bisphosphate

SD – standard deviation

SEM – standard error of the mean

sfGFP – superfolder GFP

SNX9 – sorting nexin 9

TfR – transferrin receptor

TIR-FM – total internal reflection fluorescence microscopy

CHAPTER 1 – Introduction

1.1 Vesicular transport

Compartmentalization of eukaryotic cells by membranes creates a variety of different biochemical environments and enables the resultant membrane bound organelles to perform their specialized functions (Palade, 1975). While compartmentalization is advantageous for the cell by allowing the separation of dedicated cellular processes, exchange between these compartments poses a challenge. Transport of material depends on the formation of membrane bound vesicles which move components between donor and acceptor organelles. Generation of transport vesicles is highly regulated and involves the co-ordination of an array of proteins. Vesicles are then transported through the cell and fuse with their destination compartments. The first description of transport vesicles was in 1964 by Roth and Porter who used electron microscopy to describe the presence of small (~100nm) coated vesicles that carry material into the mosquito oocyte (Roth and Porter, 1964). Later, the protein components involved in vesicle formation were characterized, including the identification of the protein clathrin as the major component of the coat that surrounds these transport vesicles (Pearse, 1976).

The subsequent decades led to the identification of a variety of different coat proteins (COPI, COPII, caveolin) and characterization of vesicles that transport material between different cellular locations (Praefcke et al., 2004; Behnia and Munro, 2005; Bonifacino and Glick, 2004) (Figure 1A). COPI vesicles function in the transport of molecules from the cis-Golgi back to the endoplasmic reticulum (ER) while COPII vesicles transport molecules from the ER to the Golgi apparatus. Clathrin-coated vesicles can transport molecules between a variety of different intracellular compartments

Figure 1 – Intracellular vesicular transport and mechanisms of endocytosis

(A) Schematic showing sites of vesicular transport between different intracellular organelles. The different coat proteins known to mediate vesicle formation at each site are shown. Adapted from (Hsu et al., 2009). **(B)** Schematic showing the different mechanisms of endocytosis that can exist in cells. Adapted from (Mayor and Pagano, 2007).

A

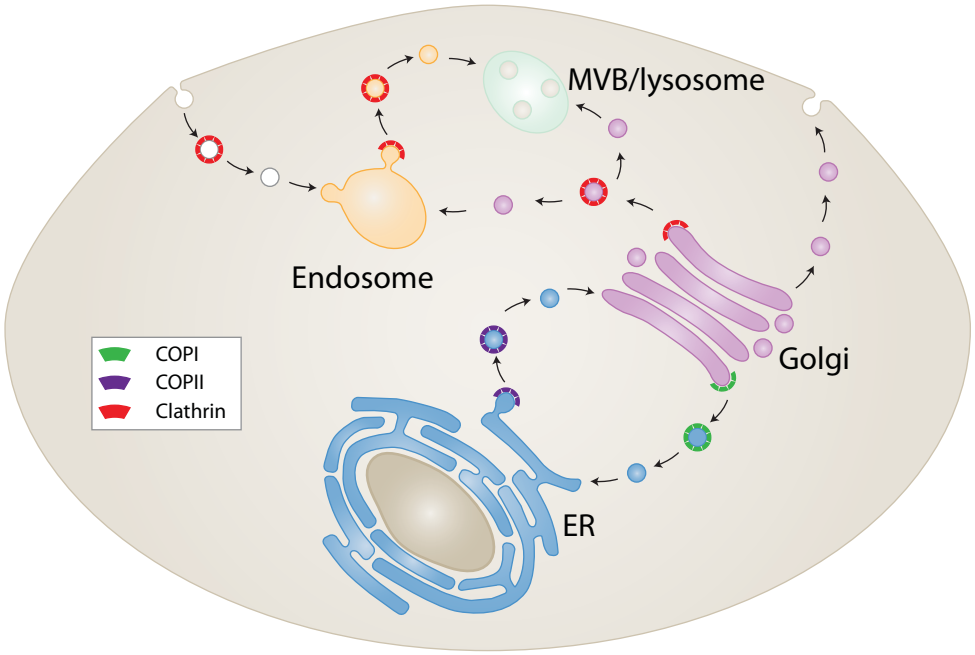
MVB/lysosome
Endosome
Golgi
ER
COPI
COPII
Clathrin

B

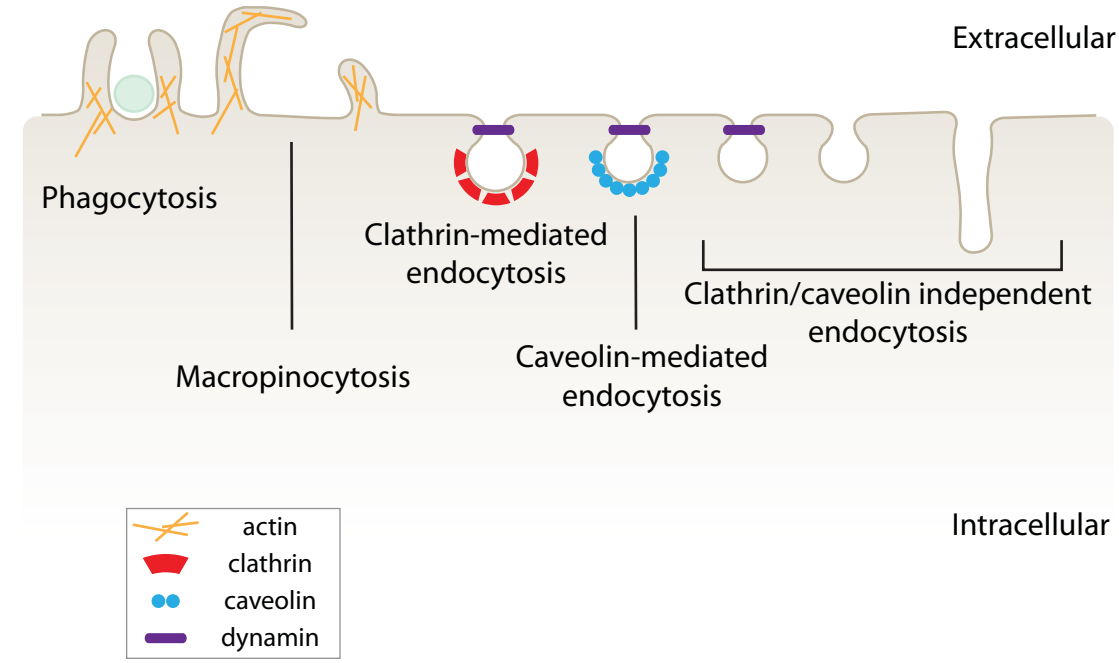
Extracellular
Phagocytosis
Clathrin-mediated endocytosis
Clathrin/caveolin independent endocytosis
Macropinocytosis
Caveolin-mediated endocytosis
Intracellular
actin
clathrin
caveolin
dynamin

including transport between Golgi and endosomes, between Golgi and lysosomes and between endosomes and lysosomes. Clathrin also functions in the exocytosis of post-Golgi vesicles at the plasma membrane (Jaiswal et al., 2009). In addition to involvement in these intracellular trafficking steps, clathrin coated vesicles also internalize plasma membrane proteins and molecules from outside the cell in the process of clathrin-mediated endocytosis.

1.2 Clathrin-mediated endocytosis

Depending on cell-type and species, there are a wide variety of different endocytic mechanisms by which cells can internalize molecules across the plasma membrane (Figure 1B) (Kumari et al., 2010; Doherty and McMahon, 2009). These processes are major regulators of plasma membrane activity and internalize a vast array of molecules thereby controlling many cellular processes. The different endocytic mechanisms are characterized not only by the different cargo that they internalize but also by the protein machinery that they employ.

Clathrin-mediated endocytosis is one of the best studied mechanisms of endocytosis and is important for the uptake of a range of transmembrane proteins from signaling receptors to nutrients. The formation of clathrin-coated vesicles at the plasma membrane involves a complex array of proteins that form an expansive network of possible interactions (Figure 2B) (Praefcke et al., 2004; McMahon and Boucrot, 2011). The advent of live-cell fluorescence imaging has allowed the dissection of the dynamics of the individual proteins involved in vesicle formation in both yeast and mammalian cells. The steps involved in the formation of a clathrin-coated vesicle at the plasma

membrane can be divided into various stages: initiation, cargo selection and coat recruitment, vesicle scission, and uncoating (Figure 2A). These stages are characterized by the proteins that are present and by the morphology of the forming clathrin-coated pit.

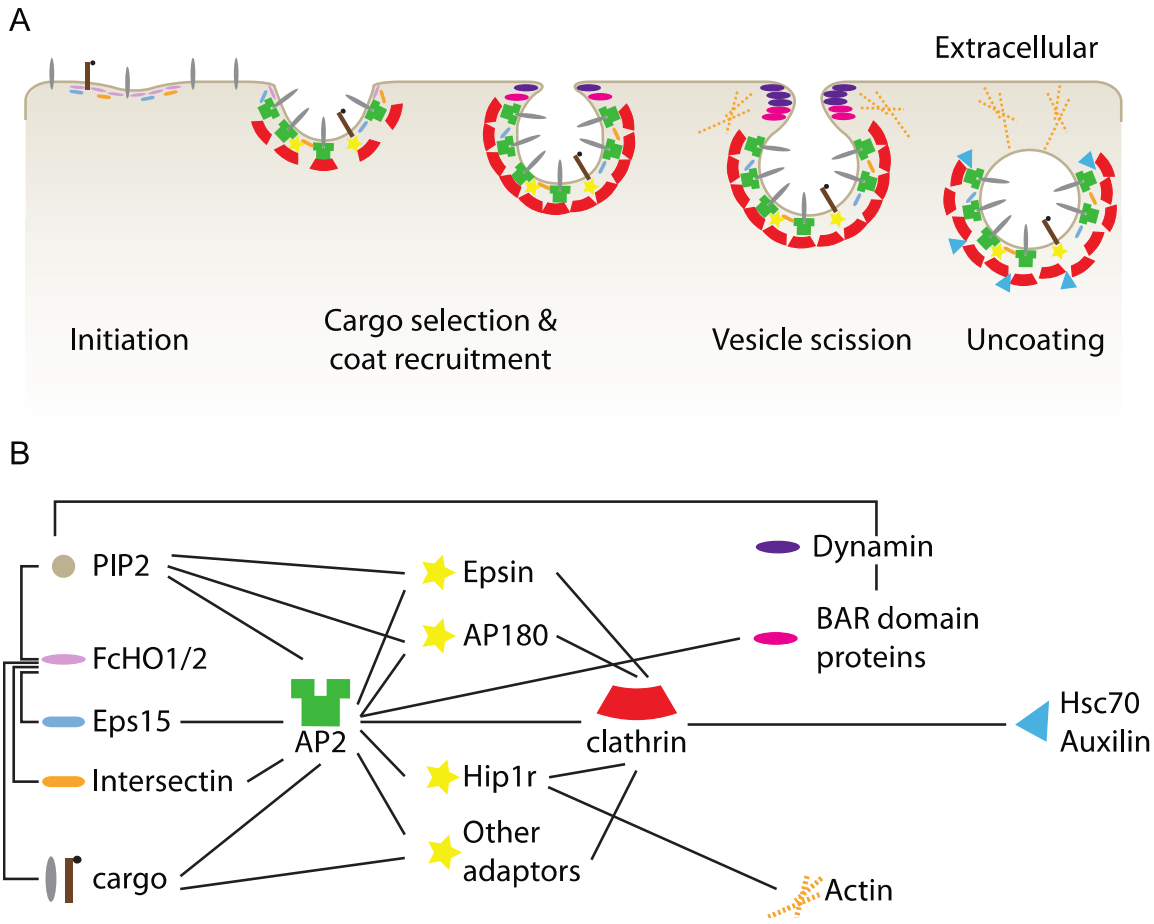

Figure 2 – The clathrin-coated vesicle cycle and protein interaction network

(A) Schematic showing the morphological steps and proteins involved in the formation of a clathrin-coated vesicle. **(B)** Schematic showing the different protein-protein interactions that exist between the proteins involved in clathrin-mediated endocytosis. Adapted from (McMahon and Boucrot, 2011)

Initiation

In mammalian cells, the determining factor for initiation of a *de novo* clathrin-coated vesicle is still unclear. The proteins FCHo1/2, Eps15/Eps15R and intersectin1/2 have been identified as "early" proteins since they mark plasma membrane sites where clathrin will later appear and their presence is required for continuation to vesicle formation. When FCHo1/2 are depleted by RNAi, clathrin coated vesicles do not form and endocytosis of a variety of clathrin cargos is blocked. FCHo1/2 appear to be nucleators of clathrin-coated pits since the number of productive pits directly corresponds to the level of FCHo1/2 expression (Henne et al., 2010). Furthermore, the yeast homolog of FCHo1/2, Syp1, is part of the early module present at endocytic actin patches in yeast (Reider et al., 2009; Stimpson et al., 2009). FCHo1/2 does not appear to enter the cell with the clathrin-coated vesicle as its presence is seen to diminish from the forming vesicle before clathrin disappearance. FCHo1/2 directly binds to, and appears to recruit, the endocytic accessory proteins Eps15/15R and intersectin1/2 to the newly forming pit (Henne et al., 2010).

FCHo1/2 is an F-BAR domain containing protein (Henne et al., 2007). BAR domains are protein modules that recognize, bind to and stabilize/induce membrane curvature and are present in a variety of proteins involved at the various stages of clathrin-coated vesicle formation (Qualmann et al., 2011). The plasma membrane localization of FCHo1/2 can be explained by the preferential binding of its F-BAR domain to the plasma membrane phospholipid phosphatidylinositol-4,5-bisphosphate ($PI(4,5)P_2$) which has been demonstrated in liposome binding assays. Dimerization and membrane-sculpting residues were shown to be essential for clathrin-coated pit formation

(Henne et al., 2010) leading to the idea that curvature generation is fundamental to clathrin-coated vesicle formation at the plasma membrane.

Cargo Selection

Incorporation of specific plasma membrane cargo into clathrin-coated vesicles is an important step in the function of clathrin-mediated endocytosis. Not all proteins on the plasma membrane are internalized in this way, indicating a selection step. Clathrin, however, is not responsible for this selection, since it cannot bind to the membrane, or to the cargo molecules that are to be transported. This function is provided by adaptor proteins that have the ability to bind clathrin, cargo and/or phospholipids in the membrane (Owen et al., 2004) (Figure 2B). One of the central adaptors for clathrin-mediated endocytosis is the AP-2 complex (Figure 3A). AP-2 belongs to an adaptor protein complex family which has four members (AP1-4), each of which acts as an adaptor for clathrin vesicle formation at different intracellular locations (Boehm and Bonifacino, 2001). The AP-2 complex functions at the plasma membrane, where it selects cargo proteins based on short linear sorting signals in their cytosolic tails (Ohno et al., 1995). The AP-2 complex is a heterotetramer made up of two large subunits (α and β2), a medium subunit (μ2) and a small subunit (σ2) that bind to each other with high affinity (Collins et al., 2002) (Figure 3A). Cargo binding is mediated by both the μ2 and σ2 subunits, and binding to plasma membrane $PI(4,5)P_2$ is mediated by the α and μ2 subunits. AP-2 binds clathrin via several domains located in the α and β2 subunits. Although the AP-2 complex subunits bind each other tightly, a large conformational change is necessary to allow the $PI(4,5)P_2$ and cargo binding sites to interact at the

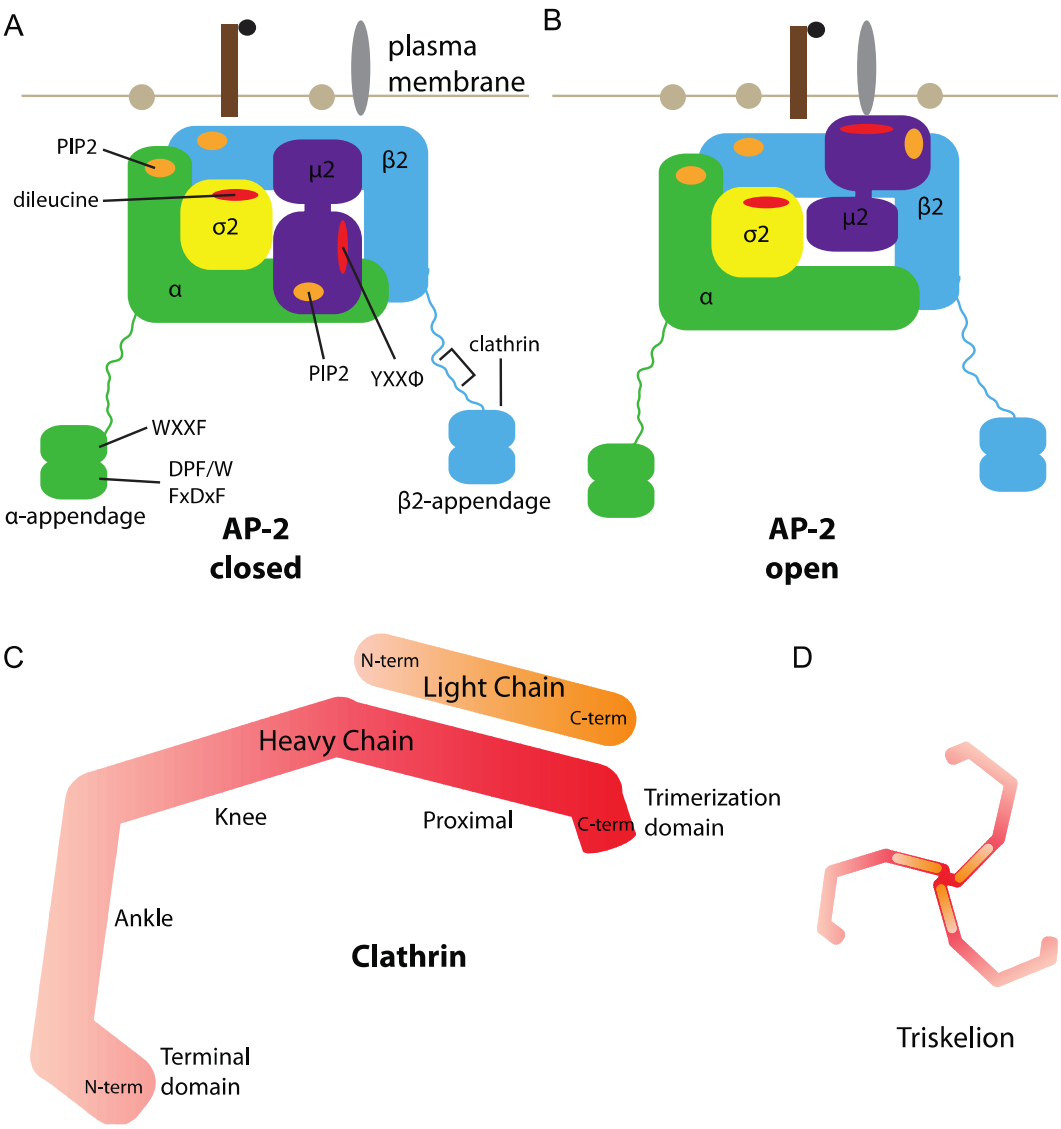

Figure 3 – AP-2 and clathrin

(A) Schematic showing the four subunits of the AP-2 complex in its closed conformation. PI(4,5)P_2, cargo (YXXΦ, dileucine), adaptor protein (WXXF, DPF/W, FxDxF) and clathrin binding sites are labeled. **(B)** AP-2 in its open conformation. The μ2 subunit moves to allow interaction of the cargo and PI(4,5)P_2 binding sites with the membrane. **(C)** Schematic showing the different domains of the clathrin heavy chain and clathrin light chain proteins. **(D)** A triskelion is formed from 3 dimers of clathrin heavy and light chains, triskelions come together to form the clathrin lattice.

membrane simultaneously (Jackson et al., 2010) (Figure 3B). Phosphorylation of the μ2 subunit on Thr156 has been shown to be important for cargo uptake *in vivo* and for *in vitro* binding to endocytic motifs (Olusanya et al., 2001; Ricotta et al., 2002) but whether this residue plays any structural role is unknown. The appendage domains of the α and β2 subunits also mediate binding to many other endocytic accessory proteins, including Eps15/Eps15R (Benmerah et al., 1995) and intersectin1/2 (Pechstein et al., 2010) thus linking the early nucleating module and the clathrin-binding and cargo selection modules (Figure 2B). The variety of interactions possible allows for adaptability of the clathrin-mediated endocytic pathway depending on cell type and signaling events and makes the AP-2 complex an important "hub" molecule (Praefcke et al., 2004). Indeed, in mammalian cells dependence on AP-2 for internalization is often considered a test for whether a cargo enters by clathrin-mediated endocytosis. The central role AP-2 plays in the formation of clathrin-coated vesicles is demonstrated by the block of internalization of cargo upon knockdown of AP-2 by RNAi (Motley et al., 2003; Hinrichsen et al., 2003). This is true even if AP-2 is not the direct cargo binding adaptor (e.g. low density lipoprotein receptor (LDLR), epidermal growth factor receptor (EGFR)) (Sorkin and Zastrow, 2009; Huang et al., 2004; Boucrot et al., 2010) suggesting its appendage interactions are just as essential to clathrin-mediated endocytosis as its cargo binding domains.

In addition to AP-2 there are a variety of other adaptor proteins which can bind to clathrin and/or AP-2 and their corresponding cargo molecules (Figure 2B). Similar to AP-2 these adaptors recognize and bind to specific peptide motifs in the cytoplasmic portions of their cargo and mediate their internalization. These adaptor molecules tend to

be more specific for particular cargo molecules or endocytic motifs as entry of these specific cargos is blocked upon removal of the adaptor molecule. For example, Dab2 binds to the FxNPxY motif in LDLR and is required for its internalization (Maurer and Cooper, 2006).

Interestingly, in yeast there are no endocytic phenotypes associated with AP-2 subunit knockouts (Yeung et al., 1999; Huang et al., 1999) and cargos dependent on AP-2 to act as their adaptor have not been found. One potential cargo that has been identified was the K28 toxin; its uptake was blocked in an AP-2 dependent manner but its dependence on clathrin and its internalization from endocytic patches was not shown (Carroll et al., 2009). Furthermore, very few other cargo-selective adaptors have been demonstrated in yeast which has led to speculation about evolution of the clathrin-mediated endocytic pathway and suggests that dependence on AP-2 and/or adaptor-cargo specificity evolved later.

Coat Recruitment

Soluble clathrin triskelia are recruited from the cytoplasm, along with AP-2, to the forming vesicle where they polymerize into hexagons and pentagons. This polyhedral lattice is believed to act as a scaffold for vesicle formation by stabilizing curvature (Hinrichsen et al., 2006). Each clathrin triskelion is made up of 3 dimers of a ~190kDa clathrin heavy chain (CHC) non-covalently bound to a 25-29kDa clathrin-light chain (CLC) (Figure 3C) (Ungewickell and Branton, 1981; Kirchhausen and Harrison, 1981). These dimers form the triskelion by interacting at the C-terminus of CHC (Figure 3D). The N-terminus of the CHC is a β-propeller and is responsible for many of the

interactions with other proteins of the endocytic network (Haar et al., 1998). Many endocytic accessory proteins have a clathrin box motif that binds to a defined site on this CHC terminal domain (Haar et al., 2000). The segment in between the N- and C-terminal regions of CHC is made up of repeats of short α-helices separated by flexible bends (Haar et al., 1998; Ybe et al., 1999). The geometry of the clathrin lattice is such that the N-terminal domains extend inside the lattice, presumably to interact with various adaptor molecules (Vigers et al., 1986; Heuser and Kirchhausen, 1985; Musacchio et al., 1999). CLC binds to CHC along the length of the C-terminal third of CHC via electrostatic interactions and regulates lattice formation by preventing assembly of clathrin triskelia with each other at physiological pH (Ybe et al., 1998). CLC inhibition can be reversed by binding to AP-2 and/or the Hip proteins, thus lattice assembly may be stimulated only upon adaptor binding at a forming endocytic pit (Greene et al., 2000; Chen and Brodsky, 2005; Legendre-Guillemin et al., 2005).

Whether clathrin polymerization into a lattice mediates membrane bending is unclear. It has been proposed that the force transmission for membrane bending from clathrin polymerization is unlikely due to it having to pass through many flexible adaptors. Instead the direct membrane interaction of curvature effectors may generate bending that is then stabilized by the clathrin lattice (McMahon and Boucrot, 2011). Indeed, many of the accessory proteins that bind to AP-2 and clathrin can sense, stabilize and/or induced membrane curvature. An example is the protein epsin, whose N-terminal domain (ENTH, epsin N-terminal homology) can induce membrane curvature while its C-terminus can simultaneously bind cargo (Ford et al., 2002; Hawryluk et al., 2006). Furthermore, a variety of BAR domain proteins, with different curvatures, are involved in

clathrin-mediated endocytosis including FCHo, sortin nexin 9 (SNX9), amphiphysin and endophilin (Qualmann et al., 2011). These proteins can tubulate liposomes *in vitro* and are recruited to clathrin-coated pits where they presumably are involved in membrane shaping and/or sensing processes (Henne et al., 2010; Pylypenko et al., 2007; Takei et al., 1999; Farsad et al., 2001; Taylor et al., 2011).

Recruitment of clathrin is essential for progression of vesicle formation, knockdown of clathrin in mammalian cells blocks entry of all clathrin-mediated endocytic cargo and halts vesicle formation (Motley et al., 2003; Hinrichsen et al., 2003; Henne et al., 2010). In yeast, knockout of the CHC or CLC genes by homologous recombination does not fully block endocytosis, therefore, although it is important for the process, clathrin is not essential. This highlights the significant differences that exist between the formation of endocytic vesicles between yeast and mammals and suggests that mammalian dependence on coat proteins may have evolved later.

Whether all productive clathrin-coated vesicles arise from *de novo* formation is unclear since in some cell types clathrin is seen in on the membrane as large flat lattices made up only of hexagons (Heuser, 1980). In order to form curvature, pentagons must be introduced; it has been proposed that this could only occur at the edge of these sheets (Kirchhausen, 2000). These structures have a slower turnover but are still capable of forming endocytic vesicles although their significance to endocytic functions is unclear (Merrifield et al., 2005; Rappoport and Simon, 2003; Gaidarov et al., 1999; Saffarian et al., 2009).

Scission

The fully formed vesicle is still connected to the plasma membrane by a vesicle neck that must be separated to allow the vesicle to move into the cell. In mammalian cells the GTPase dynamin is proposed to mediate scission of this neck. This is based on the localization of dynamin to the neck of clathrin-coated vesicles, and on evidence that mutations in dynamin arrest clathrin-coated pits at highly invaginated states (Koenig and Ikeda, 1989; Damke et al., 1994; Takei et al., 1995). Additionally, *in vitro* studies have shown that dynamin binds to membrane tubules as a helical polymer and is sufficient to mediate membrane fission upon GTP addition (Hinshaw and Schmid, 1995; Sweitzer and Hinshaw, 1998). Although the exact mechanism is unclear, a conformational change mediated by GTP hydrolysis is followed by membrane fission. Other membrane bending proteins, such as the N-BAR containing proteins amphiphysin and endophilin, and the BAR domain containing SNX9 all have a role in vesicle scission by recruiting dynamin and possibly helping to form the neck (Ferguson et al., 2009). Mammalian endocytosis is fully dependent on the presence of a functional dynamin. Dynamin can be inhibited through a variety of methods including depletion by RNAi, use of dominant negative mutants and through the use of small molecule inhibitors (van der Bliek et al., 1993; Macia et al., 2006).

In yeast, there are three dynamin genes but they do not appear to function in scission (Gammie et al., 1995; Nothwehr et al., 1995). Recently, one of the yeast dynamins (Vps1p) has been seen at a subset of endocytic patches and, although it may play a role in yeast scission, endocytosis is not fully dependent on its presence. Furthermore, Vps1p has been proposed to function in assisting amphiphysin in membrane

curvature which is different from the proposed dynamin function in mammalian cells (Smaczynska-de Rooij et al., 2010). Effects of Vps1p on other trafficking steps that may in turn affect endocytosis have also not been fully discounted.

In yeast, actin assembly is required for endocytosis (Kübler and Riezman, 1993; Ayscough et al., 1997). In mammalian cells, a burst of actin polymerization coincides with clathrin-coated vesicle internalization (Merrifield et al., 2002) and experiments using a vesicle scission assay measured actin polymerization peaking at the time of scission (Taylor et al., 2011). Despite this, actin is not required in all cells for clathrin-mediated endocytosis (Fujimoto et al., 2000). It is thought that the higher turgor pressure present in yeast requires more force generation to create membrane bending necessary for coated pit progression. The additional force comes from the polymerization of actin and thus makes actin indispensible for endocytosis in yeast. When turgor pressure is reduced in yeast, the requirement for actin in normal endocytosis is removed (Aghamohammadzadeh and Ayscough, 2009). In yeast, the BAR-domain containing protein homolog of amphiphysin, Rvs167p, covers the vesicle neck and its appearance correlates with a large inward movement of the vesicle, believed to correspond to scission (Idrissi et al., 2008; Kaksonen et al., 2005). The membrane deformation provided by these BAR domains combined with the force from actin polymerization may be enough to pinch off the vesicle neck.

The lipid phosphatase synaptojanin, which hydrolyses $PI(4,5)P_2$, may also be important for scission (Sun et al., 2007), as well as uncoating (see below). A theoretical model of endocytosis in yeast suggests that an uneven distribution of $PI(4,5)P_2$ between the budding vesicle and the vesicle neck can create line tension to drive scission (Liu et

al., 2009). This is supported by evidence that synaptojanin phosphatase activity is dependent on curvature (Chang-Ileto et al., 2011); $PI(4,5)P_2$ is hydrolyzed at the bud while the neck is protected due to BAR-domain protein binding. This results in a lipid phase boundary that creates a lateral force constricting the neck and leading to scission (Liu et al., 2009). Whether this can be extended to mammalian cells remains to be seen but it is possible that dynamin and other BAR domain proteins could prevent the accumulation of synaptojanin at the neck of vesicles.

Uncoating

Once the vesicle has been pinched off the plasma membrane it is free to move into the cell to deliver cargo to its destination. This process requires removal of the clathrin coat to allow fusion with target endosomes and membranes. In mammalian cells uncoating is mediated by the proteins auxilin, HSC70 and synaptojanin (Schlossman et al., 1984; Ungewickell et al., 1995; Cremona et al., 1999). Auxilin binds to the terminal domain of CHC, sitting directly below the trimerization area. Auxilin recruits HSC70 which initiates the uncoating reaction upon hydrolysis of ATP (Scheele et al., 2001; Fotin et al., 2004). Regulation of the timing of uncoating is unclear but it is possible these proteins can only access the clathrin cage at the gap left by the vesicle neck, which becomes exposed only after scission (McMahon and Boucrot, 2011). Hydrolysis of $PI(4,5)P_2$ by synaptojanin is also likely to cause dissociation of many of the adaptor molecules whose membrane binding affinity is dependent on the presence of $PI(4,5)P_2$.

1.3 Microscopic assays of clathrin-mediated endocytosis

The advent of green fluorescent protein (GFP) and fluorescence imaging allowed visualization of the formation of clathrin-coated vesicles (Gaidarov et al., 1999; Merrifield et al., 2002; Rappoport and Simon, 2003). Fluorescent tagging of clathrin and various other endocytic proteins revealed their dynamics but, since clathrin is also present on intracellular vesicles, it is impossible to distinguish endocytic events at the plasma membrane from intracellular budding events (Gaidarov et al., 1999). Furthermore, the fluorescent signals originating from deeper inside the cell also contribute to background fluorescence that can obscure visualization of the plasma membrane. The application of total internal reflection fluorescence microscopy (TIR-FM) has therefore been crucial to the study of endocytosis (Merrifield et al., 2002; Rappoport and Simon, 2003).

TIR-FM is a microscopy technique that allows selective excitation of the plasma membrane attached to the coverslip while molecules found deeper in the cell are not excited (Figure 4) (Axelrod, 2001). This is achieved by the creation of an evanescent wave at the interface between the coverslip and the sample that decays exponentially with increasing distance from the coverslip. This means that only molecules within ~100nm of the coverslip are excited. TIR-FM results in lower photodamage, since only a small portion of the cell is excited, and significantly increases the signal-to-noise ratio due to removal of background fluorescence. TIR-FM lends itself to the study of endocytic vesicle dynamics since the TIR-FM field depth is about the same size as a vesicle (Mattheyses et al., 2010). When imaged by TIR-FM, formation of a clathrin-coated vesicle at the plasma membrane shows a signature whereby clathrin can be seen accumulating in a punctum which then disappears from the TIR-FM field as it is pinched

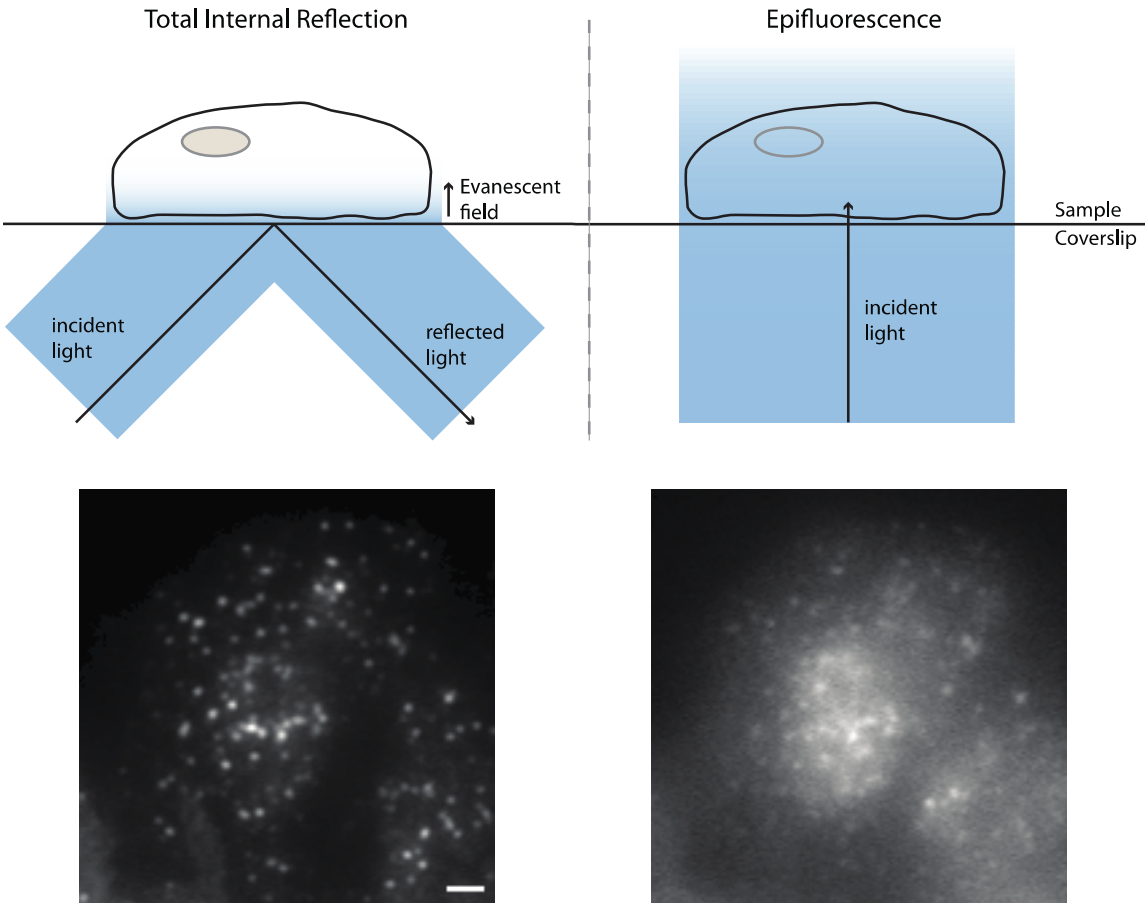

Figure 4 – Schematic of total internal reflection and wide-field microscopy

Schematic showing the different illumination of the cell volume achieved using TIR or wide-field microscopy. In TIR an exponentially decaying field is created at the coverslip-sample interface allowing selective visualization of the plasma membrane and an increase in signal to noise due to removal of background from out of focus light. An example of a cell expressing GFP tagged clathrin imaged by TIR and wide-field microscopy is shown. Scale bar = 1μm.

off and moves into the cell (Figure 5). A variety of other clathrin behaviors in addition to disappearance have been observed at the plasma membrane including lateral movement, fission and fusion of puncta and static behaviors. Variability in the lifetime of individual clathrin puncta from seconds to minutes is also observed (Merrifield et al., 2002; Rappoport and Simon, 2003; Ehrlich et al., 2004).

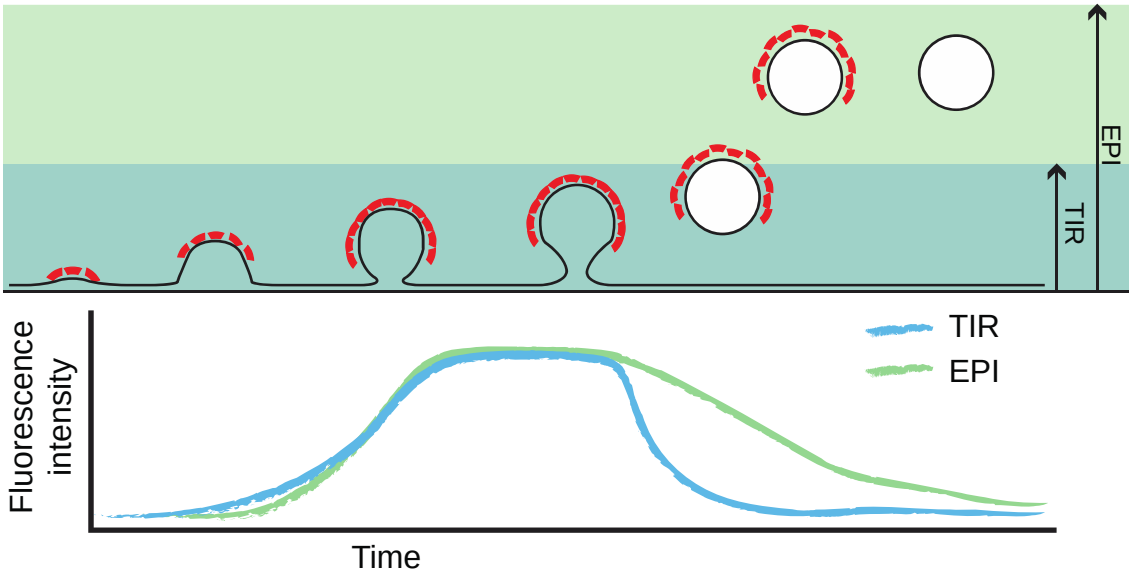

Figure 5 – Behavior of a clathrin-coated vesicle in TIR and EPI

Schematic showing the formation of a clathrin-coated vesicle labeled with a fluorescent protein (red boxes). The depth of the TIR (blue) and EPI (green) illumination is shown. As the vesicle forms the fluorescence intensity increases in both channels. When the vesicle pinches off the membrane it leaves the TIR field but is still detected by the EPI illumination.

While disappearance of clathrin from the membrane is a consequence of endocytosis, disappearance as the sole criteria for endocytosis is insufficient as it is also observed when the clathrin coat disassembles during uncoating and from photobleaching (Merrifield et al., 2005; Mattheyses et al., 2011). Thus, a robust measure for clathrin-mediated endocytosis requires demonstration of cargo internalization together with the disappearance of clathrin from the cell membrane. In mammalian systems endocytosis has been demonstrated by imaging individual endocytic vesicles as they carry cargo molecules and move into the cell (Ehrlich et al., 2004; Merrifield et al., 2005; Rappoport et al., 2005; Mattheyses et al., 2011). Another technique used to robustly monitor endocytosis from the plasma membrane is to monitor clathrin-coated pits by alternating between wide-field (EPI) and TIR-FM (Figure 4 & 5). Since the TIR field decays with a space constant of ~100nm but the EPI field has a focal depth of ~500nm, puncta that are internalized can be detected with EPI illumination after disappearing from the TIR field (Merrifield et al., 2002; Mattheyses et al., 2011) This technique has been extremely informative in defining the detailed dynamics of proteins during the formation of a clathrin-coated vesicle.

Protein dynamics measured with TIR-FM have also been combined with a scission assay (Merrifield et al., 2005; Mattheyses et al., 2011; Taylor et al., 2011). This has allowed spatiotemporal information on protein dynamics to be combined with a physical property of the endocytic process. This technique requires tagging of cargo molecules on their extracellular side with pH sensitive GFP. Switching of the pH of the external solution is read out by the brightness of the GFP fluorescence emission. Stabilization of the GFP fluorescence emission indicates that the inside of the vesicle is

no longer accessible to the extracellular fluid, and indicates that the vesicle has either pinched off or is in a state that is so highly invaginated that protons can only diffuse into the interior slowly. These experiments have demonstrated heterogeneity in the behavior of clathrin-coated vesicles and allowed scission to be compared to events such as dynamin, or clathrin, arrival and disappearance from the TIR-FM field (Mattheyses et al., 2011).

In mammalian cells, clathrin lifetimes and behaviors on the cell surface are highly variable compared to yeast where the spatiotemporal order of events appears to be more uniform (Ehrlich et al., 2004; Rappoport et al., 2006; Mattheyses et al., 2011; Kaksonen et al., 2003; 2005). The variability seen in mammalian cells could be explained by the fact that clathrin-mediated endocytosis is used for the internalization of a wide variety of different cargos compared to yeast. However, a recent study in mammalian cells indicates that the variability in clathrin dynamics may be caused by the use of overexpressed fluorescently tagged proteins. When proteins where fluorescently tagged and expressed from their endogenous promoters, rather than overexpression, clathrin and dynamin lifetimes were shorter and dynamin recruitment was less varied. This suggests the dynamics between yeast and mammalian cells may actually be more similar than previously thought and the variability previously observed simply due to the experimental set-up (Doyon et al., 2011). The importance of this finding, and whether it extends for all endocytic proteins, is yet to be determined.

1.4 Physiological functions of clathrin-mediated endocytosis

The process of clathrin-mediated endocytosis is essential to higher eukaryotic life and loss of clathrin is lethal in multicellular organisms such as *Drosophila*, *C.elegans* and *Mus musculus* (Bazinet et al., 1993; Inoue et al., 2007; McMahon and Boucrot, 2011). Further evidence for the essentiality of clathrin-mediated endocytosis in these organisms comes from the lethality of knockouts in endocytic accessory proteins such as AP-2 (González-Gaitán and Jäckle, 1997), dynamin (Ferguson et al., 2007; 2009), synaptojanin (Cremona et al., 1999), intersectin (Koh et al., 2004), auxilin (Greener et al., 2001), Eps15 (Koh et al., 2007) and endophilin (Verstreken et al., 2002). Due to the lethality of knockouts most experiments are performed on either conditional knockouts or using RNAi to knockdown expression levels of proteins.

Cargos can be internalized by clathrin-mediated endocytosis both constitutively and in a stimulated fashion. In constitutive endocytosis, receptors are internalized regardless of whether its ligand is bound. Examples include the uptake of cholesterol by the LDLR (Anderson et al., 1977) and the uptake of iron bound to transferrin by the transferrin receptor (TfR) (Pearse, 1982). A large number of these receptors are recycled back to the surface after release of their cargo (Anderson et al., 1982; Dautry-Varsat et al., 1983). Stimulated endocytosis occurs when a ligand binds to its receptor triggering its internalization. EGFR, a receptor tyrosine kinase, is taken up upon EGF binding-induced dimerization (Carpenter and Cohen, 1976; Haigler et al., 1978; Schlessinger et al., 1978; Huang et al., 2004; Rappoport and Simon, 2009). The G-protein coupled receptor (GPCR) β_2 adrenergic receptor is another example that undergoes a conformational change upon ligand binding. These conformational changes then mediate interactions

with the clathrin machinery (Zastrow and Kobilka, 1992; Ferguson, 2001). Once internalized, the receptors can be recycled back to the surface or sorted to the lysosome for degradation. Thus, internalization serves as an important control point for signal transduction regulation. Control of the receptor repertoire on the cell surface affects many cellular processes downstream of these receptors including cell growth, division, differentiation, chemotaxis, immune responses and synaptic transmission (Sorkin and Zastrow, 2009). This function of clathrin-mediated endocytic during development may explain the embryonic lethality of clathrin-mediated endocytosis knockouts. Upon Wnt ligand binding, the receptor Frizzled is internalized, and signaling terminated by channeling the receptor to lysosomal degradation. Aberrant embryonic development is observed upon disruption of this internalization (Yu et al., 2007).

In polarized epithelial cells, such as Madin-Darby canine kidney (MDCK) cells, plasma membrane phospholipids are distributed unevenly; $PI(4,5)P_2$ is preferentially localized to the apical surface while phosphatidylinositol-3,4,5-bisphosphate ($PI(3,4,5)P_3$) accumulates at the basolateral surface (Gassama-Diagne and Payrastre, 2009; Shivas et al., 2010; Gassama-Diagne et al., 2006). Since $PI(4,5)P_2$ is important for binding of many endocytic proteins, endocytosis may influence polarity through preferential internalization or altered endocytic rates at the different domains. In mammalian cells, a role for clathrin in sorting and proper localization of basolateral proteins was shown, but this was believed to be due to effects on internal trafficking pathways rather than on endocytosis from the plasma membrane (Deborde et al., 2008). In *Drosophila*, perturbations of endocytosis affected apical-basal epithelial polarity indicating that endocytosis does play a fundamental role in establishment and

maintenance of polarity (Lu and Bilder, 2005). The details of this mechanism, and of the trafficking routes, that are important for polarity in both *Drosophila* and mammals remain to be seen (Shivas et al., 2010).

In single cell eukaryotes, such as *S.cerevisiae* and *Dictyostelium*, clathrin and its accessory proteins are not essential genes (Payne and Schekman, 1985; Lemmon and Jones, 1987; O'Halloran and Anderson, 1992; Ruscetti et al., 1994; Huang et al., 1999; Yeung et al., 1999) raising the question whether clathrin conveys specific advantages for multicellularity. Loss of clathrin in unicellular organisms has been shown to affect uptake of GPI anchored proteins, global plasma membrane uptake and fluid-phase endocytosis (macropinocytosis) (Allen et al., 2003; O'Halloran and Anderson, 1992; Aguado-Velasco and Bretscher, 1999). Additionally, there are only a few identified transmembrane cargos that are specifically internalized by clathrin-mediated endocytosis pointing at divergent physiological functions and indicating specialization probably occurred in higher eukaryotes. It has been proposed that clathrin-mediated endocytosis may, therefore, serve as a generic non-specialized endocytic portal in unicellular organisms (McMahon and Boucrot, 2011).

The similarities and differences between clathrin-mediated endocytosis in mammals and yeast have been informative. Functional and domain homology conservation in the machinery and spatiotemporal protein-protein interactions suggests that these are central to the process. Indeed, phylogenetic studies indicate that the last eukaryotic common ancestor already possessed genes for the COPI vesicle coat and for all the AP complexes. These components therefore have ancient common precursors and subsequently evolved independently, interrupted by the major speciation events, which

may have led to independent specialization and diversification between the eukaryotic supergroups (Boehm and Bonifacino, 2001; Dacks et al., 2008; Field and Dacks, 2009). This hypothesis is exemplified by a recent study that identified genes of a potential fifth AP complex. This complex appears to be ancient and present in the last eukaryotic common ancestor but was subsequently lost in yeast, green algae, haptophyta and stramenopiles (Hirst et al., 2011). Since most of the conclusions regarding the functions of clathrin-mediated coated proteins and adaptors are based on evidence from yeast or mammals, there is a need to study these processes in other systems.

1.5 *Dictyostelium discoideum* as a model system

One model system where clathrin has been studied is the organism *Dictyostelium discoideum* (Schaap, 2011; Williams, 2010). *Dictyostelium* is an advantageous system as it exhibits the features of both yeast (unicellular growth) and mammalian cells (multicellular development). The *Dictyostelium* lineage appears to have diverged from a common eukaryotic ancestor before the fungi-animal split (Williams, 2010). *Dictyostelium* is a free-living soil amoeba that undergoes a developmental program upon starvation whereby individual cells aggregate into mounds by chemotaxis towards cAMP. These mounds then form multicellular slugs that culminate in the development of fruiting bodies after 24 hours. This process of multicellular morphogenesis provides a unique opportunity to study some basic principles of development. Conserved processes during development such as chemotaxis, morphogenesis, signaling, spatial patterning, and differentiation, must all occur in a co-ordinated fashion in *Dictyostelium* to create an organized multicellular structure. The ability to make knockouts or knock-ins by

homologous recombination (De Lozanne and Spudich, 1987), and the availability of the *Dictyostelium* genome sequence (Eichinger et al., 2005), makes for a powerful model organism to study complex cellular processes. Furthermore, fluorescence microscopy can be used to monitor dynamic processes at all stages of the *Dictyostelium* life cycle. This includes imaging the transition from single cells to a multicellular structure as well as imaging of individual cells during their unicellular growth stage (Müller-Taubenberger, 2006; Dormann and Weijer, 2006).

1.6 Endocytic pathways and clathrin in *Dictyostelium*

Dictyostelium has been used as a model system for studying trafficking due to its capacity to perform both phagocytosis and macropinocytosis. These endocytic mechanisms are used to internalize solid particles, such as bacteria (phagocytosis), and large pockets of extracellular fluid (macropinocytosis). Phagocytosis and macropinocytosis are distinct from clathrin-mediated endocytosis and involve the generation of larger (≥0.5μm) endosomes that are created by actin polymerization rather than coat proteins (Kumari et al., 2010; Doherty and McMahon, 2009). In wild isolates of *Dictyostelium,* which feed by phagocytosis of bacteria, macropinocytic rates are low (Kayman, 1983). However, in axenic lab strains, which grow independently of bacteria on a liquid medium, the primary mechanism of endocytosis is uptake of growth medium by macropinocytosis into large pinosomes (Kayman, 1983; Thilo and Vogel, 1980). Axenic cells still retain the ability to phagocytose bacteria when offered as a food source. Macropinosomes are formed by large actin ruffles that protrude from the plasma membrane engulfing a large volume of liquid into a fluid filled vesicle (Hacker et al.,

1997). Upon uptake of fluid, macropinosomes proceed through a somewhat linear pathway of maturation. After uptake at the plasma membrane, the macropinosome is acidified followed by delivery of lysosomal enzymes. After about 30 minutes the pH returns to neutral and undigestable material is released back into the extracellular space by exocytosis (Padh et al., 1993; Aubry et al., 1993; Nolta et al., 1994; Neuhaus et al., 2002).

In addition to phagocytosis and macropinocytosis, *Dictyostelium* possess many genes encoding homologs of the clathrin-mediated endocytic pathway (Table 1). Indeed small coated pits can be visualized invaginating from the plasma membrane in *Dictyostelium* by electron microscopy (Swanson et al., 1981). One of the major phenotypes of genetic deletions of clathrin heavy chain (c*hcA*-), however, is a block of macropinocytosis (O'Halloran and Anderson, 1992; Ruscetti et al., 1994). It is thought this phenotype may be a downstream effect from disruption of overall membrane trafficking. Measurement of macropinocytosis does not quantify membrane uptake and the two have been shown to be independent processes. Membrane uptake measurements in *chcA*- cells shows they internalize their surface slower than wild-type cells, however, this reduction is only by 30% indicating clathrin independent mechanisms may also exist for membrane uptake in *Dictyostelium* (Aguado-Velasco and Bretscher, 1999). Disruption of clathrin also affects a variety of other processes including cytokinesis, development and osmoregulation (O'Halloran and Anderson, 1992; Ruscetti et al., 1994; Niswonger and O'Halloran, 1997a; b; Wessels et al., 2000). Since clathrin functions at numerous membrane transport steps it has been difficult to resolve whether clathrin-mediated endocytosis from the plasma membrane is important for any of these processes.

Table 1 – Mammalian clathrin-mediated endocytosis proteins and their D*ictyostelium* homologs

Proteins shaded in gray indicate proteins shown to function with clathrin in *Dictyostelium*

Protein	Human gene	Function	*Dictyostelium* homolog
Clathrin	CLTC CLTA CLTB	Coat protein	ChcA clc
AP2	AP2A1 AP2A2 AP2B1 AP2M1 AP2S1	Adaptor protein	Ap2A1 Ap1B1 apm2 Ap2S1
EPS15/EPS15R	EPS15 EPS15R	Scaffolding protein	DDB_G0287325 EH domain
AP180/CALM	SNAP91 PICALM	$PI(4,5)P_2$ binding ANTH domain	clmA
HIP1/HIP1R	HIP1 HIP1R	$PI(4,5)P_2$ binding ANTH domain and actin binding	hipA
Epsin	EPN1 EPN2	Membrane bending ENTH domain	epnA
BAI1AP2L2	BAIAP2L2	localizes to clathrin-coated pits	ibrA
Arp3	ARP3	localizes to clathrin-coated pits	Arp2/3 complex
N-WASP	WASP	localizes to clathrin-coated pits	wasA
Dynamin	DNM1 DNM2 DNM3	Scission	dymA dymB dlpA dlpB dlpC
Amphiphysin	AMPH1 BIN1	N-BAR domain, recruits dynamin	DDB_G0288895 BAR domain and SH3 domain
Auxilin, GAK	DNAJC6 GAK	Uncoating	DDB_G0276447 BAR domain and DNAJ domain; similarity with plant auxilin-like protein

HSC70	HSPA8	Uncoating	hspB hspE-2 DDB_G0293674 hspH
β-arrestin	ARRB1 ARRB2	Cargo specific adaptor (GPCRs)	adcA adcB adcC acdD adcE adcF
Synaptojanin	SYNJ1 SYNJ2	Lipid phosphatase	Dd5P3 sac1
SHIP2	INPP1L	Lipid phosphatase	Dd5P1
OCRL	OCRL1	Lipid phosphatase	Dd5P4
CVAK104	SCYL2	Phosphorylates AP-2 β subunit	scy2 scy1
DYRK1A	DYRK1A	Phosphorylates several endocytosis proteins	dyrk1 dyrk2 yakA
Cortactin	CTTN	Recruits actin	DDB_G0288379 cortactin family protein
AAK1	AAK1	Phosphorylates AP-2 μ2 subunit	?
FCHo	FCHO1 FCHO2	F-BAR domain	?
Intersectin	ITSN1 ITSN2	Scaffolding protein	?
SNX9	SNX9	BAR domain	?
ARH	LDLRAP1	Cargo specific adaptor (LDLR)	?
DAB2	DAB2	Cargo specific adaptor (megalin and LDLR)	?
Stonin	STON1 STON2	Cargo specific adaptor (synaptotagmin)	?
HRB	AGFG1	Cargo specific adaptor (VAMP7)	?
NECAP	NECAP1 NECAP2	Potential cargo specific adaptor	?
Numb	NUMB	Cargo specific adaptor (Notch)	?
Endophilin	SH3GL1 SH3GL2 SH3GL3	N-BAR domain, recruits dynamin and synaptojanin	?

Evidence for clathrin-mediated endocytosis in *Dictyostelium* is based on the observation that clathrin forms plasma membrane puncta that co-localize with the AP-2 α and β1/2 subunits, epsin, Hip1r, and AP180 (Stavrou and O'Halloran, 2006; Repass et al., 2007; Brady et al., 2008; Wen et al., 2009; Sosa et al., 2012). An antibody to the α or β1/2 subunits of AP-2 showed they localized to clathrin puncta (Wen et al., 2009; Sosa et al., 2012), in addition the β1/2 subunit has been shown to interact with the μ2 subunit; however the existence of the full heterotetrameric AP-2 complex similar to that in mammalian cells has not been established.

The ability to easily generate knockouts has allowed the functional dissection of a variety of clathrin adaptors in *Dictyostelium* (Stavrou and O'Halloran, 2006; Repass et al., 2007; Brady et al., 2008; Wen et al., 2009; Brady et al., 2010; Sosa et al., 2012). These studies have been able to show interactions between epsin and Hip1r and revealed that the ENTH domain of epsin is required for the recruitment and phosphorylation of Hip1r to membrane puncta (Brady et al., 2008). Furthermore, the lifetime of clathrin puncta is increased in the absence of epsin and Hip1r, but not AP180 (Brady et al., 2010). While clathrin puncta have been observed to disappear at the plasma membrane coincident with a burst of actin (Brady et al., 2010) evidence of internalization of specific plasma membrane cargo via clathrin-mediated endocytosis has not been seen in *Dictyostelium*. Furthermore, due to the use of fixed cell imaging based assays for clathrin-mediated endocytosis in *Dictyostelium* there is limited dynamic information about the endocytosis of clathrin-coated vesicles. Dynamic information would allow for better comparison with yeast and mammalian systems and inform as to whether certain features of endocytosis such as dependence on clathrin and AP-2 are features of multicellularity.

1.7 Contractile vacuole

Knockout of many endocytic proteins in *Dictyostelium* results in a defect in osmoregulation. Osmoregulation in *Dictyostelium* is controlled by the contractile vacuole, a specialized organelle found in freshwater and soil protozoa (Gerisch et al., 2002). The contractile vacuole is a tubulo-vesicular network that allows for the removal of excess water that accumulates as a consequence of living in a hypotonic environment. The contractile vacuole network goes through cycles of filling, followed by fusion with the plasma membrane and emptying of the excess fluid from the cell. This continual cycle allows the cells to survive a wide array of tonicities in their environment.

Osmoregulation phenotypes are observed in both *chcA*- and clathrin light chain knockouts (*clc*-) as well as in knockouts of the α, β1/2 or μ2 subunits of AP-2 and AP180 (O'Halloran and Anderson, 1992; Wang et al., 2003; Stavrou and O'Halloran, 2006; Wen et al., 2009; Sosa et al., 2012).

AP-2 α and μ2 knockouts have a mild osmoregulation phenotype with only slight enlargement of the contractile vacuole in hypotonic buffer (Wen et al., 2009; Sosa et al., 2012). In these cells the contractile vacuole localized protein dajumin-GFP (Gabriel et al., 1999) is localized normally (Sosa et al., 2012). By comparison, in AP-1 μ1 knockouts the contractile vacuole is completely absent and the cells swell in hypoosmotic conditions (Lefkir et al., 2003). The contractile vacuole proteins Rh50 and dajumin-GFP are mislocalized to punctate structures inside the cell (Lefkir et al., 2003; Sosa et al., 2012), suggesting at least some contractile vacuole components are trafficked in a clathrin-coated vesicle dependent mechanism. Since AP-1 is localized to the Golgi, and it is thought to transport proteins between internal compartments, the defect seen in μ1

knockouts is believed to come from the inability to sort newly synthesized contractile vacuole proteins.

Knockout of the β1/2 subunit, which is shared by the AP-1 and AP-2 complexes in *Dictyostelium*, mimics the more severe osmoregulation defect seen in μ1 and *chcA*-knockouts where contractile vacuoles are completely absent. In β1/2 knockouts dajumin-GFP is found primarily on the plasma membrane, this indicated that AP-2 may function in dajumin-GFP internalization only in the context of AP-1 knockouts and mis-sorting of dajumin-GFP to the plasma membrane (Sosa et al., 2012). Hints for a role of clathrin-mediated endocytosis in contractile vacuole biogenesis also come from experiments using a fusion protein with the cytoplasmic tail of Rh50 that showed that it traffics via the plasma membrane en route to the contractile vacuole (Mercanti et al., 2006a).

Knockout of the endocytic adaptor AP180 shows an enlarged contractile vacuole phenotype. This is believed to be a consequence of increased homotypic fusion between vacuoles caused by lack of Vamp7B retrieval from the contractile vacuole membrane (Wen et al., 2009). These varied phenotypes indicate that there may be multiple roles for clathrin-mediated endocytosis at the contractile vacuole. Whether these functions of clathrin and its adaptors are conserved or represent a specialization in *Dictyostelium* remains to be seen.

1.8 Perspectives

Many of the mechanistic details of clathrin-coated vesicle formation have been resolved from studies in mammalian and yeast cells. The varied physiological functions of clathrin-mediated endocytosis between these organisms has, however, led to speculation about the importance of this process in simple eukaryotes. The functions of clathrin and coat proteins in different organisms are therefore important to establishing the common features of this process. This information can be used to speculate on the function of these proteins in the last eukaryotic common ancestor. For this reason, I have decided to study clathrin and the AP-2 complex in the organism *Dictyostelium discoideum*. As discussed above, visualization of internalization from the cell surface via clathrin-mediated endocytosis requires rigorous testing not previously carried out in *Dictyostelium*. Further dissection of the physiological roles of clathrin and AP-2 in *Dictyostelium* may also shed light on the conserved functions of endocytosis across the eukaryotic braches of life.

CHAPTER 2 – Identification of endocytic cargo in *Dictyostelium*

Studies of clathrin-mediated endocytosis in *Dictyostelium* have been limited by the lack of identified membrane cargo, therefore one of my objectives was to identify plasma membrane proteins that were internalized by clathrin-mediated endocytosis. In this chapter I will describe a biochemical strategy that was devised to isolate and identify proteins that are internalized by endocytosis in *Dictyostelium*.

2.1 The biotin internalization assay

In this experiment (summarized in Figure 6) plasma membrane proteins are first reversibly labeled with a biotin group, this is then followed by a step whereby cells can internalize these biotinylated cell surface proteins. Next, any biotin groups remaining on the cell surface are removed by incubation with a cell impermeable reducing agent. Internalized proteins will not be exposed to the reducing agent and will retain their biotin label. Neutravidin (NtAv) agarose beads can then be used to isolate these proteins from cell lysates. Isolated proteins can be separated by SDS-PAGE and identified by mass spectrometry. This labeling approach has been used previously in *Dictyostelium* to label cell surface proteins and assay internalization in various knockouts (Ingalls et al., 1986; Bacon et al., 1994; Novak et al., 1995; Neuhaus and Soldati, 2000). Characterization of the proteins labeled by this technique has not been carried out.

2.2 Biotinylation of plasma membrane proteins

The water soluble and membrane impermeable small molecule sulfo-NHS-SS-biotin was selected to label plasma membrane proteins. The N-hydroxysulfosuccinimide

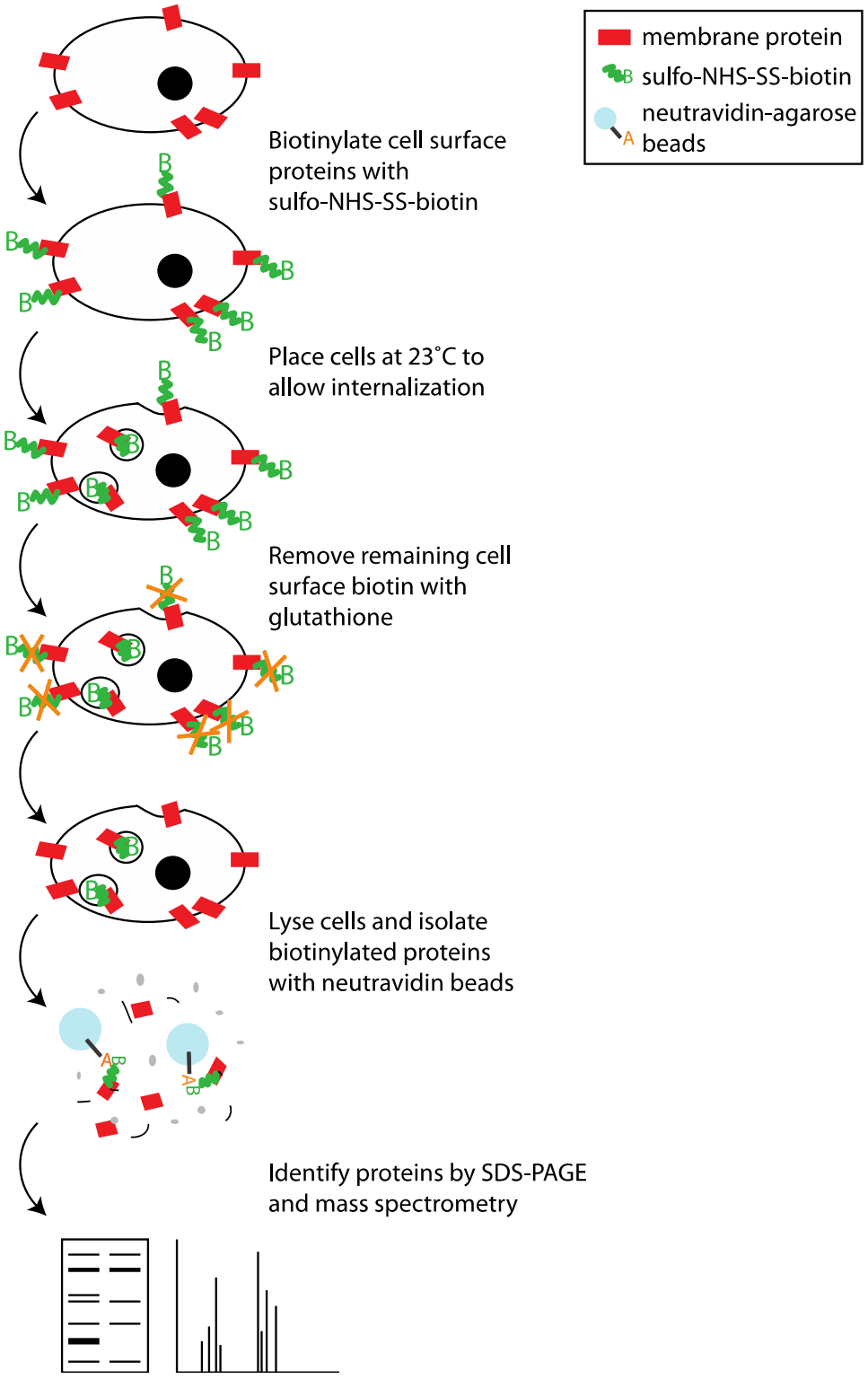

Figure 6 – Schematic of the biotin internalization assay

Steps involved in the biotin internalization assay.

(NHS) ester group reacts with the amine group of lysine residues by nucleophilic attack, resulting in a covalently attached biotin group. This biotin group can then be removed by cleavage of the disulfide bond by addition of various reducing agents.

As a first step in this protocol I tested if it was possible to biotinylate the cell surface and separate the biotinylated proteins with NtAv beads. Figure 7A shows the proteins that were isolated from cell lysates by NtAv beads with, and without, the addition of sulfo-NHS-SS-biotin to cells. Upon addition of sulfo-NHS-SS-biotin many proteins were isolated compared to the non-biotinylated control. Various parameters of the protocol were tested to attain the best results including optimizing the number of cells, concentration of sulfo-NHS-SS-biotin, quantity of NtAv beads and the duration of biotinylation step (data not shown). There were a small number of proteins that bound to the NtAv beads in the non-biotinylated sample. These appeared to be proteins that bound to the agarose part of the beads, endogenous biotin containing proteins or avidin released from the beads (16kDa bands); this was confirmed by mass spectrometry (Table 2). Labeling of the cell surface using the devised biotinylation protocol was confirmed using fluorescence microscopy (Figure 7B); biotin was visualized with streptavidin-AF568 and biotinylation of the cell surface was observed only in cells treated with sulfo-NHS-SS-biotin.

Before any further experiments were performed the full spectrum of biotinylated cell surface proteins were identified by LC-MS/MS mass spectrometry. The peptides identified by mass spectrometry were used to search the *Dictyostelium* database using Mascot (Matrix Science) and produced a list of 400 proteins that matched with the sequences of the fragmented peptides. The data was refined by filtering the protein hits

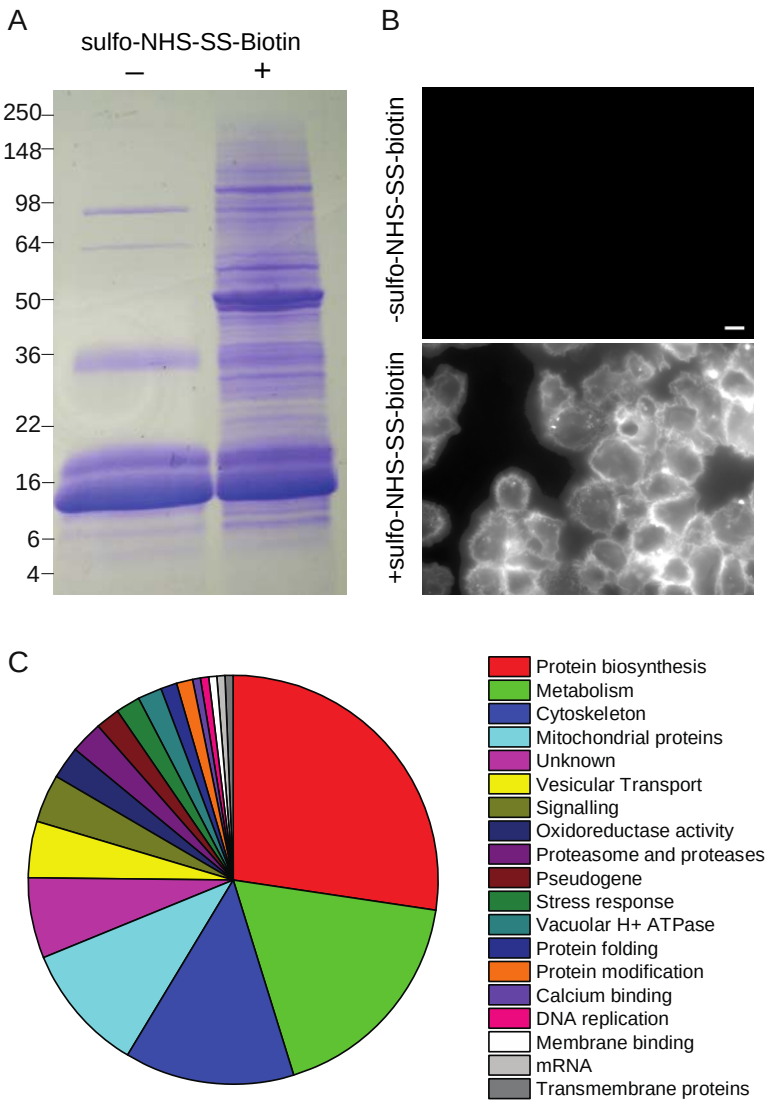

Figure 7 – Biotinylation of cell surface proteins

(A) Coomassie stained SDS-PAGE gel of proteins isolated with NtAv beads from cell lysates. Cells were treated with sulfo-NHS-SS-biotin for 20mins at 4°C, no internalization step was performed. **(B)** Wide-field microscopy images of cells treated with sulfo-NHS-SS-biotin for 20mins at 4°C. Biotin was visualized using streptavidin-AF568. Scale bar = 5µm. **(C)** Pie chart showing the proteins identified in (A) grouped based on their protein function.

Table 2 - Proteins identified by mass spectrometry in non-biotinylated controls

Name	Gene DDB ID	Score	Mass	Number of Peptides	Other
acetyl-CoA-carboxylase	accA	37	257657	23	Biotin binding
propionyl-CoA carboxylase	pccA	409	80344	30	Biotin binding
methylcrotonyl-CoA carboxylase Alpha subunit	mccA	250	77326	39	Biotin binding
methylcrotonyl-CoA carboxylase Beta subunit	mccB	543	64497	51	Biotin binding
bromodomain-containing protein	DDB0220693	71	173495	7	
ADP/ATP translocase	ancA	71	33619	4	Exchanges ADP and ATP across mitochondrial membrane. Six predicted TM domains.
avidin precursor (Gallus gallus)		2908	16873	137	

based on their Mascot protein score. The protein score is calculated from the probability that the individual peptide matches are random. Only proteins with scores over 50 ($p \leq 0.05$) were considered positive identifications and this reduced the number of proteins to 211. After removal of proteins present in the non-biotinylated control and removal of duplicates the final number of positive protein identifications was reduced to 157. A full list of these proteins can be found in Appendix I.

The proteins listed in Appendix I were sorted into functional groups using gene ontology descriptions of protein function (Figure 7C). Of the 157 proteins only one (cmfB) was identified as a transmembrane protein and the vast majority were proteins involved in processes inside the cell. A total of 43 proteins (27.4%) were involved in protein biosynthesis, with most of these proteins comprising subunits of the ribosome. A further 28 proteins (17.8%) were classed as metabolic proteins and 16 were mitochondrial proteins (10.2%). Proteins associated with the cytoskeleton were also highly represented (21 proteins; 13.4%). A small set of proteins involved in vesicular transport were identified (7 proteins; 4.5%; chcA, rab14, vps35. copG, cap, sarA, rab1C) along with three subunits of the vacuolar H+ ATPase.

The large number of intracellular proteins represented by this method was surprising, especially since the microscopy experiments had indicated that the labeling conditions minimize internalization of the biotin. Interestingly, proteomic analysis of purified phagosomes by three different groups had similar results with many intracellular proteins from the same functional groups predominating (Gotthardt et al., 2006; Shevchuk et al., 2009; Urwyler et al., 2009). All these studies showed a low representation of transmembrane proteins, even when using a variety of detergents and/or

a carbonate extraction step in their protocols. Similar trends were also seen when the proteome of macropinosomes was analyzed, although in this study 24% of the proteins identified contained a membrane spanning domain (Journet et al., 2012). The proteins identified in this thesis were cross-referenced with the proteins identified in these other proteomic studies, as well as, with the secreted proteome of developing *Dictyostelium* (Bakthavatsalam and Gomer, 2010) (Table 3). Nearly all the proteins identified in the biotin labeling experiment were also present in the macropinocytic proteome (91.7%). In addition, a significant percentage of the proteins were also present in the phagosome proteome (23.6-59.9%).

Table 3 - Comparison of biotinylated proteome data with published data

Data set	Percentage of hits also present in other proteome data sets
Conditioned Media Proteome (350 proteins) (Bakthavatsalam and Gomer, 2010)	15.9% (25 proteins)
Macropinocytic Proteome (2108 proteins) (Journet et al., 2012)	91.7% (144 proteins)
Phagosome Proteome 1 (179 proteins) (Gotthardt et al., 2006)	59.9% (94 proteins)
Phagosome Proteome 2 (566 proteins) (Urwyler et al., 2009)	25.5% (40 proteins)
Phagosome Proteome 3 (157 proteins) (Shevchuk et al., 2009)	23.6% (37 proteins)

2.3 Summary

The identification of a large number of intracellular proteins via the cell-surface biotinylation technique indicates that this technique may not be appropriate for the isolation of clathrin-mediated endocytic cargo. Many macropinocytic and phagocytic intracellular proteins were identified. It was not possible to tell if the proteins identified are directly biotinylated or if they may have been isolated via indirect interactions with other biotinylated proteins. The identification of proteins present in macropinosomes and phagosomes is not completely unexpected since these organelles are derived from the plasma membrane. The high overlap with the macropinocytic proteome suggests that macropinocytosis may not be adequately inhibited at 4°C. This would allow internalization of the biotinylation reagent and access to intracellular proteins during the twenty minute labeling step. It is possible that this high macropinocytic background signal overwhelms any signal that was derived from non-macropinocytic pathways. Alternative labeling strategies, enrichment for clathrin-coated vesicles, more stringent washing and improved membrane protein extraction methods were not explored further. These changes could significantly alter the protein repertoire identified by this technique.

CHAPTER 3 – Generation of a labeled AP-2 complex

Fluorescently tagged forms of clathrin have been used in *Dictyostelium* to study the localization and dynamics of clathrin-coated vesicles (Damer and O'Halloran, 2000; Wang et al., 2006). Since clathrin-coated vesicles are involved in many different transport steps within the cell it was first necessary to specifically visualize the population of clathrin associated with endocytosis. In mammalian cells, AP-2 is a key determinant for entry by clathrin-mediated endocytosis and is specific to this pathway. I therefore selected AP-2 as a candidate marker to visualize clathrin puncta associated with endocytosis in *Dictyostelium*. In this chapter I will describe the generation of a functional GFP tagged AP-2 complex.

3.1 Cloning and characterization of the *Dictyostelium* AP-2 complex

Genes corresponding to the subunits of AP-1, AP-2, AP-3 and AP-4 in *Dictyostelium* were inferred from homology to their mammalian counterparts (Table 4). Experimental evidence has confirmed these annotations for the γ, β1/2 and μ1 subunits of AP-1 (Lefkir et al., 2003; Sosa et al., 2012), for the δ, β3 and μ3 subunits of AP-3 (Bennett et al., 2008) and for the β1/2 and μ2 subunits of AP-2 (Sosa et al., 2012). To investigate the AP-2 complex in *Dictyostelium* both the *apm2* (μ2 subunit) and *Ap2A1* (α subunit) genes were cloned from a cDNA library generated from vegetative *Dictyostelium* wild-type (AX2) cells.

Table 4 - *Dictyostelium* AP complex genes

	Gene	Percent identity with human (name and accession number)	Divergence	Experimental evidence
AP-1 γ subunit	ap1g1	44.4 (AP-1 gamma-1b, NP_001119)	84.2	(Lefkir et al., 2003)
AP-1 β subunit	ap1b1	52.2 (AP-1 beta-1 isoform b, NP_663782)	68.4	(Sosa et al., 2012)
AP-1 μ subunit	apm1	67.4 (AP-1 mu-1 isoform 2, NP_115882)	38.4	(Lefkir et al., 2003)
AP-1 σ1 subunit	ap1s1	44.9 (AP-1 sigma-2, NP_003907)	89.1	
AP-1 σ2 subunit	ap1s2	57.8 (AP-1 sigma-2, NP_003907)	53.1	
AP-2 α subunit	ap2a1-1 ap2a1-2	38.3 (AP-2 alpha-2-2, NP_036437)	100.3	This study
AP-2 β subunit	ap1b1	51.9 (AP-2 beta isoform b, NP_001273)	70.0	This study, (Sosa et al., 2012)
AP-2 μ subunit	apm2	50.8 (AP-2 mu isoform a, NP_004059)	64.0	This study, (Sosa et al., 2012)
AP-2 σ subunit	ap2s1	62.0 (AP-2 sigma isoform AP17, NP_004060)	52.6	This study
AP-3 δ subunit	ap3d1	35.9 (AP-3 delta-1 isoform 2, NP_003929)	102.5	(Bennett et al., 2008)
AP-3 β subunit	ap3b-1 ap3b-2	31.6 (AP-3 beta-2, NP_004635)	113.5	(Bennett et al., 2008)
AP-3 μ subunit	apm3	47.4 (AP-3 mu-1, NP_036227)	74.6	(Bennett et al., 2008)
AP-3 σ subunit	ap3s1	64.9 (AP-3 sigma-1, NP_001275)	39.5	
AP-4 ε subunit	ap4e1	21.6 (AP-4 epsilon-1, NP_031373)	170.5	
AP-4 β subunit	ap4b1	24.0 (AP-4 beta-1, NP_006585)	157.9	
AP-4 μ subunit	apm4	21.6 (AP-4 mu-1, NP_004713)	148.2	
AP-4 σ subunit	ap4s1	55.4 (AP-4 sigma-1 isoform 2, NP_001121598)	59.3	

3.1.1 Tagging of the μ2 subunit of AP-2

The μ2 subunit was tagged on its C-terminus with GFP (apm2-GFP) and expressed in wild-type (AX2) cells under the control of the constitutive actin 6 promoter. Stable cell lines were generated but detection of the tagged protein by western blot of cell lysates was unsuccessful using an antibody to GFP. Visual examination of the cell lines showed they were very heterogeneous; punctate staining was seen in some cells while the rest of the cells showed a dim cytosolic fluorescence (Figure 8A). It is likely that the expression level was low and/or only a small portion of cells within the population expressed apm2-GFP.

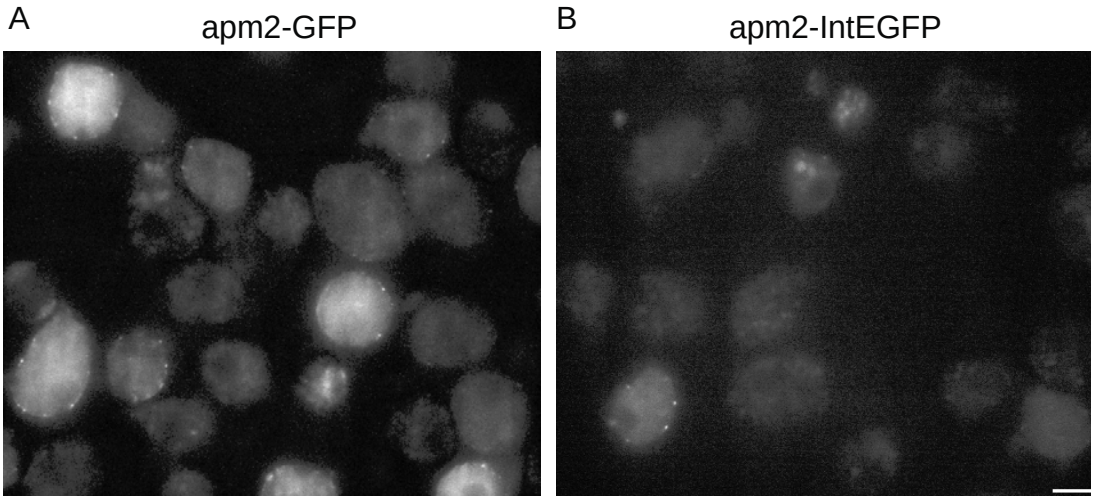

Figure 8 – Tagging of the μ2 subunit of AP-2

Wide-field microscopy images of AX2 cells transformed with a plasmid encoding **(A)** apm2-GFP or **(B)** apm2-IntEGFP. Scale bar = 5μm.

In mammalian cells, the placement of tags at the N and C terminus of the μ2 subunit of AP-2 has been shown to render the protein non-functional and unable to incorporate into AP-2 complexes. Instead epitope tags have been added between residues 236 and 237 located in a flexible linker in the molecule (Nesterov et al., 1999; Collins et al., 2002). These tagged constructs are believed to assemble into the AP-2 complex based on the observation that they co-immunoprecipitate and co-localize with the other AP-2 subunits (Nesterov et al., 1999). I therefore used a similar approach and inserted EGFP into the apm2 sequence at amino acid 241, an equivalent site to that used in the mammalian constructs (apm2-IntEGFP). When expressed in wild-type cells apm2-IntEGFP showed no improvement over apm2-GFP; cell lines were heterogeneous (Figure 8B) and tagged protein expression could not be detected by western blot using a GFP antibody.

3.1.2 Tagging of the α subunit of AP-2

Following unsuccessful tagging of the μ2 subunit, I attempted to tag the α subunit with GFP on the N-terminus (GFP-Ap2A1). Expression of GFP-Ap2A1 in wild-type cells (AX2) resulted in the expression of a single 140kDa protein, in agreement with the predicted size for GFP-Ap2A1 (Figure 9A). GFP-Ap2A1 localized to membrane puncta (see Chapter 4) and was uniformly expressed in all cells. Expression of this protein showed no detectable effect on cell growth (Figure 9C) or time taken by cells to undergo development on non-nutrient agar plates (Figure 9D).

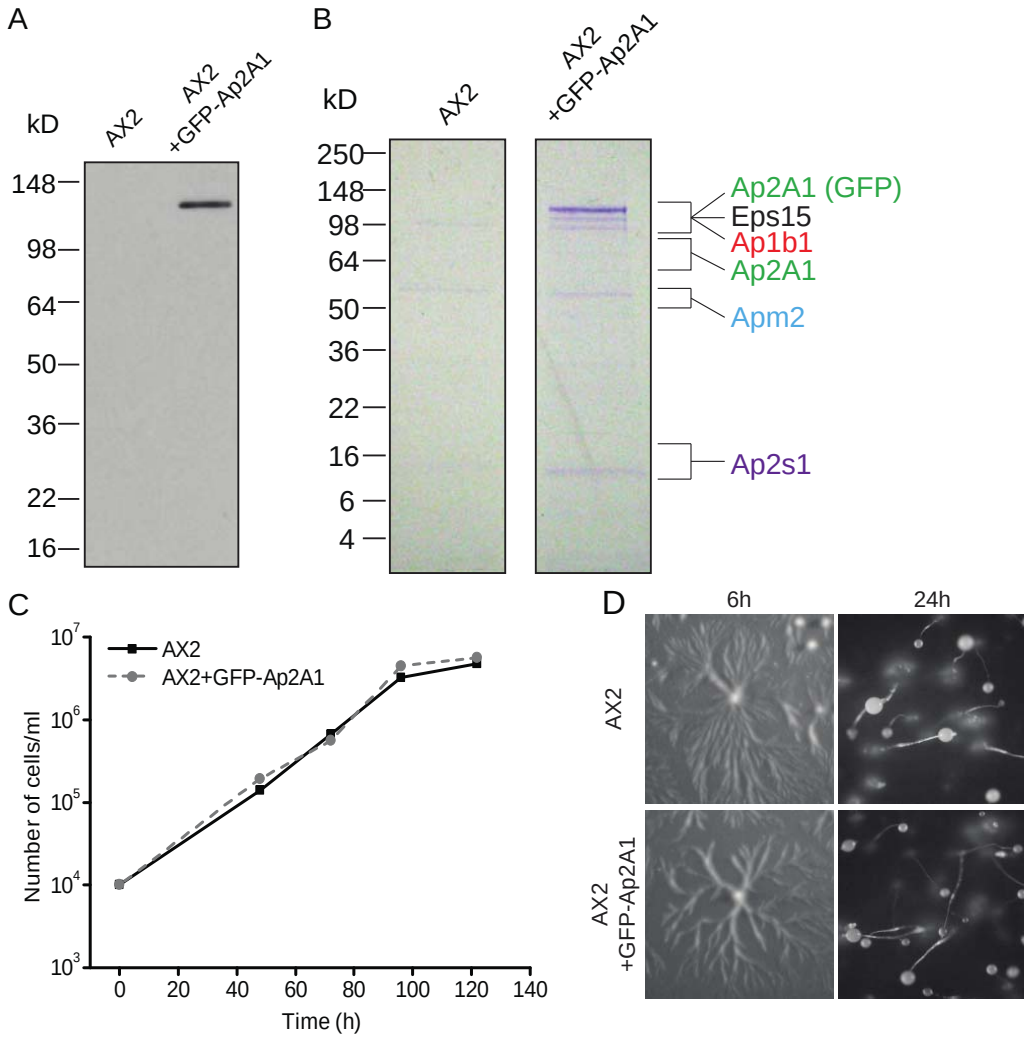

Figure 9 – Tagging of the α subunit of AP-2

(A) Western blot for GFP in lysates from wild-type cells (AX2) and from AX2 cells expressing GFP-Ap2A1. **(B)** Coomassie stained SDS-PAGE gel of proteins immunoprecipitated with anti-GFP antibodies from AX2 cells and from AX2 cells expressing GFP-Ap2A1. A list of all proteins identified by LC-MS/MS is in Table 5 and Appendices II & III. **(C)** Growth curve of AX2 cells and AX2 cells expressing GFP-Ap2A1. **(D)** Pictures of AX2 cells and AX2 cells expressing GFP-Ap2A1 induced to undergo fruiting body formation on non-nutrient agar plates. Representative images taken at 6h and 24h after the onset of starvation are shown.

3.2 Identification of proteins that interact with GFP-Ap2A1

To identify proteins that interact with GFP-Ap2A1 and form the AP-2 complex, cells expressing GFP-Ap2A1 were lysed and incubated with an anti-GFP antibody. The co-immunoprecipitated proteins were separated by SDS-PAGE and identified by LC-MS/MS mass spectrometry. Proteins identified included the predicted α, β, μ and σ subunits of the AP-2 complex (Figure 9B and Table 5). A full list of proteins that co-immunoprecipitated with GFP-Ap2A1 is found in Appendix II, proteins are only listed if they were identified in two separate experiments. Of all the proteins identified in the first experiment 65% (83 of 127) were also found in the second experiment. In the second experiment 19% (83 of 445) of the proteins were found in the first experiment. The increased number of proteins identified in the second experiment was due to improvements in the mass spectrometry. Within the proteins that were identified twice the gene *Ap1B1* was identified as encoding the β subunit, independently confirming the recent report that AP-1 and AP-2 use the same β subunit in *Dictyostelium* (Sosa et al., 2012). The gene *apm2* was also identified as encoding the μ2 subunit and *Ap2S1* as encoding the σ2 subunit. Other AP complex subunits were not identified indicating that GFP-Ap2A1 does not incorporate into the other AP complexes present in cells. The *Dictyostelium* homolog of Eps15 was also identified. Eps15 is a clathrin adaptor known to bind to the AP-2 α subunit in mammalian cells (van Delft et al., 1997). Interestingly the transmembrane subunit of the vacuolar H+ ATPase was also identified (*VatM*). This protein could be a potential cargo for endocytosis from the plasma membrane. A variety of other proteins involved in different intracellular processes were also identified (Appendix II) but the significance of these interactions and their specificity remains to be

Table 5 – Mass spectrometry data for GFP-Ap2A1 interacting proteins

Name	DDB_G ID	Score	Percent coverage	Number of unique peptides (total # of peptides)	MW (kDa)
ap1b1	DDB_G0279141	2253.82	36.31	30 (75)	106.5
		3548.85	40.76	35 (103)	
ap2a1	DDB_G0273439	5947.12	37.21	32 (191)	110.6
		15463.93	47.02	46 (429)	
ap2s1	DDB_G0289721	939	ND	(95)	17.0
		750.00	43.66	7 (36)	
apm2	DDB_G0277139	366.48	20.27	9 (16)	49.8
		2453.18	31.21	13 (71)	
EPS15 homology domain-containing protein	DDB_G0287325	175.09	7.19	5 (6)	131.3
		4728.43	40.89	34 (118)	

validated. Some of these proteins were identified in the biotinylation experiments in Chapter 2 (marked with a B) indicating that they may be non-specific proteins routinely identified during LC-MS/MS analysis.

A further list of 30 proteins that were co-immunoprecipitated with GFP-Ap2A1 can be found in Appendix III. This table comprises of proteins that were only identified in one of the two experiments but seemed interesting candidates for GFP-Ap2A1 interactors based on their biological function. These proteins included seven proteins (2% of proteins identified (362)) involved in vesicular transport including the SNARE binding protein nsfA and both clathrin heavy and light chains. Seven different (2% of identified proteins) Rab proteins were identified, as well as four membrane associated proteins (1% of identified proteins). Two further transmembrane proteins (0.6% of identified proteins) were identified which could be possible endocytic cargo molecules. Again, whether any of these proteins directly bind to AP-2 or are just random noise remains to be validated.

3.3 Identification of proteins that interact with GFP-clc

I also used this co-immunoprecipitation technique to identify proteins that interact with the labeled form of the clathrin light chain I would be using in further experiments. Cell lysates from *clc*- cells expressing GFP tagged clathrin light chain (GFP-clc) were used (Wang et al., 2006). Western blot confirmed the expression of the GFP tagged protein in these cells (Figure 10A).

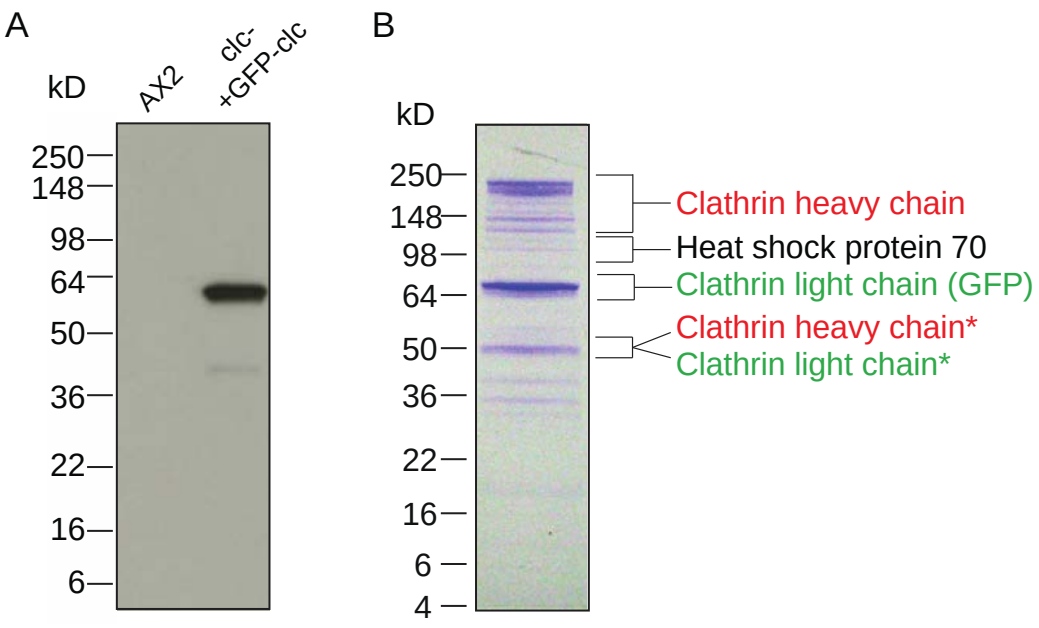

Figure 10 – Identification of GFP-clc interacting proteins

(A) Western blot for GFP in lysates from wild-type cells (AX2) and from *clc*- cells expressing GFP-clc. **(B)** Coomassie stained SDS-PAGE gel of proteins immunoprecipitated with anti-GFP antibodies from *clc*- cells expressing GFP-clc. Degradation products are labeled with an asterisk. A list of all proteins uniquely identified by LC-MS/MS is in Appendix IV.

As above, co-immunoprecipitated proteins were separated by SDS-PAGE and proteins identified by LC-MS/MS mass spectrometry (Figure 10B). Thirty one proteins were identified and these included the clathrin heavy chain and a heat shock protein 70 family member with 32% identity to the mammalian clathrin uncoating protein Hsc70 (*HSPA8*) (Schlossman et al., 1984). Both clathrin heavy chain (~190kDa) and GFP tagged clathrin light chain (~60kDa) were identified in bands that migrated corresponding to the sizes of the full-length proteins. Additionally, degradation products

of these two proteins (Figure 10B, asterisks) were identified as fragments migrating around 50kDa. This degradation could be due to the co-immunoprecipitation procedure. A full list of the other proteins identified can be found in Appendix IV. Again, four of these proteins were identified in the biotinylation experiment described in Chapter 2.

3.4 Summary

The results presented here demonstrate the existence of a functional AP-2 complex in *Dictyostelium* that is homologous to the AP-2 complex found in mammals. Additionally, I was able to tag the α subunit of the complex with GFP and show expression of this protein does not affect cell growth or development. Furthermore, co-immunoprecipitation shows GFP-Ap2A1 is able to incorporate into the AP2 complex and, at the level of expression used here, does not localize to any other AP protein complexes in the cell. GFP-Ap2A1 was also able to interact with a variety of other proteins. Some of these have proposed functions in endocytosis indicating that an endocytic protein-protein interaction network may exist in *Dictyostelium* similar to that found in mammals (Praefcke et al., 2004).

Functionality of the tagged form of clc was demonstrated previously by rescue of *clc*- phenotypes upon expression of GFP-clc (Wang et al., 2006). The results shown here demonstrate that GFP-clc is able to interact with clathrin heavy chain, in addition to several other proteins. In combination, the results presented in this chapter support the conclusion that the tagged forms of both AP-2 and clathrin are functional and are good reporters to measure the localization and dynamics of these protein complexes within the cell.

CHAPTER 4 – Dynamics of clathrin and AP-2

In this chapter I will describe the use of GFP tagged AP-2 complex and GFP-clc to measure the localization and dynamics of clathrin and AP-2 puncta in wild-type cells. In order to investigate their function further the localization of clathrin and AP-2 were assessed in various clathrin and AP-2 knockout cell lines.

4.1 Intracellular localization and dynamics of AP-2

The intracellular localization of GFP-Ap2A1 was investigated using confocal microscopy and total internal reflection fluorescence microscopy (TIR-FM). In wild-type cells (AX2), confocal slices through the middle of the cell volume showed GFP-Ap2A1 localized to distinct puncta that were distributed around the cell periphery (Figure 11A), in agreement with a previous study that used antibodies raised against Ap2A1 (Wen et al., 2009). Imaging of cells by TIR-FM, which only excites molecules within ~100nm of the coverslip, allowed me to establish that AP-2 puncta are at, or close to, the plasma membrane (Figure 11B). Only puncta present at the basal cell surface attached to the coverslip can be measured using TIR-FM. TIR-FM timelapse imaging of GFP-Ap2A1 revealed the dynamic nature of the cell-surface AP-2 puncta - puncta appear at the membrane, remain there for various lengths of time and subsequently disappear from the TIR-FM field (Figure 11D & E). Occasionally, AP-2 puncta could be seen to localize in rings or circles by TIR-FM (Figure 11C), closely resembling AP-2 puncta localization on bladders of the contractile vacuole (Wen et al., 2009). These were excluded from further kinetic analysis of puncta. When imaged for a short time (streaming acquisition for a total of 7.5s) three different puncta behaviors were observed: 78 ± 8% remained static,

Figure 11 – Intracellular localization and dynamics of AP-2

(A) Confocal sections showing the intracellular localization of GFP-Ap2A1 in wild-type (AX2), *Ap2A1*-, *apm2*-, *clc*- and *chcA*- cells. Scale bar = 1μm. **(B)** TIR-FM images of GFP-Ap2A1 puncta in AX2, *Ap2A1*-, *apm2*-, *clc*- and *chcA*- cells. Scale bar = 1μm **(C)** TIR-FM images of GFP-Ap2A1 showing an example of puncta localized in a ring most likely around a contractile vacuole bladder. **(D)** Examples of the dynamics of individual GFP-Ap2A1 puncta imaged by TIR-FM in AX2. Top row shows a disappearing punctum (red arrow) and a static punctum (yellow arrow). Bottom row shows a laterally moving punctum, whose track is shown in green. Scale bar = 0.5μm. **(E)** Examples of the dynamics of individual GFP-Ap2A1 puncta imaged by TIR-FM in AX2, **(F-G)** *chcA*- and **(H)** *apm2*- cells. Normalized fluorescence intensity is plotted as a function of time for each punctum. Scale bar = 0.5μm.

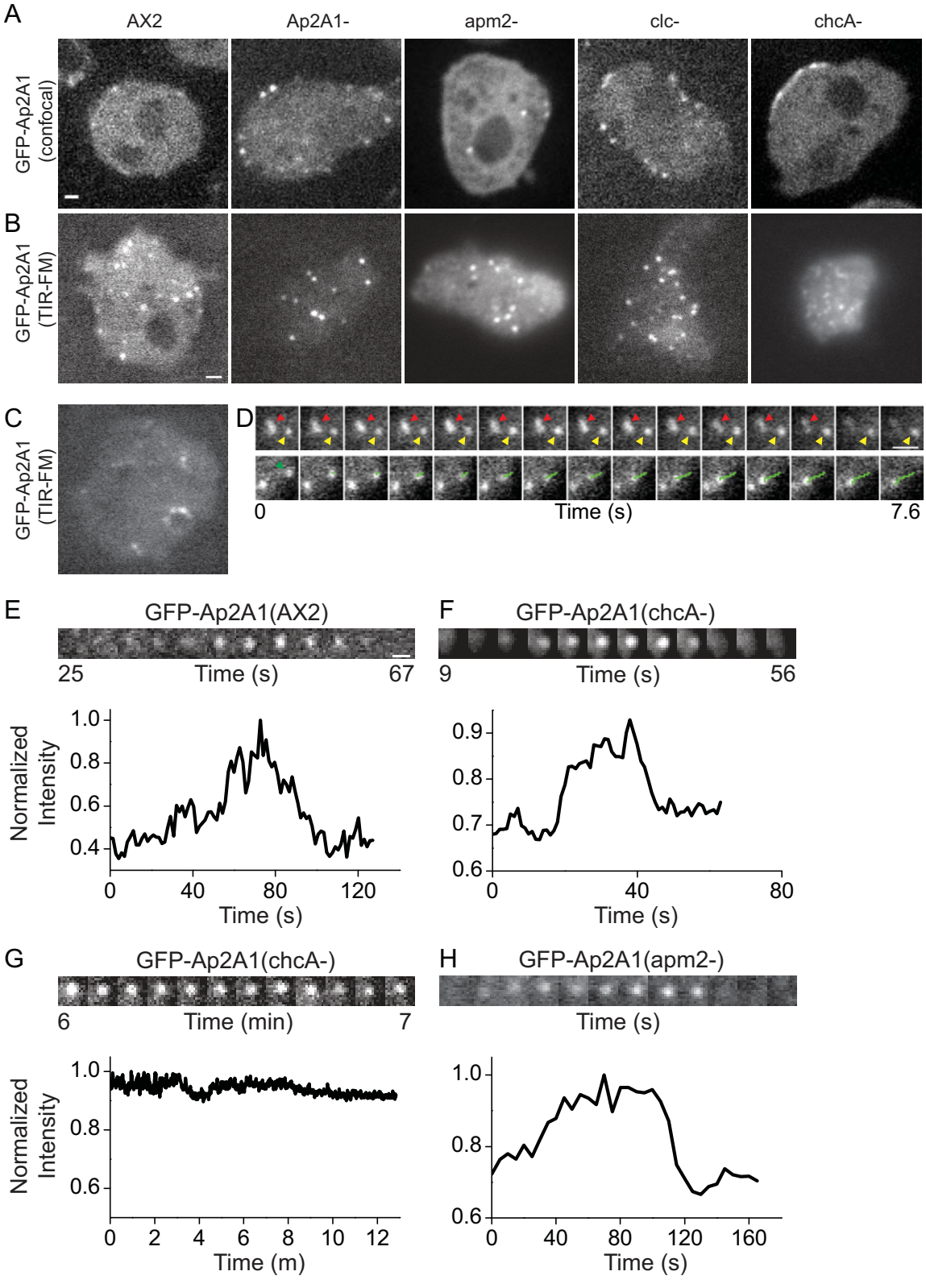
A
AX2
Ap2A1-
apm2-
clc-
chcA-
GFP-Ap2A1 (confocal)
B
GFP-Ap2A1 (TIR-FM)
C
GFP-Ap2A1 (TIR-FM)
D
0
Time (s)
7.6
E
GFP-Ap2A1(AX2)
25
Time (s)
67
Normalized Intensity
1.0
0.8
0.6
0.4
0
40
80
120
Time (s)
F
GFP-Ap2A1(chcA-)
9
Time (s)
56
0.9
0.8
0.7
0.6
0
40
80
Time (s)
G
GFP-Ap2A1(chcA-)
6
Time (min)
7
Normalized Intensity
1.0
0.8
0.6
0
2
4
6
8
10
12
Time (m)
H
GFP-Ap2A1(apm2-)
Time (s)
1.0
0.8
0.6
0
40
80
120
160
Time (s)

16 ± 8% disappeared and 7 ± 5% moved laterally (mean ± standard deviation (SD), n=363 puncta; 12 cells; 4 experiments) (Figure 11D). When imaged for a longer time (timelapse for 10min) all the puncta observed appearing on the surface disappeared within 6 minutes with an average duration on the surface of 56.3 ± 4.2s (mean ± standard error of the mean (SEM), n=111 puncta; 4 cells; 2 experiments) (Figure 12A). Some puncta were lost due to the movement of cells during the course of imaging and could not be included in the kinetic analysis.

In an attempt to remove any potential bias in the manual tracking I tested the use of automated tracking to follow every punctum in the cell. This automated tracking routine counted all puncta of AP-2 that disappeared and included puncta that disappeared due to cell movement. The average durations of puncta measured by this method were therefore significantly shorter and had large errors. Thus, due to their highly motile nature, automated tracking is not a suitable approach to analyze the kinetics of endocytic puncta in *Dictyostelium*.

4.2 Intracellular localization and dynamics of clathrin

In order to compare the behavior of AP-2 with clathrin I imaged *clc*- cells expressing GFP-clc (Wang et al., 2006). In TIR-FM, GFP-clc localized to distinct membrane puncta as well as to contractile vacuoles as previously observed (Figure 13A & B) (Wen et al., 2009; Brady et al., 2010). I performed the same analysis as for GFP-Ap2A1 puncta. Imaging for a short time (7.5s) revealed the dynamic behavior of clathrin puncta with 55 ± 18% remaining static, 26 ± 14% disappearing and 19 ± 5% moving laterally (mean ± SD, n=300 puncta; 6 cells; 2 experiments) (Figure 13C). When imaged

Figure 12 – Duration of AP-2 puncta on the cell surface

Histograms showing cell surface duration of GFP-Ap2A1 puncta in **(A)** AX2, **(B)** *chcA*-, **(C)** *clc*-, **(D)** *Ap2A1*- and **(E)** *apm2*- cells. The mean duration ± SEM and the number of puncta measured are given. Measurements are from a minimum of 4 different cells and 2 different experiments **(F)** Box chart showing the durations of GFP-Ap2A1 puncta in the different cell lines. Crosses = maximum and minimum values; solid square = mean; error bars = standard deviation; box = 25, 50 and 75 percentile. (G) Bar graph showing the percentage of GFP-Ap2A1 puncta present at the end of the timelapse with durations >350s.

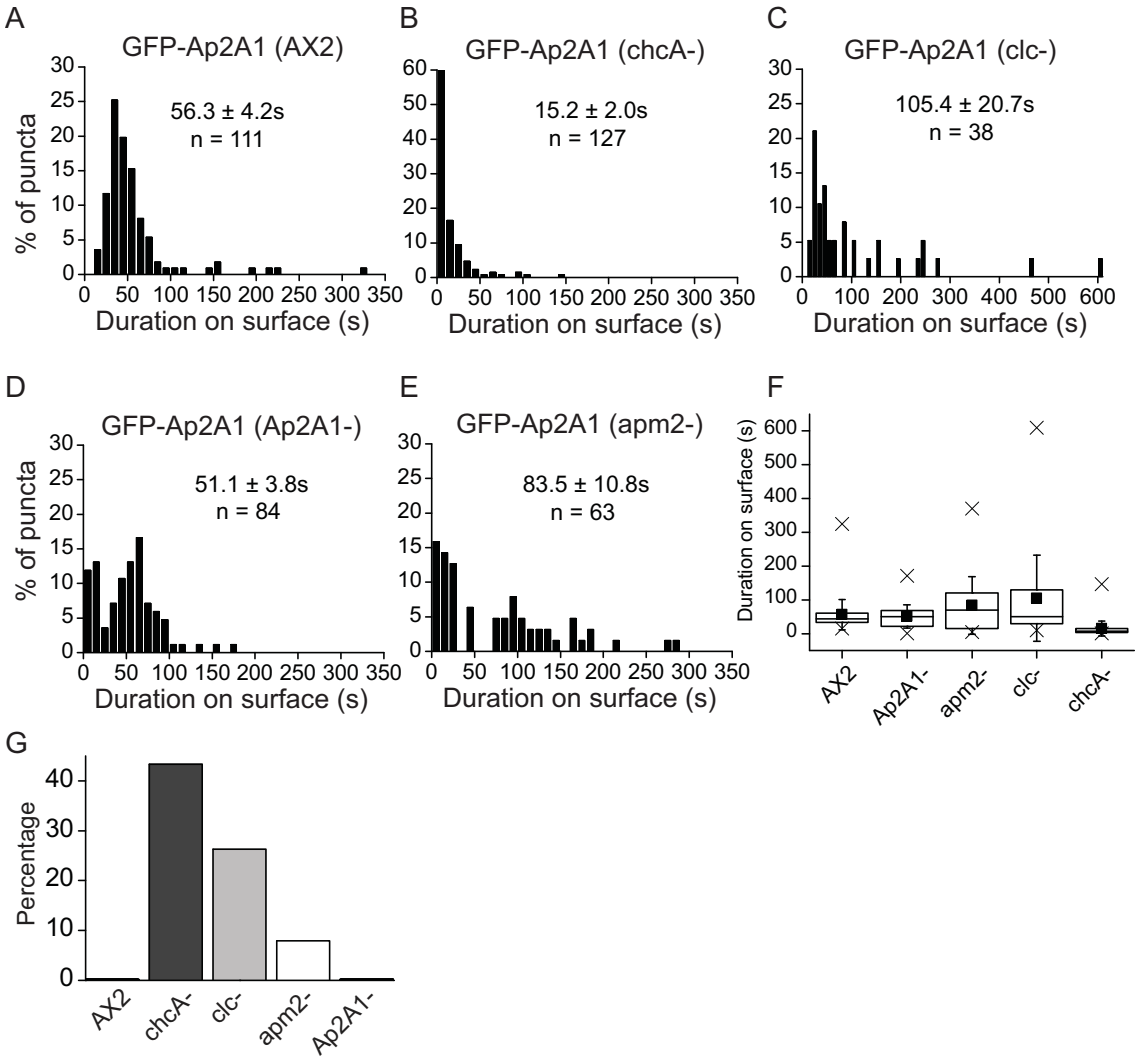
A
GFP-Ap2A1 (AX2)
56.3 ± 4.2s
n = 111
% of puncta
Duration on surface (s)
B
GFP-Ap2A1 (chcA-)
15.2 ± 2.0s
n = 127
Duration on surface (s)
C
GFP-Ap2A1 (clc-)
105.4 ± 20.7s
n = 38
Duration on surface (s)
D
GFP-Ap2A1 (Ap2A1-)
51.1 ± 3.8s
n = 84
% of puncta
Duration on surface (s)
E
GFP-Ap2A1 (apm2-)
83.5 ± 10.8s
n = 63
Duration on surface (s)
F
Duration on surface (s)
AX2
Ap2A1-
apm2-
clc-
chcA-
G
Percentage
AX2
chcA-
clc-
apm2-
Ap2A1-

Figure 13 – Intracellular localization and dynamics of clathrin

(A) TIR-FM images of mRFP-clc puncta in AX2, *Ap2A1-*, *apm2-*, *chcA-* and GFP-clc puncta in *clc-* cells. Scale bar = 1μm. **(B)** TIR-FM images of mRFP-clc showing an example of puncta localized in a ring most likely around a contractile vacuole bladder. Scale bar = 1μm. **(C)** Examples of the dynamics of individual GFP-clc puncta imaged by TIR-FM in *clc-* cells. Top row shows a disappearing punctum (red arrow) and a static punctum (yellow arrow). Bottom row shows a laterally moving punctum, whose track is shown in green. Scale bar = 0.5μm. **(D)** Examples of the dynamics of individual mRFP-clc puncta imaged by TIR-FM in AX2, **(E)** *Ap2A1-* and **(F)** *apm2-* cells. Normalized fluorescence intensity is plotted as a function of time for each punctum. Scale bar = 0.5μm.

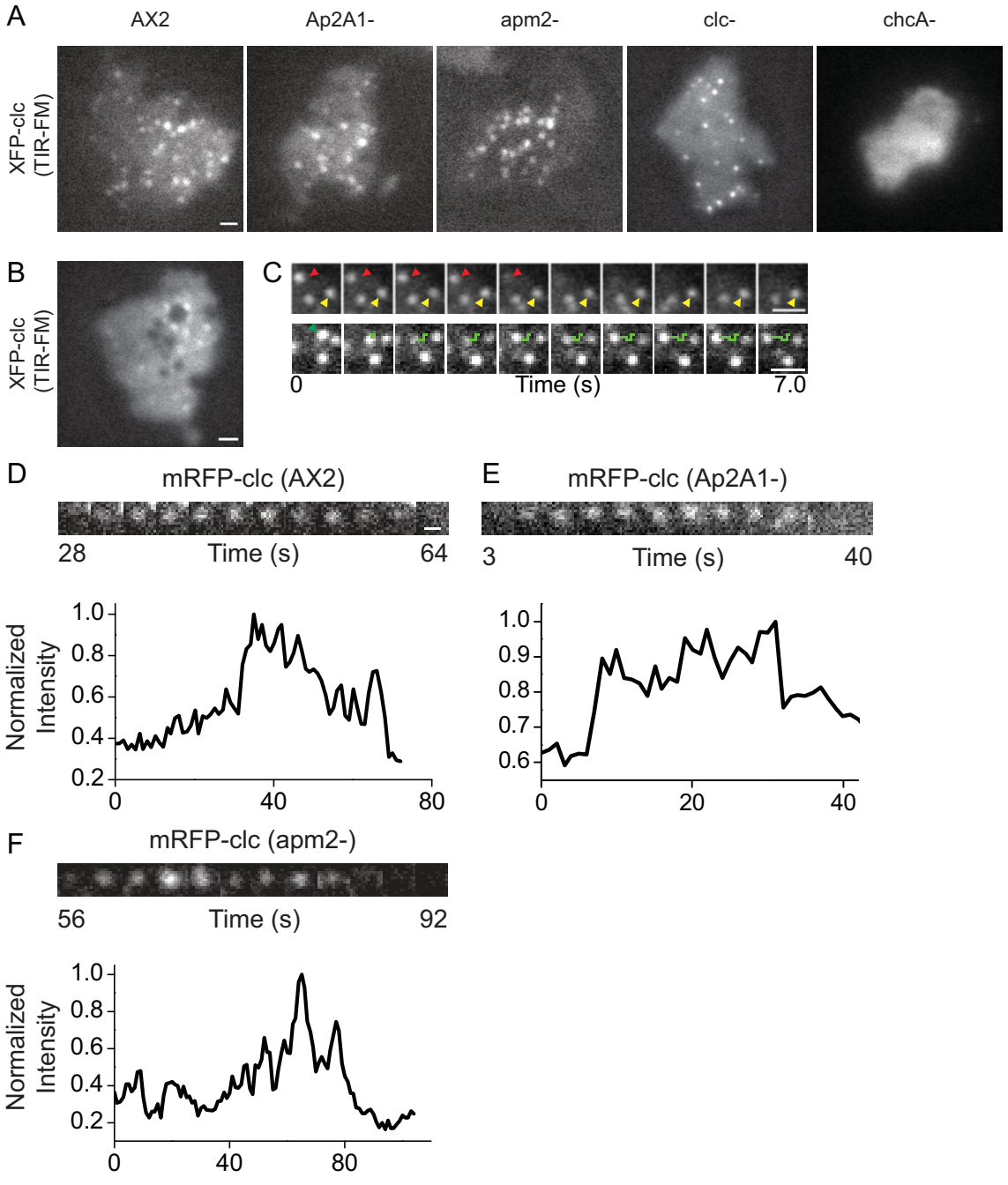
A
AX2
Ap2A1-
apm2-
clc-
chcA-
XFP-clc (TIR-FM)
B
XFP-clc (TIR-FM)
C
0
Time (s)
7.0
D
mRFP-clc (AX2)
28
Time (s)
64
Normalized Intensity
1.0
0.8
0.6
0.4
0.2
0
40
80
E
mRFP-clc (Ap2A1-)
3
Time (s)
40
1.0
0.9
0.8
0.7
0.6
0
20
40
F
mRFP-clc (apm2-)
56
Time (s)
92
Normalized Intensity
1.0
0.8
0.6
0.4
0.2
0
40
80

for a longer period (10min), all puncta observed appearing on the surface disappeared within 5 minutes with an average duration on the surface of 55.6 ± 6.0s (mean ± SEM, n=103 puncta; 9 cells; 5 experiments) (Figure 14A). Again puncta that appeared or disappeared in the TIR-FM field due to cell movement were excluded.

The experiments were also performed using *clc*- cells expressing mRFP tagged clc (mRFP-clc) that is similar to the mRFP-clc previously reported (Brady et al., 2010). Again when cells were imaged by TIR-FM for 10 minutes, all puncta observed appearing on the surface disappeared within 5 minutes with an average duration on the surface of 37.3 ± 7.7s (mean ± SEM, n=43 puncta; 5 cells; 2 experiments) (Figure 14B). This is similar to the value of 39s previously reported using mRFP-clc (Brady et al., 2010). The differences in duration observed between the GFP tagged and mRFP tagged forms of clc indicate that the fluorescent protein tags may have different effects on clc function. The ability of both the tagged clc forms to rescue the *clc*- phenotypes does, however, indicate that these proteins are functional (Wang et al., 2006; data not shown). The subtle differences in the dynamics I measured could arise from the fact that the GFP used in GFP-clc is not a monomeric form whereas the RFP used is monomeric. Dimerization of GFP-clc could affect the dynamics of the protein and therefore the duration on the cell surface.

Comparison of clathrin and AP-2 puncta showed they have similar distributions of duration times at the cell surface (Figure 12A & 14A); however there is a population of clathrin puncta which have shorter durations at the cell surface (21% of GFP-clc and 54% of mRFP-clc puncta have a lifetime < 10s vs. 0% of AP-2 puncta). I used a two-sample Kolmogorov-Smirnov (KS) test to determine whether the histograms of puncta

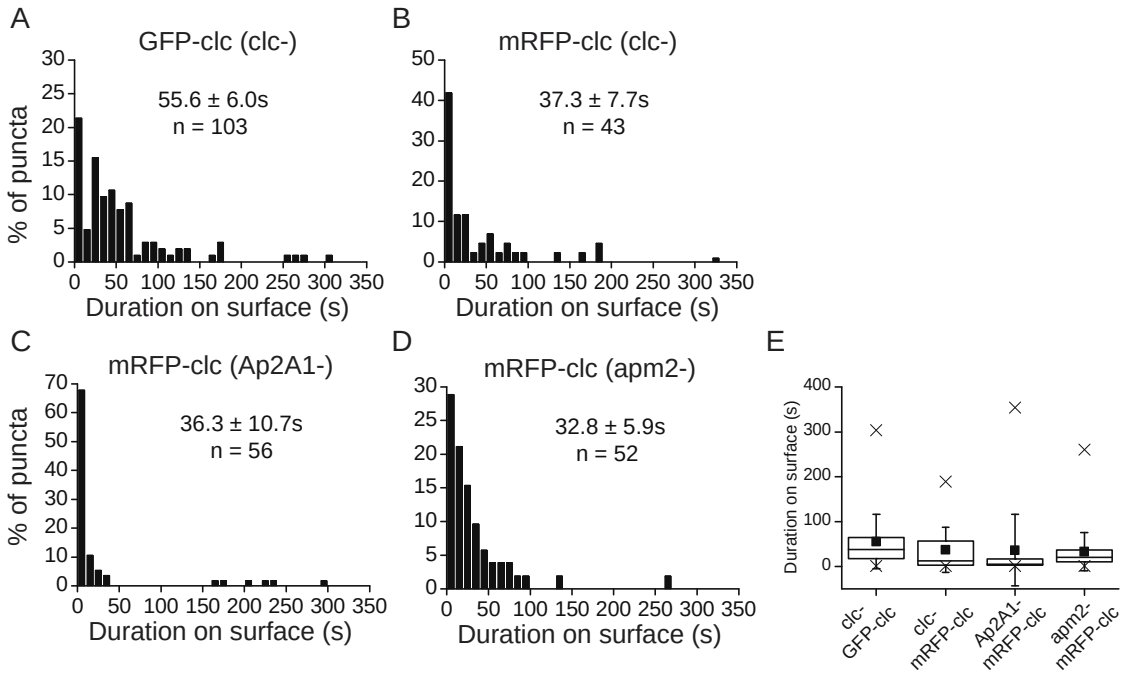

Figure 14 – Duration of clathrin puncta on the cell surface

Histograms showing cell surface duration of **(A)** GFP-clc puncta in *clc*- cells, **(B)** mRFP-clc puncta in *clc*-, **(C)** *Ap2A1*- and **(D)** *apm2*- cells. The mean duration ± SEM and the number of puncta measured are given. Measurements are from a minimum of 4 different cells and 2 different experiments **(E)** Box chart showing the durations of XFP-clc puncta in the different cell lines. Crosses = maximum and minimum values; solid square = mean; error bars = standard deviation; box = 25, 50 and 75 percentile.

duration on the surface showed similar distributions. I found the distributions of durations were significantly different between AP-2 and GFP-clc (KS test, p=0.046) and between AP-2 and mRFP-clc (KS test, $p=2.16 \times 10^{-8}$). This difference was eliminated if puncta with durations <10s were removed from the clathrin populations (GFP-clc KS test, p=0.066; mRFP-clc KS test, p=0.075) (Table 6). It is possible this population corresponds to clathrin-coated intracellular vesicles that move close to the plasma membrane during imaging thus being detected using TIR-FM (Keyel et al., 2004).

When the population of puncta with durations <10s were removed from the clathrin data set the average durations changed to 69.5 ± 6.8s (mean ± SEM, n=81 puncta) for GFP-clc and to 62.0 ± 10.8s (mean ± SEM, n=25 puncta) for mRFP-clc. Interestingly, comparison of the distribution of durations using the KS test showed that when the <10s populations are removed from the GFP-clc and mRFP-clc data sets they are no longer significantly different (KS test, p=0.530). This suggests that the differences in dynamics measured with GFP-clc vs. mRFP-clc could be caused by differences in the endosomal population of clathrin rather than in the endocytic dynamics.

4.3 Clathrin heavy chain is required for the dynamic behavior of AP-2 puncta

The formation and maturation of a clathrin-coated pit involves the recruitment of a complex array of proteins. It has been difficult to study the requirements for individual components of the clathrin-coated vesicle cycle in mammalian cells due to redundancy and incomplete knockdowns. I therefore took advantage of the availability of knockouts in *Dictyostelium* to investigate if clathrin is necessary for the localization of AP-2. GFP-Ap2A1 was expressed in cells with disrupted clathrin light chain (*clc*-) (Wang et al.,

Table 6 - Kolmogorov-Smirnov (KS) test *P* values

Data Set 1	**Data Set 2**	**KS *P* value**
GFP-clc (*clc*-)	mRFP-clc (*clc*-)	0.00584
GFP-clc minus 10s (*clc*-)	mRFP-clc minus 10s (*clc*-)	0.52934
GFP-clc (*clc*-)	GFP-Ap2A1 (AX2)	0.04594
GFP-clc minus 10s (*clc*-)	GFP-Ap2A1 (AX2)	0.06564
mRFP-clc (*clc*-)	GFP-Ap2A1 (AX2)	2.15915×10^{-8}
mRFP-clc minus 10s (*clc*-)	GFP-Ap2A1 (AX2)	0.0747
mRFP-clc (*clc*-)	mRFP-clc (*Ap2A1*-)	0.04744
mRFP-clc (*clc*-)	mRFP-clc (*apm2*-)	0.04795
GFP-Ap2A1 (AX2)	GFP-Ap2A1 (*Ap2A1*-)	0.00937
GFP-Ap2A1 (AX2)	GFP-Ap2A1 (*apm2*-)	2.22786×10^{-5}
GFP-Ap2A1 (AX2)	GFP-Ap2A1 (*clc*-)	0.01449
GFP-Ap2A1 (AX2)	GFP-Ap2A1 (*chcA*-)	3.80114×10^{-32}

2003) or with disrupted clathrin heavy chain (*chcA*-) (Ruscetti et al., 1994). Confocal and TIR-FM imaging of GFP-Ap2A1 in *clc*- cells showed that AP-2 was able to localize to membrane puncta that behaved with similar dynamics to wild-type cells (Figure 11A & B; Figure 12C & F).

In *chcA*- cells GFP-Ap2A1 was also able to form membrane puncta; puncta with a normal appearance were observed but there was also a increased number of diffuse puncta compared to wild-type cells (Figure 11B). In addition there was cell-to-cell variability with some cells showing no puncta. Confocal imaging of GFP-Ap2A1 in *chcA*- cells showed that although GFP-Ap2A1 could bind to the membrane the puncta often all stuck together and localized to one side of the cell (Figure 11A). Furthermore, timelapse TIR-FM imaging showed high variability in the behavior of individual AP-2 puncta; several puncta were very short lived (<10s), some had wild-type dynamics (Figure 11F), while other puncta that were present at the beginning of imaging did not disappear for over a 12 minute period (Figure 11G). Analysis of the surface duration of the dynamic GFP-Ap2A1 puncta showed an increased proportion of puncta with durations of less than 10s, causing a significantly shorter average surface duration of 15.2 ± 2.0s (mean ± SEM, n=127 puncta; 11 cells; 7 experiments) compared to wild-type cells (56.3 ± 4.2s) (Figure 12B); correspondingly the distribution of durations was significantly different between wild-type and *chcA*- cells (KS test, $p=3.80 \times 10^{-32}$) (Table 6). In order to have a measurable duration on the surface, appearance and disappearance must be observed during the timelapse. Therefore, GFP-Ap2A1 puncta that were present for the whole timelapse were not measured in the histogram of the distribution of durations (Figure 12B). To analyze these, the puncta present at the end of the timelapse

were tracked backwards through the timelapse and I quantified their time of arrival; for wild-type cells I did not observe any puncta with a duration >350s. However, in *chcA*- cells I found 43% of the puncta present in the last frame of the timelapse were abnormally long lived. This number was also elevated in *clc*- cells (26%) (Figure 12G).

These results indicate that while clathrin is not required for the plasma membrane localization of AP-2, its presence is required for normal dynamics of the AP-2 puncta at the cell surface. Loss of clathrin results in the appearance of two abnormal AP-2 puncta populations, one that is very short lived (average duration 15.2s), and one that is long lived (durations over 350s).

4.4 AP-2 μ2 is not required for AP-2 α puncta formation

I next investigated the effects of disrupting the α (*Ap2A1-)* (Wen et al., 2009) or μ2 (*apm2-*) (Mercanti et al., 2006b) subunits on the localization of AP-2 or clathrin in cells. In both the α and μ2 knockouts the localization and dynamics of clathrin puncta at the plasma membrane were similar to wild-type cells (Figure 13A, E & F; Figure 14C-E).

Confocal and TIR-FM imaging of GFP-Ap2A1 rescue in *Ap2A1*- cells showed puncta were localized to the membrane similar to wild-type cells (Figure 11A & B). These puncta behaved with wild-type dynamics, however the distributions of durations were significantly different (KS test, p=0.0094) due to the appearance of a population with shorter durations (<20s) (Figure 12D & F; Table 6). This could be due to an incomplete rescue of the *Ap2A1*- phenotype by the GFP-Ap2A1 protein or due to difference in the background strain used to generate the *Ap2A1*- cells (DH10).

Interestingly GFP-Ap2A1 also localized to distinct membrane puncta in μ2 knockouts (Figure 11A & B). Again some of these GFP-Ap2A1 puncta showed wild-type dynamics (Figure 11H), however, on average the duration of puncta was longer (83.5 ± 10.8s). In addition to this shift of some puncta to a longer duration, again I also observed the appearance of a population with shorter durations (<20s) and the distributions of durations were significantly different from wild-type puncta (KS test, $p=2.23x10^{-5}$) (Figure 12E & F; Table 6). Confocal imaging showed that while GFP-Ap2A1 puncta could be seen on the plasma membrane there was a higher cytoplasmic level of GFP-Ap2A1 in *apm2-* cells (Figure 11A). Western blot of cell lysates showed loss of *apm2-* does not destabilize the α subunit (Figure 15A) confirming the finding that *apm2-* does not destabilize the other large AP-2 subunit β1/2 (Sosa et al., 2012).

To investigate the composition of the GFP-Ap2A1 puncta I incubated lysates from *apm2-* cells expressing GFP-Ap2A1 with an anti-GFP antibody and separated and identified the co-immunoprecipitated proteins using SDS-PAGE and LC-MS/MS mass spectrometry (Figure 15B). Forty nine proteins were identified, a full list can be found in Appendix V. In the absence of the μ2 subunit, GFP-Ap2A1 was still able to interact with the β1/2 (*Ap1B1*) and σ2 (*Ap2S1*) subunits of the AP-2 complex. I did not find any of the other AP μ subunits but did identify the γ subunit of AP-1 (*Ap1G1*). Furthermore, the eps15 homolog and nsfA were again identified indicating that, in the absence of μ2, GFP-Ap2A1 can maintain these interactions. Again a variety of other proteins were identified (Appendix V), several of these were identified in biotinylation experiments (marked with a "B"), or in the previous GFP-Ap2A1 co-immunoprecipitations (marked with an asterisk). These results indicate that in the absence of the μ2 subunit in *Dictyostelium* a

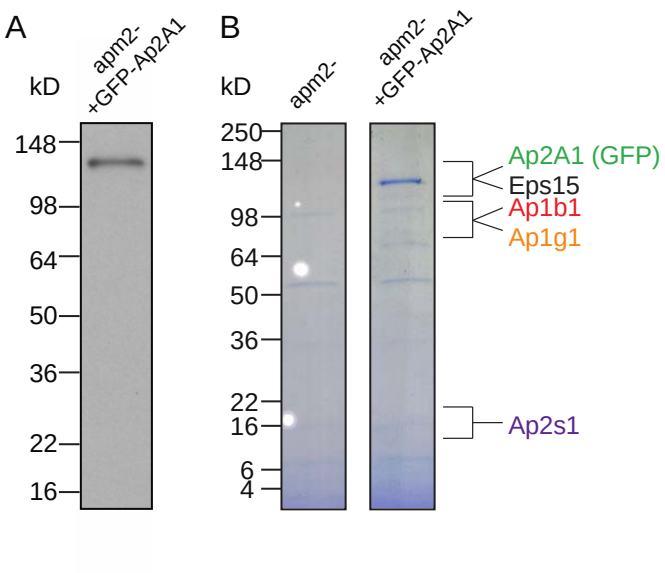

Figure 15 – Identification of GFP-Ap2A1 interacting proteins in *apm2*- cells

(A) Western blot for GFP in lysates from *apm2*- cells expressing GFP-Ap2A1. **(B)** Coomassie stained SDS-PAGE gel of proteins immunoprecipitated with anti-GFP antibodies from *apm2*- cells and *apm2*- expressing GFP-Ap2A1. A list of all proteins uniquely identified by LC-MS/MS is in Appendix V.

partial AP-2 complex can form that may contain the γ subunit. This experiment did not, however, test the relative abundance of GFP-Ap2A1 that was bound to the β1/2 and σ2 subunits, thus the partial complex detected could represent only a small amount of GFP-Ap2A1 expressed in the cell.

4.5 Summary

The results presented here show that in *Dictyostelium,* clathrin and AP-2 localize to membrane puncta. Live-cell imaging revealed these puncta are highly dynamic and exhibit similar behaviors to those seen for clathrin-coated vesicles in mammalian cells. Puncta accumulate on the membrane followed by disappearance from the TIR-FM field (Rappoport et al., 2006). In mammalian cells clathrin and AP-2 membrane puncta represent coated-pits forming on the membrane, therefore it is likely that the puncta I have observed are homologous structures and represent coated-pits in *Dictyostelium*. Clathrin and AP-2 puncta displayed similar average surface durations and dynamics. For both clathrin and AP-2 there was a wide variety of durations on the plasma membrane, again a property consistent with mammalian clathrin-coated pits (Mattheyses et al., 2011).

Deletions in clathrin and AP-2 genes in *Dictyostelium* were used to study the requirements for these proteins in clathrin-coated vesicle formation. The results showed that AP-2 can form membrane puncta in the absence of clathrin heavy chain but they had abnormal dynamics. A population with long lifetimes on the surface appeared, furthermore, I also observed a population of AP-2 puncta that have a much shorter surface duration indicating that clathrin has a role in stabilizing AP-2 at the membrane.

In the absence of the AP-2 μ2 subunit, GFP-Ap2A1 was stable and able to localize to plasma membrane puncta that represented partial AP-2 complexes as shown by co-immunoprecipitation and mass spectrometry experiments. This suggests that the AP-2 complex can assemble and target to the plasma membrane without the μ2 subunit, consistent with findings for AP-1 in *Dictyostelium* (Lefkir et al., 2003). The appearance of a short lived population of AP-2 puncta in the μ2 and α knockouts indicated that the individual subunits may also play a role in stabilizing the binding of the AP-2 complex to the membrane. The μ2 and α knockouts did not appear to affect dynamics of clathrin puncta in *Dictyostelium*.

CHAPTER 5 – Clathrin and AP-2 puncta correspond to endocytic vesicles

Since clathrin and AP-2 puncta behaved with similar dynamics at the plasma membrane, I next investigated their co-localization and dynamics in the same cell. Furthermore, to test the hypothesis that clathrin and AP-2 puncta corresponded to clathrin-coated pits I used an optical assay used to determine if disappearing puncta corresponded to sites of endocytosis.

5.1 Clathrin and AP2 puncta co-localize and disappear together

In order to image AP-2 and clathrin in the same cell clc was tagged with mRFP on its N terminus (mRFP-clc). This construct is similar to the RFP-clc previously described (Wen et al., 2009). A clc tagged with mRFP on its C terminus (clc-mRFP) was also generated, this site is believed to be less likely to interfere with clathrin functions due to its positioning at the trimerization domain. Both fusion proteins were able to rescue *clc*- phenotypes and were used interchangeably. When co-expressed and imaged by TIR-FM, both mRFP-clc and GFP-Ap2A1 co-localized in puncta at the plasma membrane in live cells, in agreement with observations in fixed cells (Figure 16A) (Wen et al., 2009). Co-localization analysis demonstrated that 76 ± 18% of AP-2 puncta were positive for clathrin and 57 ± 19% of clathrin puncta were positive for AP-2 (mean ± SD, n=33 cells) (Figure 16C). Co-localization of less than 100% is consistent with observations of clathrin and AP-2 in mammalian cells (Rappoport et al., 2003) and *Dictyostelium* (Wen et al., 2009).

Two color TIR-FM time-lapse imaging of puncta showed that GFP-Ap2A1 and mRFP-clc display similar dynamics at the plasma membrane (Figure 16B). As seen with

Figure 16 - Simultaneous imaging of the dynamics of clathrin and AP-2

(A) Two-color TIR-FM images of GFP-Ap2A1 and mRFP-clc puncta. Scale bar = 2μm. **(B)** Example of the dynamics of an individual punctum imaged by TIR-FM. Scale bar = 0.5μm. **(C)** Quantification of co-localization between GFP-Ap2A1 and mRFP-clc puncta imaged by TIR-FM. The percentage overlap is plotted for GFP–Ap2A1 vs. mRFP-clc (gray bar) and for mRFP-clc vs. GFP-Ap2A1 (white bar). Data is represented as mean ± SD (n=33 cells). **(D)** Normalized fluorescence intensity for the punctum shown in **(B)** is plotted as a function of time for GFP-Ap2A1 (green, open circles) and mRFP-clc (red, filled circles). **(E)** Histogram of the time between mRFP-clc and GFP-Ap2A1 disappearance from the TIR-FM field (n=132 puncta, 15 cells, 2 experiments).

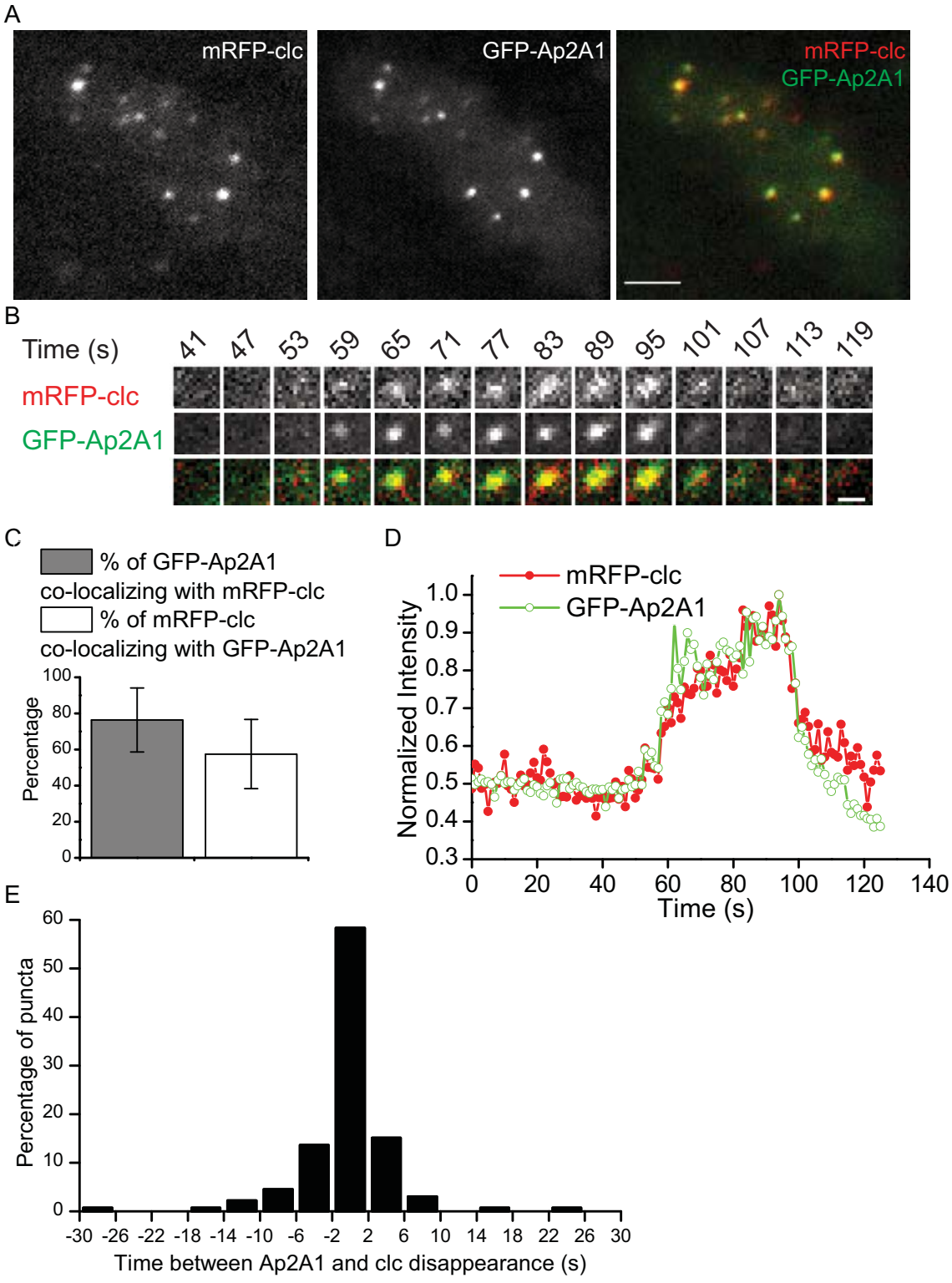
A
mRFP-clc
GFP-Ap2A1
mRFP-clc
GFP-Ap2A1
B
Time (s)
41 47 53 59 65 71 77 83 89 95 101 107 113 119
mRFP-clc
GFP-Ap2A1
C
% of GFP-Ap2A1
co-localizing with mRFP-clc
% of mRFP-clc
co-localizing with GFP-Ap2A1
Percentage
100 80 60 40 20 0
D
mRFP-clc
GFP-Ap2A1
Normalized Intensity
1.0 0.9 0.8 0.7 0.6 0.5 0.4 0.3
0 20 40 60 80 100 120 140
Time (s)
E
Percentage of puncta
60 50 40 30 20 10 0
-30 -26 -22 -18 -14 -10 -6 -2 2 6 10 14 18 22 26 30
Time between Ap2A1 and clc disappearance (s)

single color experiments, individual puncta could be seen accumulating at the membrane, remaining there for variable amounts of time, before disappearance from the TIR-FM field (Figure 16D). Individual puncta were analyzed by calculating the time of initiation of disappearance from the TIR-FM field for both GFP-Ap2A1 and mRFP-clc (n=132 puncta, 15 cells, 2 experiments) (Figure 16E). This analysis showed that for 58% of puncta AP-2 disappeared within 4s of clathrin disappearance indicating that AP-2 and clathrin leave the TIR field at the same time and behave with similar dynamics at the plasma membrane.

5.2 Clathrin and AP-2 disappearance corresponds to endocytosis

As discussed in Chapter 1, disappearance of puncta from TIR-FM is insufficient to distinguish between endocytosis, coated-pit disassembly, and/or photobleaching. Therefore, additional criteria were required to determine if the disappearing puncta observed here correspond to endocytic events. One criterion that can be used to distinguish endocytic events is the movement of clathrin and AP-2 coated vesicles inside the cell.

To further investigate the nature of AP-2 and clathrin disappearance I monitored puncta by alternating between wide-field (EPI) and TIR illumination. Since the TIR field decays with a space constant of ~100nm but the EPI field has a focal depth of ~500nm, puncta that are internalized should continue to be detected with EPI illumination after disappearing from the TIR field (Merrifield et al., 2002; Mattheyses et al., 2011). This technique allows distinction between three main behaviors based on the fluorescence intensity signatures puncta produce in the EPI and TIR channels.

Cells expressing GFP-Ap2A1 and clc-mRFP were imaged by alternating EPI and TIR illumination and the fluorescence intensity of individual puncta was quantified for each channel (Figure 17). Two criteria were used to determine whether puncta were analyzed further. Firstly, puncta had to be positive for both AP-2 and clathrin. Secondly, puncta had to show the typical dynamics already observed whereby AP-2 and clathrin accumulate in TIR followed by disappearance. Quantification of the fluorescence intensity of individual puncta over time for both the EPI and TIR illumination was used to group puncta based on their behavior. For some puncta the clathrin EPI signal could not be detected above the background; in these cases only the AP-2 EPI signal was used for analysis and classification.

A vesicle that forms in TIR, pinches off the membrane and moves into the cell, consistent with endocytosis, was observed for 32 ± 17% of puncta (mean ± SD, n=93 puncta, 9 cells, 2 experiments) (Figure 17A). In these puncta the fluorescence appeared in EPI simultaneously with, or soon after, the TIR signal, consistent with the *de novo* formation of a clathrin-coated pit at the plasma membrane. When these puncta disappear from the TIR field they continued to be observed in EPI-illumination, indicating movement of a vesicle away from the plasma membrane into the cell.

For 17 ± 13% (mean ± SD) of puncta the EPI signal appeared and disappeared simultaneously with the signal in TIR (Figure 17B). These events could correspond to endocytic vesicles that either lose their clathrin and AP-2 coincident with the vesicle leaving the plasma membrane, or to vesicles internalizing faster than the imaging speed. Alternatively, the loss of signal could be due to an unproductive clathrin-coated pit where clathrin and AP-2 disassemble at the cell membrane. Both of these behaviors have been

Figure 17 – EPI-TIR assay of AP-2 and clathrin puncta

Examples of the dynamics of individual GFP-Ap2A1 and clc-mRFP puncta imaged by two-color alternating EPI and TIR illumination. Kymographs are a maximum intensity projection of the four pixels surrounding the center of the punctum. Normalized fluorescence intensity is plotted as a function of time for GFP-Ap2A1 TIR signal (top graph, black line), GFP-Ap2A1 EPI signal (top graph, gray line), clc-mRFP TIR signal (bottom graph, black line), clc-mRFP EPI signal (bottom graph, gray line). Dashed lines indicate the time of either appearance or disappearance for each channel. **(A)** Example of an individual punctum where the EPI and TIR signals appear together and the TIR signal disappears before the EPI signal. **(B)** Example of an individual punctum where the EPI and TIR signals appear and disappear together. **(C)** Example of an individual punctum where the EPI signal appears before the TIR signal.

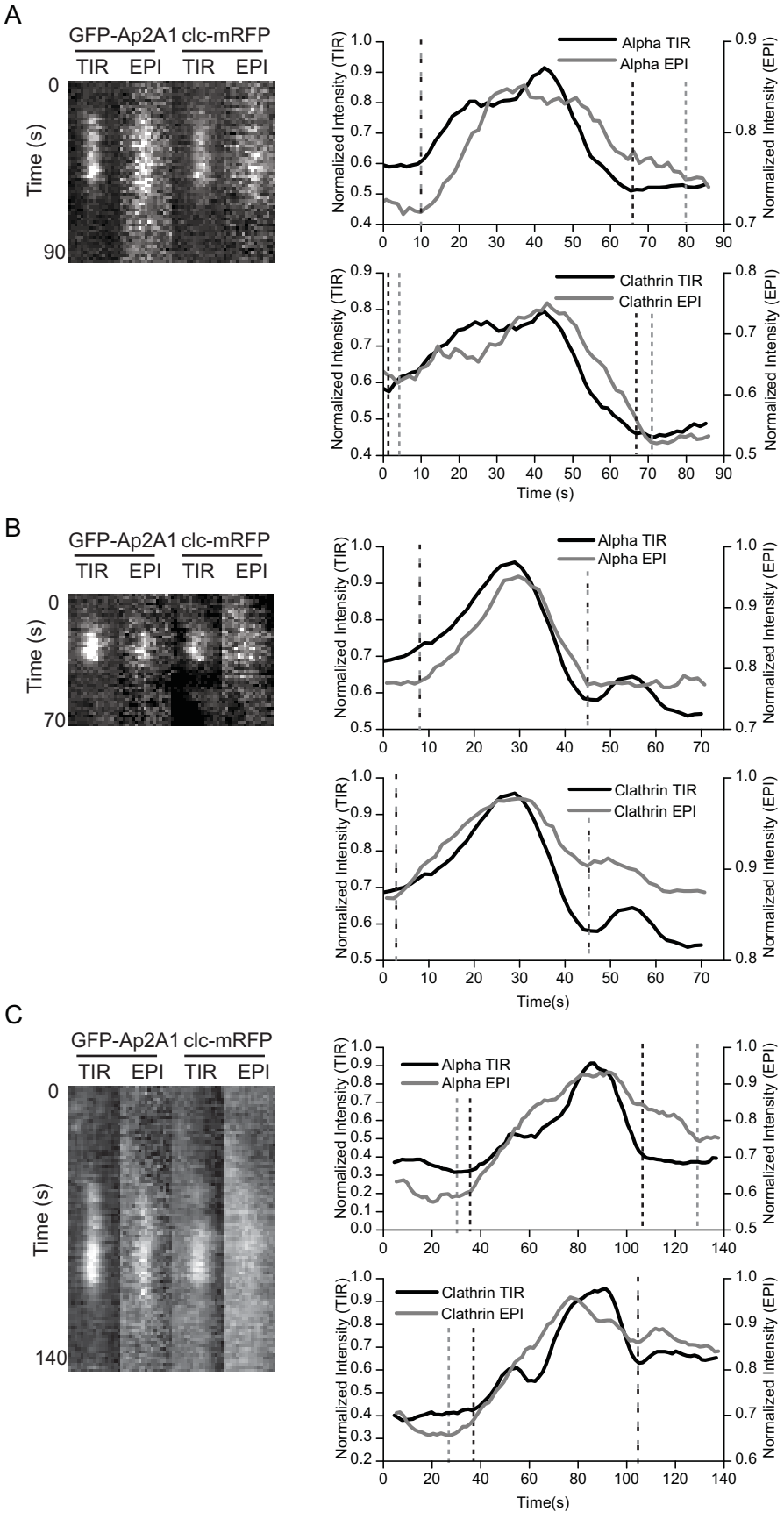
A
GFP-Ap2A1 clc-mRFP
TIR EPI TIR EPI
Time (s)
0
90
Alpha TIR
Alpha EPI
Clathrin TIR
Clathrin EPI
Normalized Intensity (TIR)
Normalized Intensity (EPI)
Time (s)
B
GFP-Ap2A1 clc-mRFP
TIR EPI TIR EPI
Time (s)
0
70
Alpha TIR
Alpha EPI
Clathrin TIR
Clathrin EPI
Normalized Intensity (TIR)
Normalized Intensity (EPI)
Time(s)
C
GFP-Ap2A1 clc-mRFP
TIR EPI TIR EPI
Time (s)
0
140
Alpha TIR
Alpha EPI
Clathrin TIR
Clathrin EPI
Normalized Intensity (TIR)
Normalized Intensity (EPI)
Time(s)

reported in mammalian cells (Mattheyses et al., 2011) therefore I classified this group as "possible endocytosis or uncoating".

A small percentage (12 ± 6% (mean ± SD)) of puncta had an EPI signal that appeared before the TIR signal and thus appear to be internal vesicles from the cytosol that enter the TIR field (Figure 17C) and not clathrin-coated vesicles formed *de novo* at the plasma membrane.

In 39 ± 18% (mean ± SD) of puncta the EPI signal was not bright enough to distinguish from the background fluorescence in the cytoplasm, hence their fate could not be classified. We expect that the behavior of these puncta will be equally distributed between the behaviors observed. If so, around 50% of AP-2 and clathrin puncta that disappear from the TIR field show behavior that corresponds to productive endocytic events. This number could be even higher if the "possible endocytosis or uncoating" population is included.

5.3 Summary

In *Dictyostelium,* clathrin and AP-2 co-localized in puncta and disappeared from the TIR-FM field together. I took advantage of the spatial selectivity of TIR-FM compared to wide-field illumination to image the internalization of clathrin-coated pits as they moved from the plasma membrane into the cell. When I imaged clathrin and AP-2 puncta using this technique I saw that a minimum of around 30% of disappearing puncta showed internalization behavior, with this proportion being possibly higher. Taken together, our results demonstrate that AP-2 and clathrin accumulate at clathrin-coated pits that disappear from the TIR-FM field corresponding to productive endocytic events.

CHAPTER 6 - Dajumin is internalized by clathrin-mediated endocytosis

The localization of AP-2 and clathrin on contractile vacuole bladders has been well documented, and was also observed in this work (Chapter 4) (Stavrou and O'Halloran, 2006; Wen et al., 2009). Phenotypes of clathrin and AP-2 knockouts have implied functions for clathrin and AP-2 in osmoregulation although their exact roles in the process are unclear. Furthermore, despite regular fusion of contractile vacuoles with the cell membrane, contractile vacuole proteins do not remain on the cell surface (Gabriel et al., 1999). Thus, we examined if clathrin-mediated endocytosis is involved in retrieval of the contractile vacuole proteins from the cell membrane.

6.1 Three-dimensional distribution of clathrin on the contractile vacuole

To study the contractile vacuole, dajumin-GFP was used as a marker. This protein is preferred because it labels both the bladders and tubules of the contractile vacuole network (Gabriel et al., 1999). Wild-type cells expressing dajumin-GFP and mRFP-clc were imaged by spinning disk confocal microscopy. The localization and dynamics of clathrin puncta on contractile vacuoles has been described previously and clathrin was reported to be on 47% of contractile vacuoles in transient association with bladders and tubules during all stages of the contractile vacuole cycle (Stavrou and O'Halloran, 2006).

In agreement with these previous studies, clathrin can be seen localized in puncta throughout the cytoplasm, on the plasma membrane and associated with bladders and tubules of the contractile vacuole (Fig 18A). A more detailed analysis of distribution of clathrin puncta on the contractile vacuole was then performed. Puncta could be seen in three different places; on bladders, at bladder/tubule junctions and behind the emptying

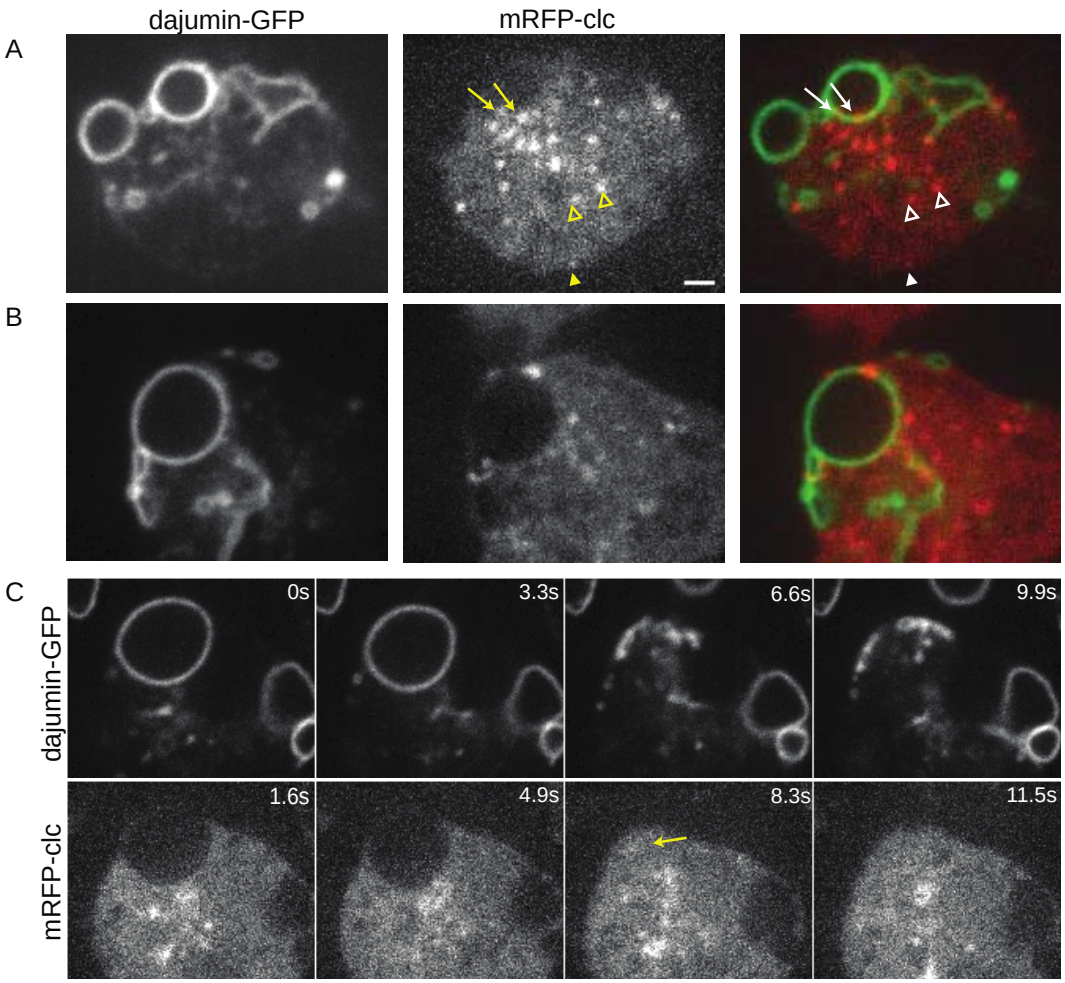

Figure 18 – Co-localization and dynamics of dajumin-GFP and clathrin

(A) Confocal section showing the intracellular localization of dajumin-GFP and mRFP-clc. Localization of clathrin puncta are indicated on a bladder of the contractile vacuole (arrows), in the cytoplasm (open triangle) and on the plasma membrane (filled triangle). Scale bar = 1μm. **(B)** Confocal section showing the localization of mRFP-clc on the bladders and tubules of the contractile vacuole and at the bladder/tubule interface. (C) Confocal section showing the localization of clathrin (arrow) closely behind an emptying of the contractile vacuole.

bladder (Figure 18B & C). The amount of time that clathrin puncta were seen in any of these locations was scored and showed that clathrin was localized on a bladder in 22 ± 10% of frames, was at a bladder/tubule junction in 38 ± 13% of frames and was behind an emptying bladder in 7 ± 5% of frames (mean ± SEM, n=7 cells). Clathrin could be scored as localized to a bladder, or to a bladder/tubule junction, in all frames since they were present at all times. Emptying bladders were only seen in 38 ± 9% of frames (mean ± SEM, n=7 cells) reducing the chance of clathrin being scored in his location. Taking this into account, localization of clathrin behind an emptying bladder was still only observed occasionally.

Contractile vacuoles were highly dynamic and could be seen filling and emptying along with rapid movements and morphological changes of the tubules. The clathrin puncta associated with the contractile vacuole were also highly dynamic. Analysis was performed to see if clathrin association was connected to the contractile vacuole cycle. In each frame, the stage of the contractile vacuole cycle (filling, filled or emptying) was assessed based on morphology of the bladder using the dajumin-GFP signal. Contractile vacuoles spent 35 ± 12% of frames filling, 27 ± 7% of frames filled and 38 ± 9% of frames emptying (mean ± SEM, n=7 cells). If clathrin puncta were associated with any part of the contractile vacuole this was scored as a positive localization. This analysis showed no clear association with contractile vacuole cycle in agreement with previous observations (Stavrou and O'Halloran, 2006). Clathrin was found on the contractile vacuole in 50 ± 17% of filling frames, in 79 ± 15% of filled frames and in 44 ± 15% of emptying frames (mean ± SEM, n=7 cells).

In order to establish the localization of clathrin on the contractile vacuole in three-dimensions the entire cell volume was imaged. This was performed in live cells since chemical fixation techniques cause vesiculation of the contractile vacuole (Fok et al., 1993; Zhu et al., 1993; Neuhaus et al., 1998). Whole cell volumes were imaged extremely fast (~5sec) to minimize artifacts that would occur from cell movement during the imaging time. Z-stacks were deconvolved and the dajumin-GFP and mRFP-clc signals reconstructed using Imaris software (Figure 19A-C). Clathrin puncta were often seen at sites where tubules and bladders joined but were also seen sitting on bladders or fully encompassing a tubule, correlating with the data from individual planes.

Analysis was performed using Imaris to create three-dimensional objects for both the clathrin and dajumin signals. For this analysis, a mask was created from the images of the individual planes using an edge detection filter followed by applying a threshold to include only the top 2% of pixels based on intensity. Examples of the masks generated are shown in Figure 19 A and B. These masks were then used to define the edges of the three-dimensional objects created in Imaris (Figure 19D). The percentage of objects that overlapped with each other was then calculated, an object was counted if any of its voxels also contained signal from the other channel. Figure 19D (left) shows all the dajumin objects overlaid with all clathrin objects, Figure 19D (right) shows only the clathrin objects that overlap with a dajumin object. This analysis showed that 26 ± 6% (mean ± SD, n=23 cells) of the clathrin objects within the cell overlapped with dajumin signal, these objects correspond to 68 ± 10% of the clathrin voxels. Conversely, 32 ± 8% of dajumin objects within the cell overlapped with clathrin signal, these objects correspond

Figure 19 – Three-dimensional localization of dajumin and clathrin

Wide-field microscopy images of **(A)** mRFP-clc and **(B)** dajumin-GFP in AX2 cells. Single focal planes from z-stacks are shown (top row) along with the corresponding segmentation mask (bottom row) used for three-dimensional analysis. Scale bar = 2μm. **(C)** Three-dimensional distribution of dajumin-GFP (green) and mRFP-clc (magenta). The deconvolved z-stacks shown in (A) and (B) were used to generate the images. Two different volume renderings are shown. Arrows show clathrin localized to bladders, tubules and bladder/tubule junctions. Scale bar = 1.5μm. **(D)** Three-dimensional analysis of dajumin-GFP and mRFP-clc. The segmentation masks shown in (A) and (B) were used to generate the images shown. Clathrin objects that did not overlap with a dajumin object were removed from the right-hand image. Scale bar = 1.5μm.

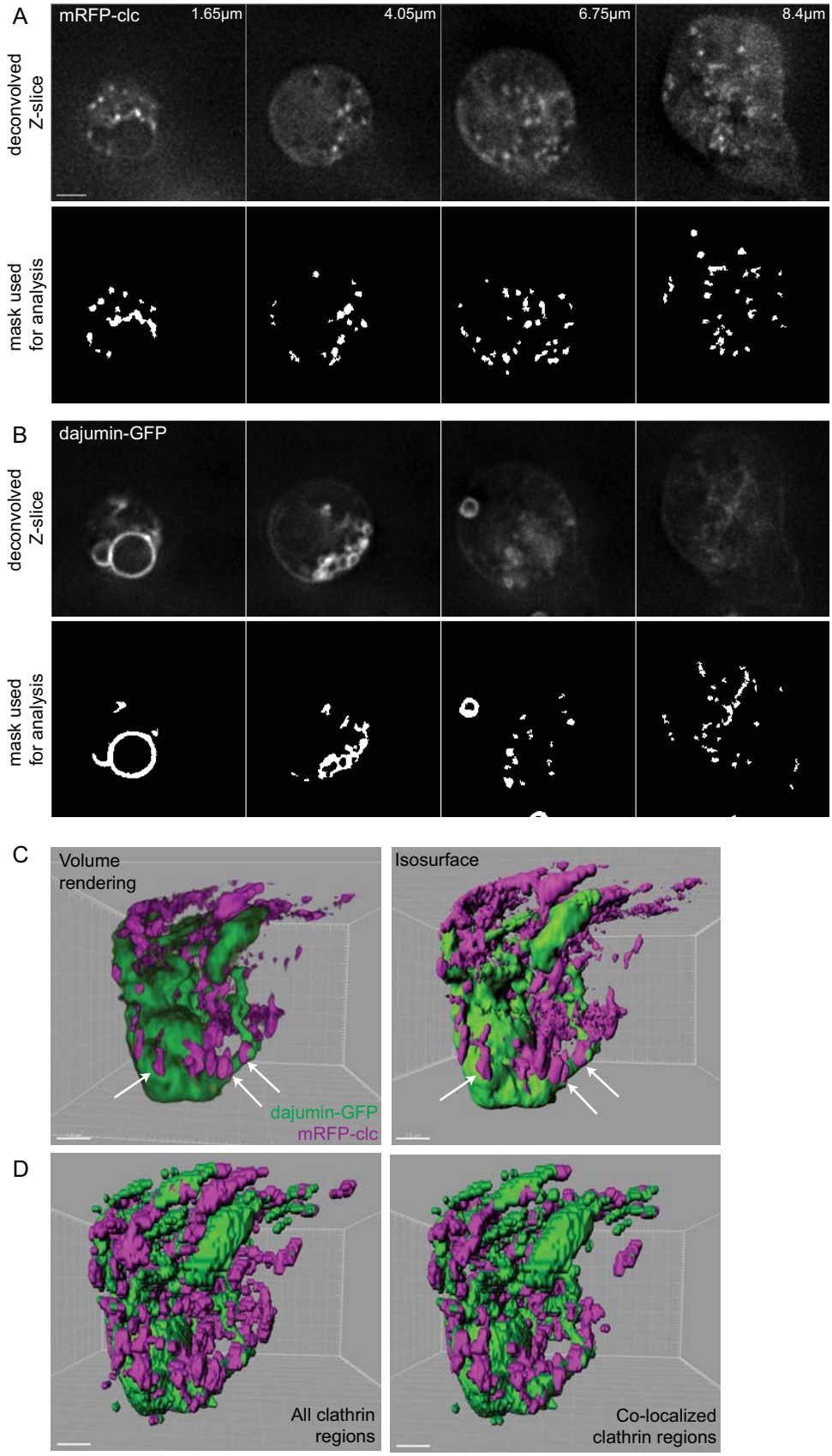
A
mRFP-clc
1.65µm
4.05µm
6.75µm
8.4µm
deconvolved Z-slice
mask used for analysis
B
dajumin-GFP
deconvolved Z-slice
mask used for analysis
C
Volume rendering
Isosurface
dajumin-GFP
mRFP-clc
D
All clathrin regions
Co-localized clathrin regions

to 85 ± 6% of the dajumin voxels, indicating that these objects included larger volume objects made up of the bladders.

Due to the highly dynamic nature of the contractile vacuole I wanted to analyze the clathrin puncta over time in three-dimensions. In order to allow sufficient time resolution z-stacks were acquired for only a 2μm section of the cell. Unfortunately, while the first few frames are informative and recapitulate the dynamics seen in individual planes, longer acquisition was prevented due to photobleaching of the mRFP-clc fluorescence (Figure 20).

6.2 TIR-FM analysis of clathrin and dajumin localization

During imaging of the three-dimensional distribution of the contractile vacuole, a dim dajumin-GFP signal was often seen on the plasma membrane (Figure 19B, 6.75μm slice). Plasma membrane localization of untagged dajumin was previously reported, but it was thought the addition of GFP altered this localization (Gabriel et al., 1999). It is probable that the localization of dajumin-GFP on the plasma membrane was not previously seen due to the overwhelming bright signal from the contractile vacuole. In order to evaluate the plasma membrane dajumin-GFP signal I imaged the dynamics of dajumin-GFP and mRFP-clc using TIR-FM. The contractile vacuole network preferentially sits near the surface attached to the coverslip thus the contractile vacuole can be seen as bright bladders and tubules close to the basal membrane (Gabriel et al., 1999). Closer inspection of the images revealed dajumin-GFP also localized to dim puncta that co-localized with mRFP-clc puncta (Figure 21A). Co-localization analysis showed that 40 ± 14% of mRFP-clc overlapped with dajumin-GFP and 22 ± 12% of

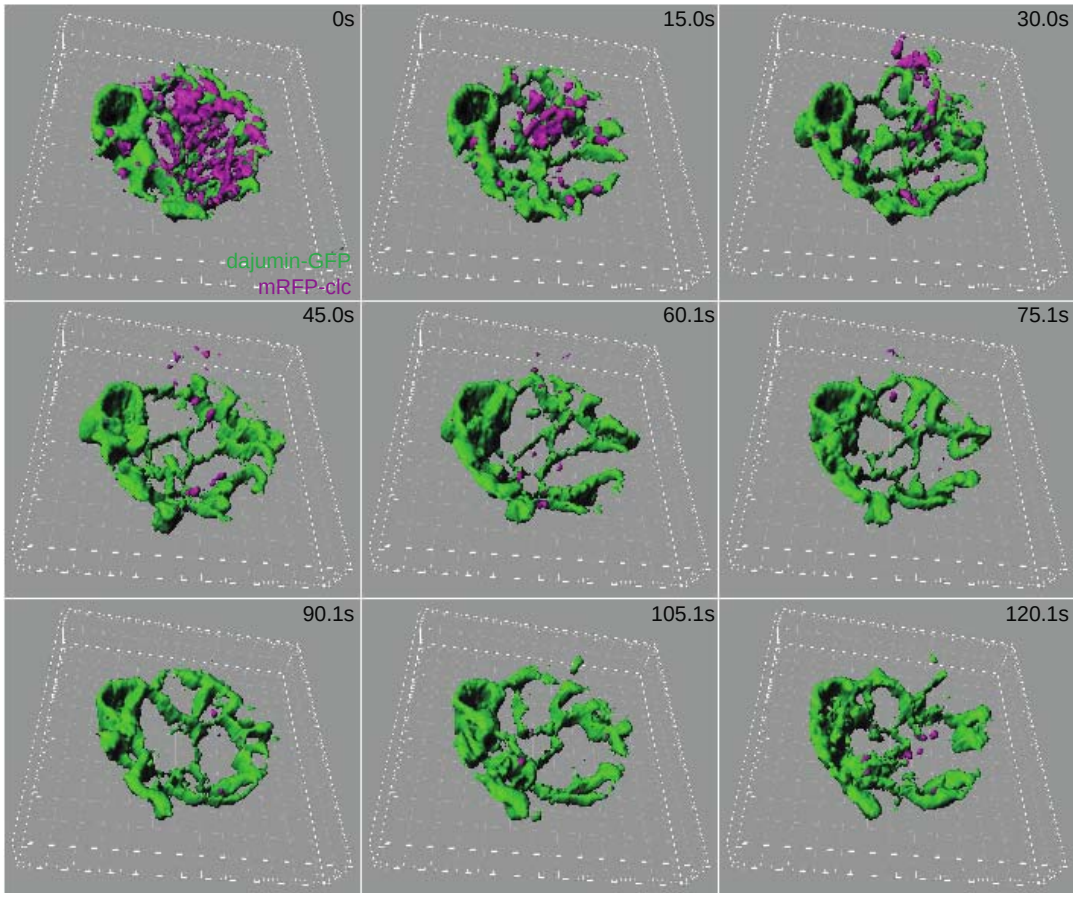

Figure 20 – Three-dimensional localization and dynamics of dajumin and clathrin

Three-dimensional distribution of dajumin-GFP (green) and mRFP-clc (magenta) over time. Deconvolved z-stacks of a 2µm section of the cell were used to generate the images.

Figure 21 - Co-localization and dynamics of dajumin-GFP and clathrin puncta

(A) & **(D)** Two-color TIR-FM images of (A) dajumin-GFP and mRFP-clc or (D) dajumin-GFP and mRFP-Ap2A1. The enlarged images allow visualization of dajumin-GFP puncta, intensities are rescaled. Scale bar = 1μm. **(B)** & **(E)** Quantification of co-localization between (B) dajumin-GFP and mRFP-clc or between (E) dajumin-GFP and mRFP-Ap2A1. Data is represented as mean ± SD ((B) n=25 cells, 2 experiments (E) n=45 cells, 2 experiments). **(C)** & **(F)** Pixel shift analysis of co-localization was performed on each cell. The graph shows the percentage overlap as a function of shifting the images one pixel to the left (negative numbers) or right (positive numbers). Data is represented as mean normalized percentage overlap ± SD. **(G)** Example of dynamics of an individual dajumin-GFP and mRFP-clc punctum imaged by TIR-FM. Scale bar = 0.5μm. **(H)** Normalized fluorescence intensity for the punctum shown in (G) is plotted as a function of time for dajumin-GFP (green, open circles) and mRFP-clc (red, filled circles). **(I)** Histogram of the time between mRFP-clc and dajumin-GFP disappearance from the TIR-FM field (n=47 puncta, 10 cells, 2 experiments).

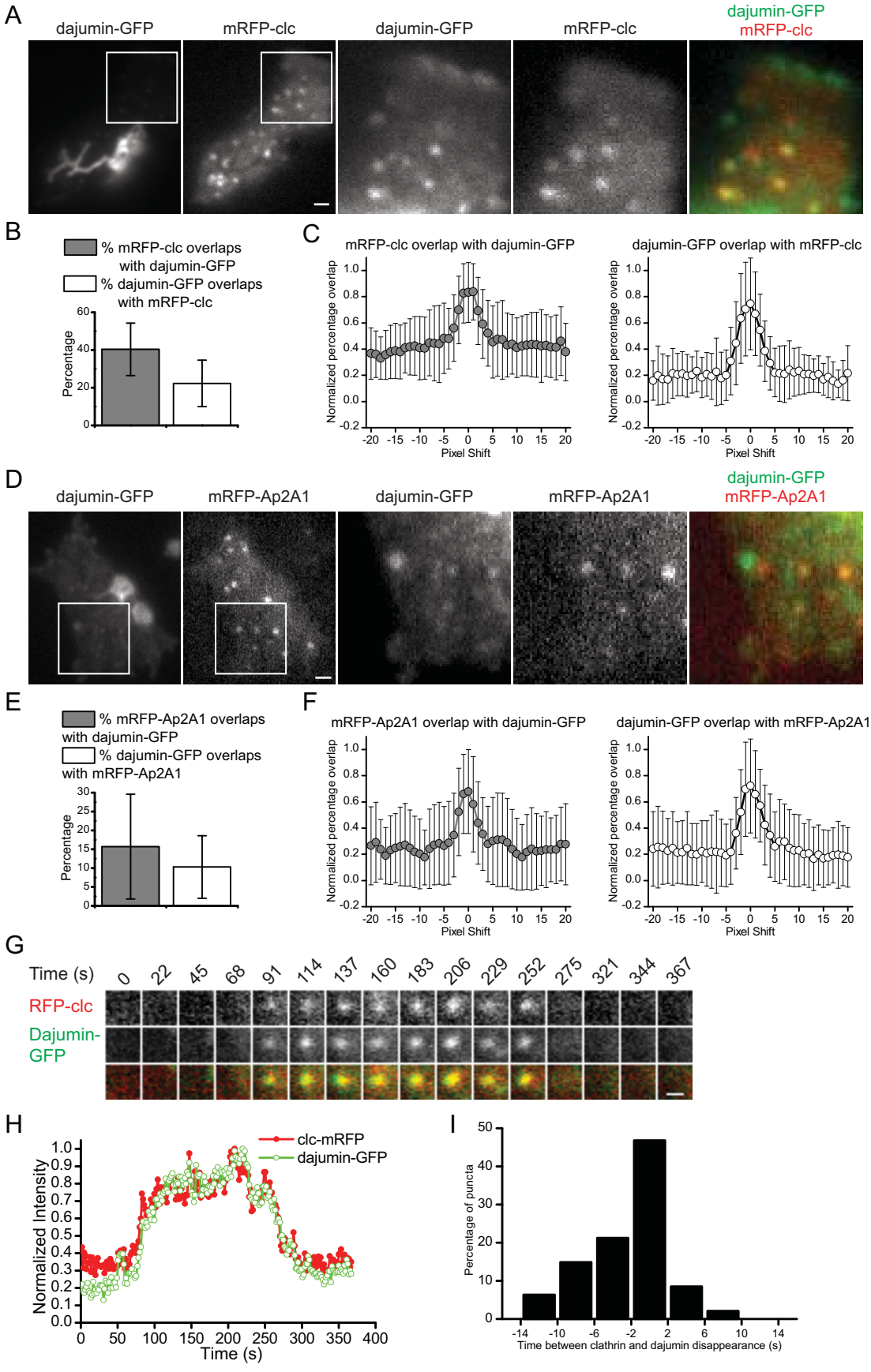
A
dajumin-GFP
mRFP-clc
dajumin-GFP
mRFP-clc
dajumin-GFP
mRFP-clc
B
% mRFP-clc overlaps with dajumin-GFP
% dajumin-GFP overlaps with mRFP-clc
Percentage
C
mRFP-clc overlap with dajumin-GFP
dajumin-GFP overlap with mRFP-clc
Normalized percentage overlap
Pixel Shift
D
dajumin-GFP
mRFP-Ap2A1
dajumin-GFP
mRFP-Ap2A1
dajumin-GFP
mRFP-Ap2A1
E
% mRFP-Ap2A1 overlaps with dajumin-GFP
% dajumin-GFP overlaps with mRFP-Ap2A1
Percentage
F
mRFP-Ap2A1 overlap with dajumin-GFP
dajumin-GFP overlap with mRFP-Ap2A1
Normalized percentage overlap
Pixel Shift
G
Time (s)
0 22 45 68 91 114 137 160 183 206 229 252 275 321 344 367
RFP-clc
Dajumin-GFP
H
clc-mRFP
dajumin-GFP
Normalized Intensity
Time (s)
I
Percentage of puncta
Time between clathrin and dajumin disappearance (s)

dajumin-GFP overlapped with mRFP-clc (mean ± SD, n=25 cells, 2 experiments) (Figure 21B). Co-localization was validated by performing a pixel shift analysis and showed the peak co-localization overlap was in the non-shifted image (dx=0) (Figure 21C). There was a high cell-to-cell variability in the percentage overlap since dim dajumin-GFP puncta were not always observed. Time-lapse imaging of dajumin-GFP showed that dim dajumin puncta can be seen in all cells but appear and disappear so are not necessarily present at all times. The co-localization of dajumin-GFP with clathrin-coated pits suggested it might also co-localize with AP-2. To perform this experiment an Ap2A1 tagged with mRFPmars (mRFP-Ap2A1) was generated and expressed in wild-type cells expressing dajumin-GFP. When imaged by TIR-FM, dajumin-GFP puncta that co-localized with mRFP-Ap2A1 puncta were observed (Figure 21D). Co-localization analysis showed 16 ± 14% of mRFP-Ap2A1 overlapped with dajumin-GFP and 10 ± 8% of dajumin-GFP overlapped with mRFP-Ap2A1 (mean ± SD, n=45 cells, 2 experiments). (Figure 21E). Again there was high cell-to-cell variability and co-localization was validated using pixel shift analysis (Figure 21F). The co-localization of this transmembrane protein with AP-2 and clathrin suggested it might be internalized in clathrin-coated vesicles.

To investigate the dynamics of dajumin-GFP puncta I used timelapse TIR-FM imaging of cells expressing dajumin-GFP and mRFP-clc (Figure 21G). Puncta were tracked over time and the fluorescence intensity was quantified (Figure 21H). Dajumin-GFP accumulated with clathrin followed by a rapid disappearance from the TIR field. The time of initiation of disappearance from the TIR field was calculated for both dajumin-GFP and mRFP-clc for each punctum (n=47 puncta, 10 cells, 2 experiments).

This analysis showed that 47% of dajumin-GFP puncta disappeared together with clathrin (<4s apart) (Figure 21I). The remaining 53% of dajumin-GFP puncta also disappeared from the TIR field but their time of disappearance was not simultaneous with the disappearance of clathrin (i.e. they disappeared before or after clathrin) (Figure 21I). Since the EPI-TIR assay in Chapter 5 showed that clathrin puncta that disappear from TIR move into the cell (Figure 17) this implies that dajumin-GFP is internalized from the plasma membrane of *Dictyostelium* via clathrin-mediated endocytosis.

6.3 Summary

Analysis of the localization of clathrin and the contractile vacuole have confirmed previous observations that clathrin puncta are localized to the contractile vacuole and have highly dynamic behavior. It appears that clathrin puncta are able to form on both the bladders and on the tubules of the contractile vacuole. Three-dimensional analysis of the localization revealed that at any one time clathrin puncta can be seen associated with 32.0% of the objects making up the contractile vacuole in the cell. This imaging also revealed the plasma membrane localization of dajumin-GFP, when imaged by TIR-FM dajumin-GFP was seen to form dim plasma membrane puncta that co-localized with clathrin and AP-2 puncta. Furthermore, dajumin-GFP puncta disappeared from TIR-FM coincident with clathrin puncta indicative of the behavior of an endocytic cargo.

CHAPTER 7 – Assaying endocytosis of dajumin with the pHluorin assay

As previously discussed, disappearance from the TIR-FM field does not necessarily correspond to endocytic events. I therefore sought to demonstrate internalization of dajumin-GFP from the plasma membrane in clathrin-coated vesicles. Initially I employed the EPI-TIR assay used in Chapter 5 to image dajumin-GFP and mRFP-clc puncta. Unfortunately the background signal in the dajumin-GFP channel was too high to allow any data to be collected thus I sought other methods to demonstrate internalization.

7.1 The pHluorin assay

One such method is the use of the pHluorin assay (Merrifield et al., 2005). In this technique the transmembrane protein of interest is tagged on its extracellular side with superecliptic pHluorin, a pH sensitive variant of GFP (Miesenböck et al., 1998). When the extracellular media is switched between pH5.8 and pH8.0, since the pHluorin is in contact with the media, the fluorescence emission switches between bright and dark states. Once the vesicle pinches off the membrane its contents are no longer in contact with the extracellular media and the pHluorin does not respond to the extracellular media changes. Since vesicles are pinched off at random half will be pinched in the bright state and can be observed as internalization events from the plasma membrane. This assay has been used extensively in the study of mammalian clathrin-mediated endocytosis (Merrifield et al., 2005; Mattheyses et al., 2011; Taylor et al., 2011).

7.2 Tagging dajumin with pHluorin

In order to perform the pHluorin assay it was necessary to tag dajumin on its extracellular domain. The sequence encoding pHluorin or superfolder-GFP (sfGFP) was placed between amino acids S247 and K248 (pH^{S247}-dajumin; $sfGFP^{S247}$-dajumin) or between amino acids L403 and S404 (pH^{L403}-dajumin; $sfGFP^{L403}$-dajumin) (Figure 22A) and expressed in wild-type cells. These sites were chosen by performing an online secondary structure prediction (PSIPRED; http://bioinf.cs.ucl.ac.uk/psipred/) and selecting unstructured regions for insertion of GFP. Unexpectedly, when cells were observed by wide-field microscopy, very little signal associated with the contractile vacuole or plasma membrane could be seen. Instead only dim signal associated with the ER was observed.

To test for the expression of the constructs western blots of cell lysates expressing dajumin-GFP were performed. These showed the full length protein (86.8kDa, runs at ~130kDa due to glycosylation) and two cleavage products (45kDa and 40kDa) are present in cells (Figure 22B). A C-terminal fragment of dajumin-GFP, and of a dajumin-contact site A (CSA) fusion protein, have both been reported previously (Barth et al., 1994; Gabriel et al., 1999). Western blot of cell lysates expressing pH^{S247}-dajumin, $sfGFP^{S247}$-dajumin, pH^{L403}-dajumin, or $sfGFP^{L403}$-dajumin revealed the full-length protein is expressed but cleavage products associated with the cell were no longer found. Western blot of media from these cells revealed that the extracellular portion of dajumin containing GFP is cleaved and released into the media (Figure 22B). It is difficult to interpret the fragment sizes due to the effects of glycosylation on the apparent molecular weight of the fragments. These results explain the lack of fluorescence signal associated

Figure 22 – Extracellular tagging of dajumin

(A) Schematic of constructs generated showing the positions where pHluorin or sfGFP was inserted. **(B)** Western blot for GFP in cell lysates and conditioned media from cells expressing the different dajumin constructs as indicated.

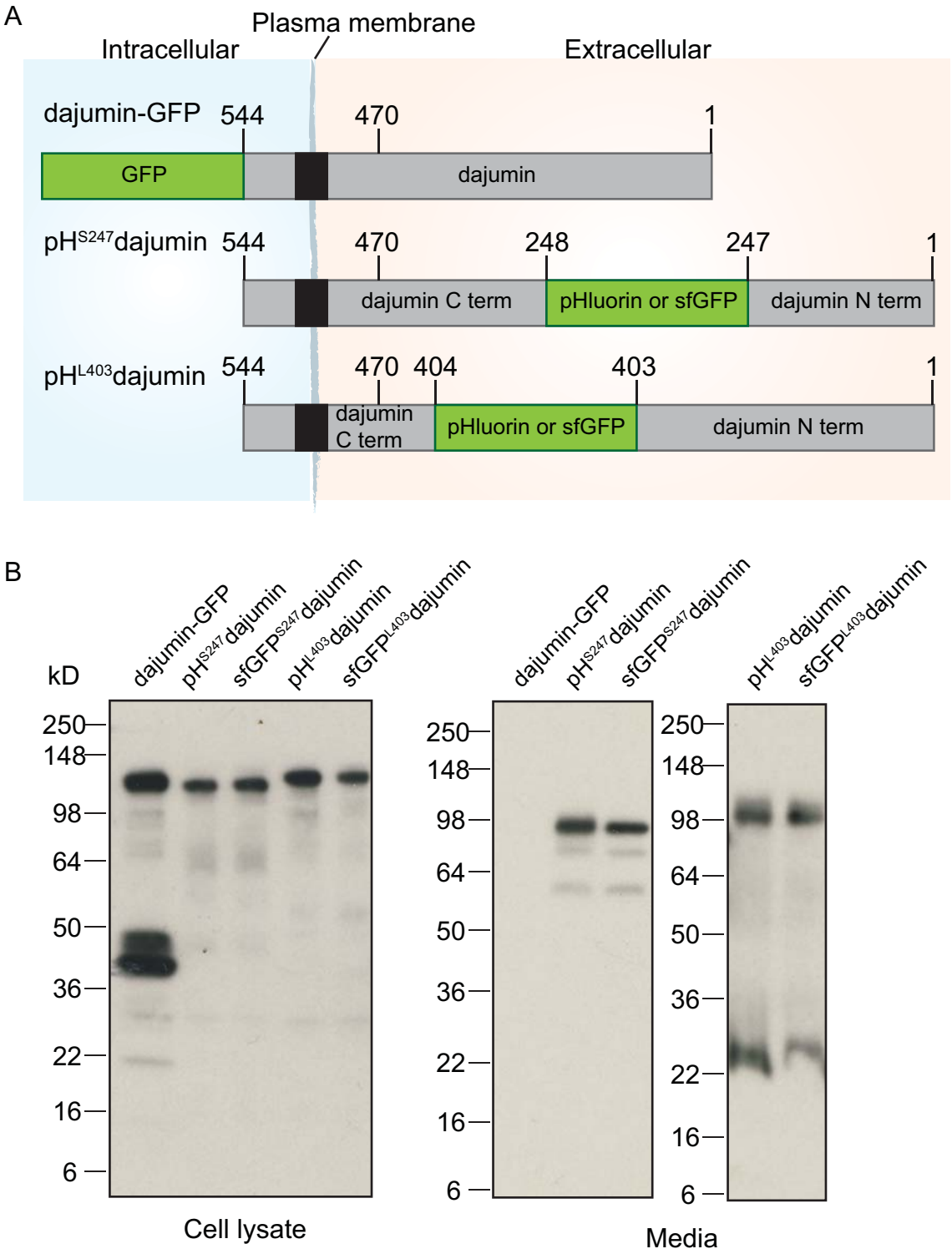
A
Plasma membrane
Intracellular
Extracellular
dajumin-GFP
544
470
1
GFP
dajumin
pHS247dajumin
544
470
248
247
1
dajumin C term
pHluorin or sfGFP
dajumin N term
pHL403dajumin
544
470
404
403
1
dajumin C term
pHluorin or sfGFP
dajumin N term
B
kD
dajumin-GFP
pHS247dajumin
sfGFPS247dajumin
pHL403dajumin
sfGFPL403dajumin
250
148
98
64
50
36
22
16
6
Cell lysate
Media

with the cell. Only GFP signal in the ER, presumably from dajumin biosynthesis before loss of GFP in the media, can be seen.

In an attempt to remove the cleavage site from dajumin I generated several constructs in which a short C-terminal region of dajumin was fused with pHluorin (pH-dajC$^{A470\text{-}T544}$) or with pHluorin and the N-terminus of dajumin (pH^{L403}dajC$^{A470\text{-}T544}$) (Figure 23A). This region (A470-T544) has been used in other chimeric proteins in *Dictyostelium* to serve as a transmembrane domain (Barth et al., 1994; Mercanti et al., 2006a). I also added the mRFP sequence to the C-terminus of these constructs in order to be able to follow the C-terminal fragment (Figure 23A). Western blot showed these constructs were cleaved extracellularly similar to the constructs already shown (data not shown). Microscopy of these cells demonstrated this cleavage; mRFP signal could be seen associated with the contractile vacuole, while GFP fluorescence was dim and could be seen only in the ER as diffuse tubular staining throughout the cytoplasm and perinuclear region (Figure 23B). This localization was the same for both constructs regardless of whether the dajumin N-terminus was present. Tagging of dajumin with multiple fluorescent proteins could render the protein dysfunctional and therefore influence the interpretation of results. However, the results from the double-labeled dajumin agreed with the data for dajumin labeled only with GFP. The results suggest that dajumin-GFP is cleaved before it reaches the contractile vacuole since no GFP fluorescence was observed either in the lumen on the contractile vacuole or associated with the membrane. Since antibodies are not available to endogenous dajumin it was not possible to establish if dajumin-GFP cleavage and localization was caused by addition of the GFP tag.

Figure 23 – Extracellular tagging of dajumin

(A) Schematic of constructs generated showing the positions where pHluorin or mRFP was inserted. (B) Wide-field microscopy images of wild-type cells expressing pH-dajC$^{A470\text{-}T544}$mRFP or pH^{L403}dajC$^{A470\text{-}T544}$mRFP. The signal from the GFP and RFP channels are shown along with an overlay. Scale bar = 1μm.

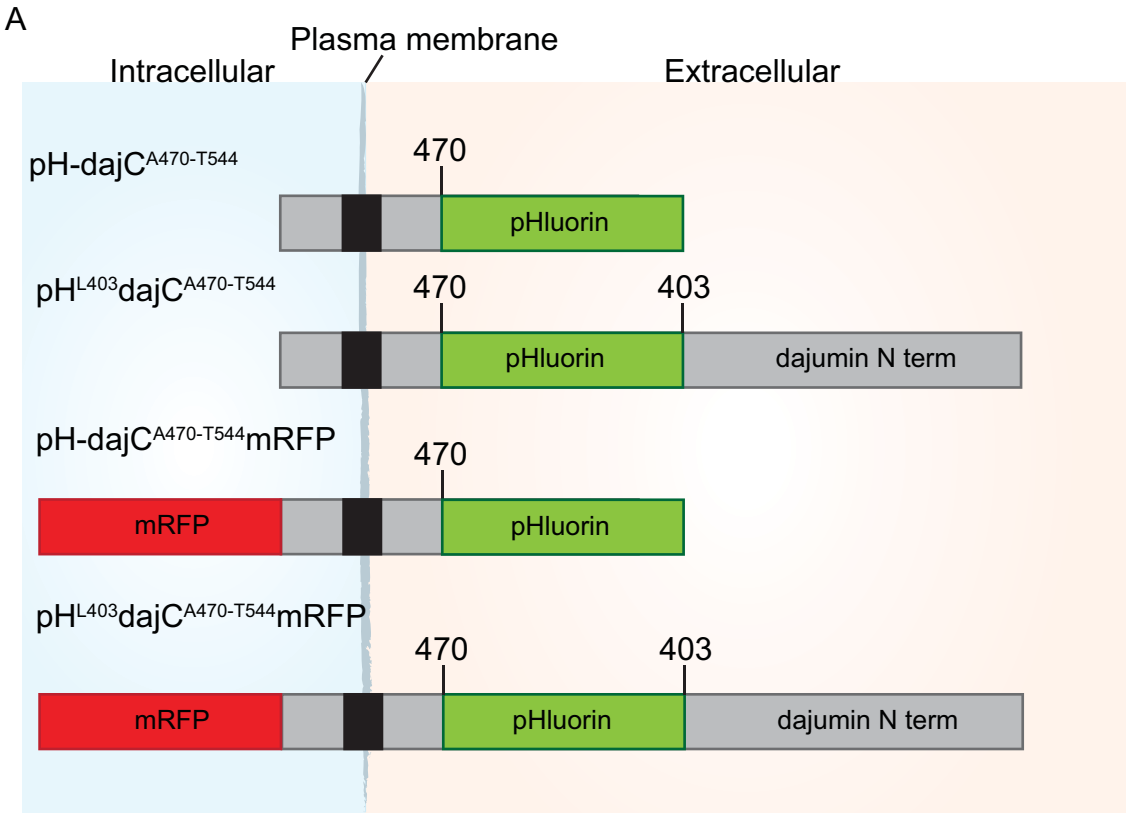
A
Plasma membrane
Intracellular
Extracellular
pH-dajC^A470-T544
470
pHluorin
pH^L403dajC^A470-T544
470
403
pHluorin
dajumin N term
pH-dajC^A470-T544mRFP
470
mRFP
pHluorin
pH^L403dajC^A470-T544mRFP
470
403
mRFP
pHluorin
dajumin N term

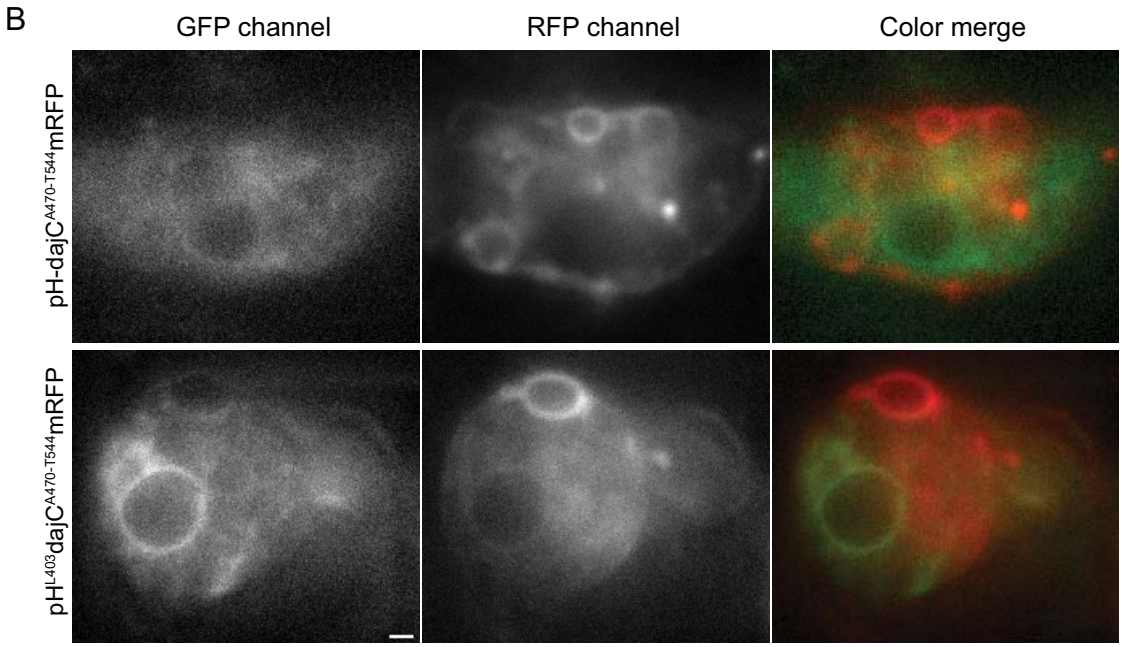
B
GFP channel
RFP channel
Color merge
pH-dajC^A470-T544mRFP
pH^L403dajC^A470-T544mRFP

In order to attempt to mutate or prevent the cleavage of dajumin it was necessary to know the exact cleavage site. The location of the dajumin cleavage site was therefore further investigated using LC-MS/MS mass spectrometry. Lysates from cells expressing dajumin-GFP were incubated with an anti-GFP antibody and the immunoprecipitated proteins were separated by SDS-PAGE (Figure 24A). Bands corresponding to the four dajumin-GFP cleavage products seen by western blot were sent for analysis by LC-MS/MS. Peptides from each band were mapped onto the dajumin protein sequence and are represented in Figure 22B. No peptides mapped to the first twenty amino acids indicating that this is a signal sequence, as predicted, and is removed from the protein during synthesis. Peptide mapping shows the protein in band A represents full length dajumin as expected. The protein in band D appears to be GFP that is cleaved from dajumin-GFP as only peptides matching the GFP sequence were observed. This band is a minor portion of the cleaved protein as seen by the western blot (Figure 22A). The proteins in bands B and C both represent cleaved versions of dajumin-GFP. The protein in band C appeared to only have significant peptide matches in the intracellular portion of dajumin-GFP. The protein in band B did have peptides that mapped onto the extracellular portion of dajumin-GFP but due to a lack of fragmented peptides generated in the transmembrane region of the protein it was not possible to precisely locate the cleavage sites.

Figure 24 – Mass spectrometry analysis of dajumin fragments

(A) Coomassie stained SDS-PAGE gel of proteins immunoprecipitated with anti-GFP antibodies from wild-type cells expressing dajumin-GFP. Bands excised and sent for mass spectrometry analysis are labeled A-D. Western blot for GFP of the immunoprecipitated proteins is also shown (right). **(B)** Representation of LC-MS/MS data. The number of peptide hits relative to their position within the dajumin-GFP sequence is shown. The positions of different domains in the dajumin molecule are shown with dashed lines.

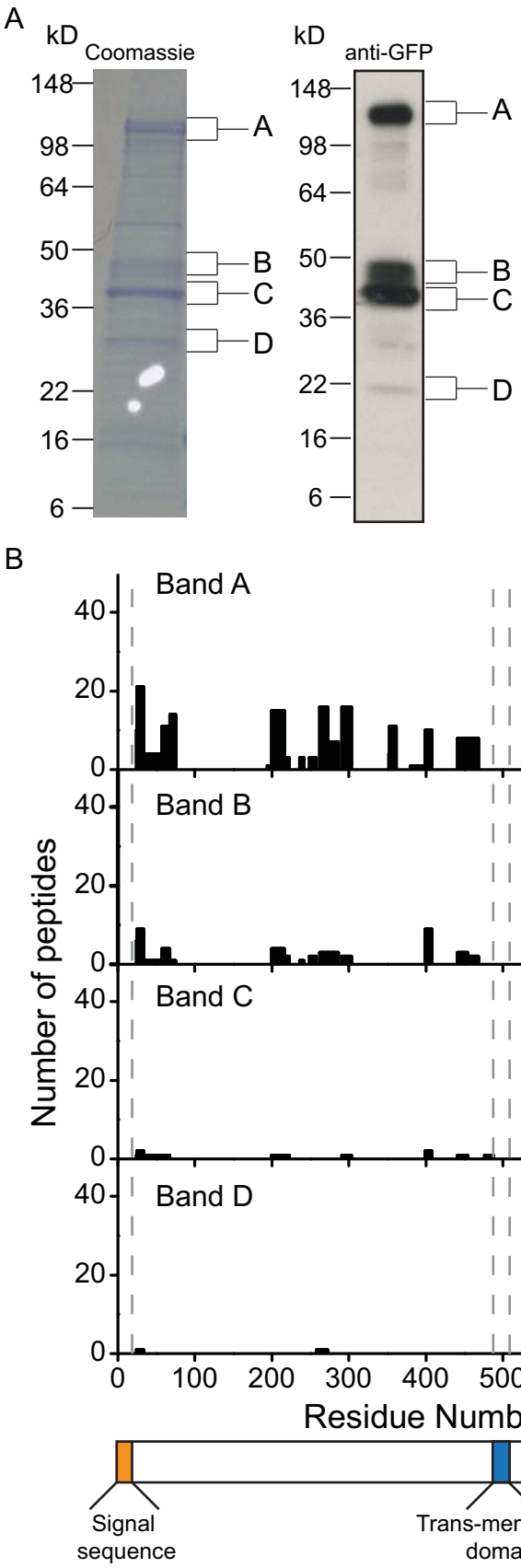
A
kD
Coomassie
148
98
64
50
36
22
16
6
A
B
C
D
kD
anti-GFP
148
98
64
50
36
22
16
6
A
B
C
D
B
Band A
Band B
Band C
Band D
Number of peptides
40
20
0
0
100
200
300
400
500
600
700
Residue Number
GFP
Signal sequence
Trans-membrane domain

7.3 Summary

Attempts at extracellular tagging of dajumin have revealed that the protein is present as a C-terminal fragment within cells. The full length protein is also present in cells but can only be seen localized to the ER, presumably where it is synthesized, suggesting dajumin-GFP is cleaved before it reaches the contractile vacuole. Tagging of the C-terminus of dajumin with mRFP and the N-terminus with GFP has revealed that the C-terminal fragment is associated with the contractile vacuole. Mass spectrometry analysis of dajumin fragments confirmed the western blot results and showed dajumin is likely cleaved at multiple sites. This cleavage may be in the extracellular domain very close to the transmembrane domain or within the transmembrane domain itself. These results have hindered execution of the pHluorin assay, which is dependent on having an extracellular tagged form of dajumin.

CHAPTER 8 - Assaying endocytosis of dajumin with the biotin internalization assay

Since extracellular tagging of dajumin was not successful, internalization of dajumin-GFP from the plasma membrane was confirmed using a modified version of the biotin internalization assay (Barth et al., 1994).

8.1 Biotin internalization assay

Plasma membrane proteins of wild-type cells expressing dajumin-GFP were reversibly biotinylated with the membrane impermeable biotin sulfo-NHS-SS-biotin. Immunoprecipitation of dajumin-GFP from cell lysates, followed by SDS-PAGE and western blot analysis with streptavidin-HRP showed that dajumin-GFP is biotinylated and thus present on the plasma membrane. Only the full-length protein and the 45kDa fragment were biotinylated, the 40kDa fragment is either not on the plasma membrane or does not have extracellular amino groups accessible to the biotinylation reagent (Figure 25A, Lane 1). This data agrees with the mass spectrometry results from Chapter 7 that indicated the 40kDa band is cleaved at or within the transmembrane domain. By microscopy it was not possible to detect the full-length protein on the cell surface (Chapter 7). Sulfo-NHS-SS-biotin primarily attaches to lysine residues therefore the degree of biotinylation of the fragments is a factor of the number of lysine residues. Full-length dajumin has 38 extracellular lysines and the 45kDa fragment has approximately 8. Thus, the signal seen for each fragment not only represents the amount of protein but is also heavily influenced by the number of lysines present and biotins attached. It is possible there is a small amount of full-length dajumin on the cell surface that is below the detection limit of the microscope but could be detected in this more sensitive

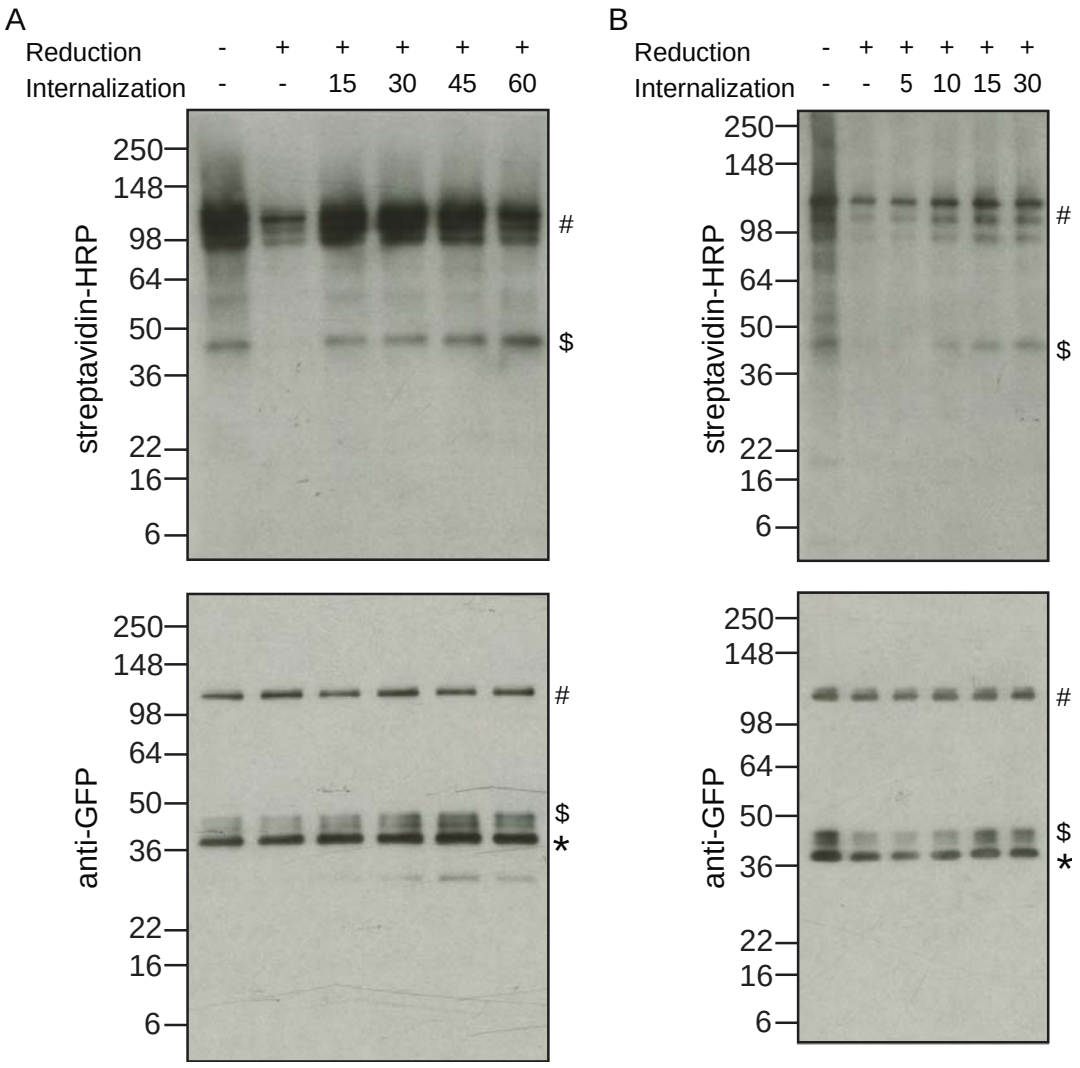

Figure 25 – Time-course of biotinylated dajumin-GFP internalization

(A) Biotin internalization assay for dajumin-GFP in wild-type cells. Dajumin-GFP was immunoprecipitated from cell lysates following cell-surface biotinylation and internalization for various times as indicated (time in min). Control samples that did not undergo internalization or cell-surface reduction are also shown. Membranes were probed for biotin with streptavidin-HRP (top) or for GFP with an anti-GFP antibody (bottom). Dajumin-GFP full length protein (#), the 45kDa fragment ($) and the 40kDa fragment (*) are indicated. **(B)** The biotin internalization assay shown in (A) was repeated with shorter internalization times as indicated.

biotinylation assay.

I next followed the fate of cell surface dajumin-GFP by allowing the cells to internalize proteins for various times (15, 30, 45 and 60 minutes) by incubation at 22°C. After internalization, any residual cell surface biotin was removed by incubation with the membrane impermeable reducing agent glutathione. In control cells that did not undergo an internalization step it was not possible to fully remove all of the biotin from dajumin-GFP (Figure 25A, Lane 2), it is likely that this represents a low level of internalization that still occurs at 4°C. The amount of biotinylated dajumin-GFP was however increased above this background level following the internalization step at 22°C demonstrating endocytosis from the cell surface. Both full-length and the 45kDa fragment were internalized within 15 minutes with little increase seen with the longer incubations (Figure 25A).

To probe the kinetics of dajumin-GFP internalization the biotin internalization experiment was repeated with shorter internalization times (5, 10, 15 and 30 minutes). Figure 25B shows the internalization of dajumin-GFP can be detected after 10 minutes of internalization and reaches its maximum by 15 minutes. For further experiments 15 minutes of internalization was used.

8.2 Biotin internalization in knockout cell lines

I assessed the requirement of clathrin and AP-2 for internalization by expressing dajumin-GFP in *Ap2A1-*, *apm2-*, *clc-* and *chcA*-cells. Again, in wild-type (AX2) cells both full length and the 45kDa fragment are biotinylated only in the presence of sulfo-NHS-SS-biotin. Both long and short exposures of the biotin signal are shown to enable

visualization of the 45kDa fragment. As seen in Figure 25, the amount of biotinylation increases above background following the 15 minute internalization step (Figure 1A). Quantification of the blots is shown, normalized to the GFP signal for each lane. In *Ap2A1-*, *apm2*- and *clc*- cells the amount of biotinylated dajumin-GFP also increased following the internalization step showing plasma membrane dajumin-GFP was internalized similar to wild-type cells (Figure 26A-D). By contrast, in *chcA*- cells dajumin-GFP was biotinylated and therefore on the plasma membrane but no internalization was ever observed (Figure 26E).

8.3 Localization of dajumin-GFP in knockout cell lines

These results were confirmed by imaging the localization of dajumin-GFP in the various cell lines (Figure 27A). Deconvolution of z-stacks showed in wild-type, *Ap2A1-*, *apm2*- and *clc*- cells the predominant localization of dajumin-GFP is to bright contractile vacuoles. Plasma membrane localization of dajumin-GFP can also be seen on individual focal planes. In contrast, dajumin-GFP was predominantly localized to the plasma membrane in *chcA*- cells. In agreement with previous reports we observed no contractile vacuoles (O'Halloran and Anderson, 1992). The absence of contractile vacuoles in *chcA*- cells was confirmed by staining with the lipophilic dye FM4-64 (Heuser et al., 1993) and with an antibody to the vacuolar proton pump (*VatM*) (Fok et al., 1993) (Figure 27B & C). In *chcA*- cells some internal dajumin-GFP positive structures could be seen, however these did not co-localize with a fluid-phase endocytic marker or a lysosomal marker (10kDa TxR-dextran; Lysotracker DND Blue; Figure 28A & B) and may represent a

Figure 26 - Internalization of biotinylated dajumin-GFP in wild-type and knockout cells

Biotin internalization assay for **(A)** AX2, **(B)** *Ap2A1*-, **(C)** *apm2*-, **(D)** *clc*- and **(E)** *chcA*- cells is shown. Dajumin-GFP was immunoprecipitated from cell lysates following cell-surface biotinylation and internalization for 15min. Control samples that did not undergo biotinylation, internalization or cell-surface reduction are also shown. Membranes were probed for biotin with streptavidin-HRP (top row, short and long exposures shown) or for GFP with an anti-GFP antibody (bottom row). Dajumin-GFP full length protein (#), the 45kDa fragment ($) and the 40kDa fragment (*) are indicated. Bar graphs show quantification of the streptavidin-HRP signal normalized to the GFP signal for each lane.

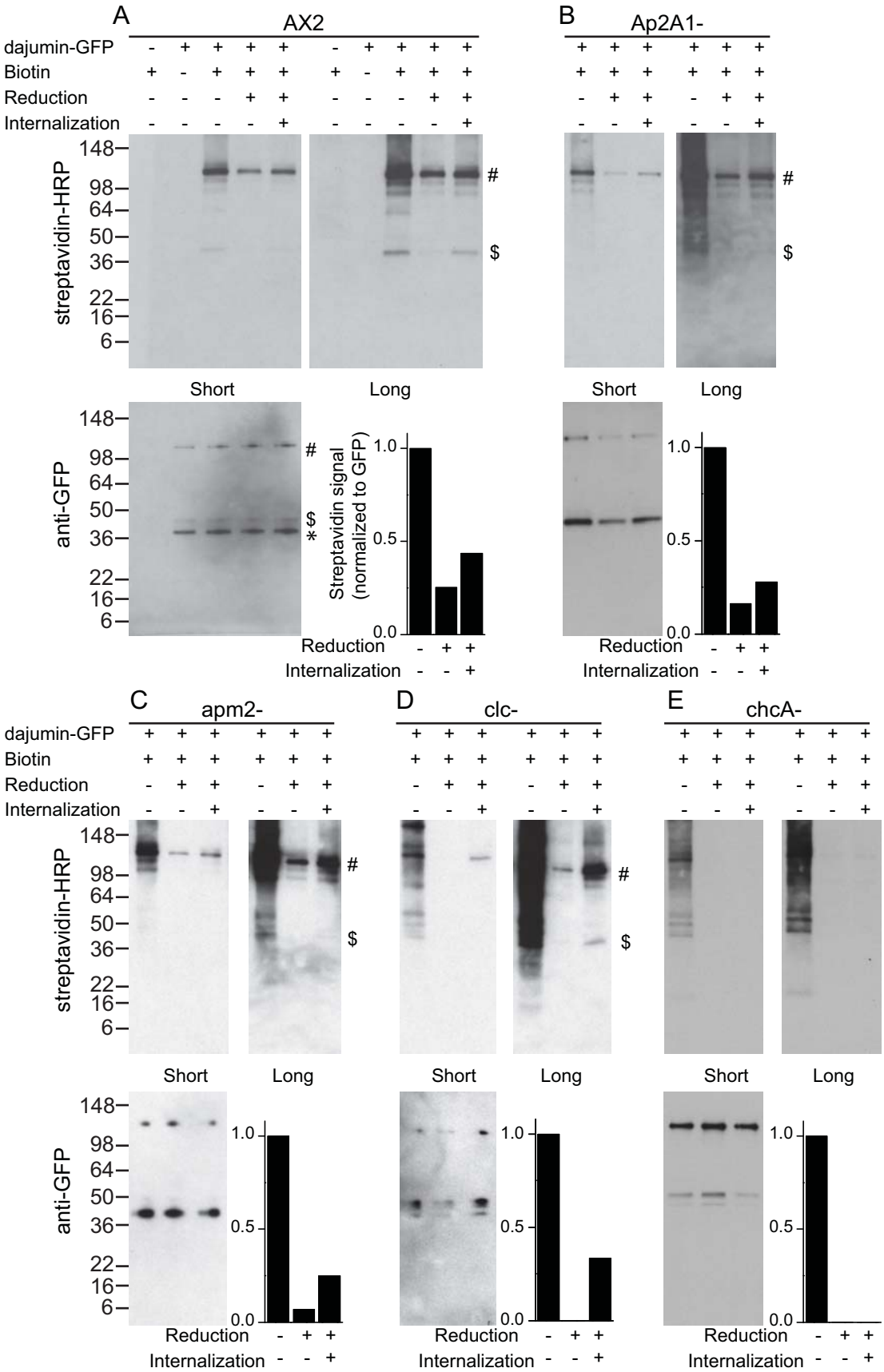
A
AX2
B
Ap2A1-
dajumin-GFP
Biotin
Reduction
Internalization
streptavidin-HRP
anti-GFP
148
98
64
50
36
22
16
6
#
$
*
Short
Long
Streptavidin signal (normalized to GFP)
1.0
0.5
0.0
C
apm2-
D
clc-
E
chcA-

Figure 27 – Localization of dajumin-GFP, VatM and FM4-64 in wild-type and knockout cells

(A) Wide-field microscopy images of dajumin-GFP in AX2, *Ap2A1-*, *apm2-*, *clc-* and *chcA-* cells. A single focal plane (top row) and a maximum intensity projection of the entire cell (bottom row) are shown. **(B)** Wide-field microscopy images of FM4-64 labeling in AX2, *Ap2A1-*, *apm2-*, *clc-* and *chcA-* cells and corresponding DIC images. **(C)** Maximum intensity projection of VatM immunostaining in AX2, *Ap2A1-*, *apm2-*, *clc-* and *chcA-* cells. Scale bars = 1μm.

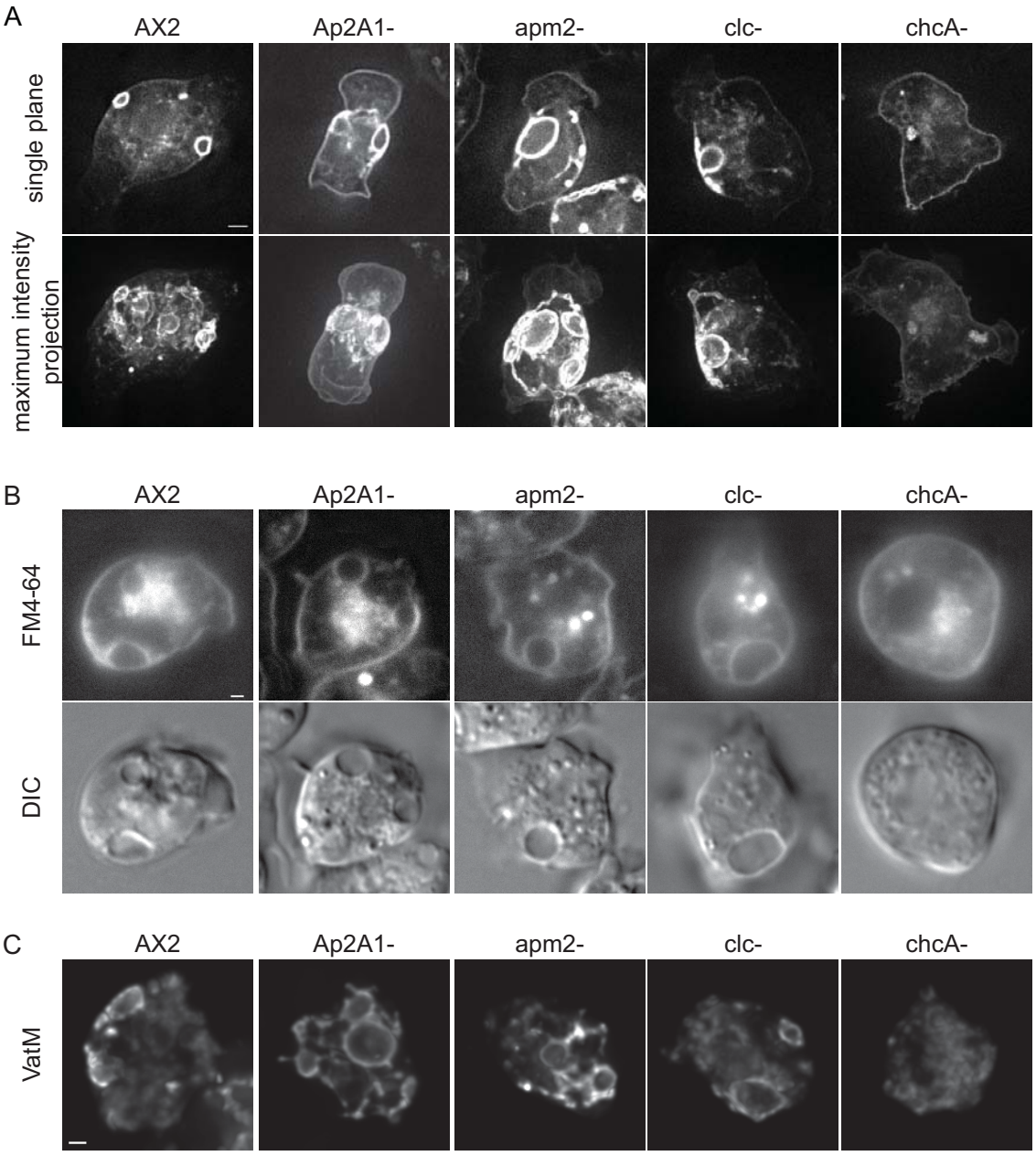
A
AX2
Ap2A1-
apm2-
clc-
chcA-
single plane
maximum intensity projection
B
AX2
Ap2A1-
apm2-
clc-
chcA-
FM4-64
DIC
C
AX2
Ap2A1-
apm2-
clc-
chcA-
VatM

Figure 28 – Localization of dajumin-GFP with macropinosomes and lysosomes in wild-type and knockout cells

Wide-field microscopy images of dajumin-GFP in AX2, *apm2*-, *clc*- and *chcA*- cells with **(A)** macropinosomes (labeled with 10kDa dextran-TxR) or, **(B)** lysosomes (labeled with Lysotracker DND Blue). A single focal plane for each channel and a color overlay is shown. Scale bars = 1μm.

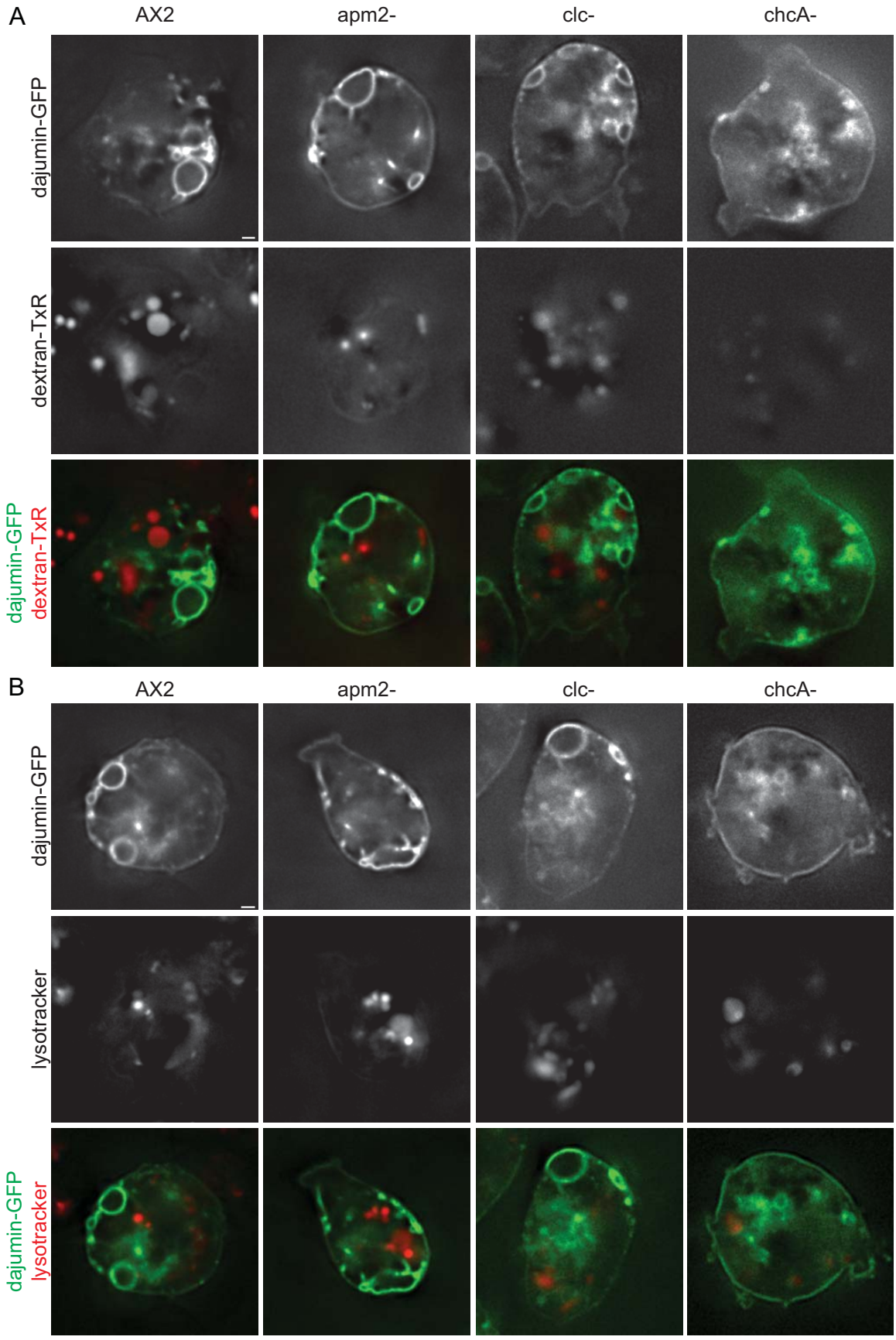
A
AX2
apm2-
clc-
chcA-
dajumin-GFP
dextran-TxR
dajumin-GFP
dextran-TxR
B
AX2
apm2-
clc-
chcA-
dajumin-GFP
lysotracker
dajumin-GFP
lysotracker

rudimentary contractile vacuole that has not fused with the plasma membrane or compartments where dajumin-GFP is synthesized.

8.4 Summary

The biotin internalization assay demonstrated that the full-length and the 45kDa fragment of dajumin-GFP are present on the plasma membrane of cells and are internalized from the cell surface within 10-15 minutes. Internalization does not appear to be affected in AP-2 knockouts or in *clc*- knockouts, however internalization of dajumin is fully dependent on the presence of chcA. Microscopy of the localization of dajumin-GFP showed it does not co-localize with markers of the macropinocytic pathway, which is also dependent on the presence of chcA. These results confirm the finding in Chapter 6 that dajumin-GFP localized to clathrin-coated pits and is internalized by clathrin-mediated endocytosis. Furthermore, microscopy of dajumin-GFP in AP-2 and clathrin knockouts showed that in *chcA*- cells dajumin-GFP is trapped on the plasma membrane in line with this hypothesis and explaining the contractile vacuole defect seen in clathrin knockouts.

CHAPTER 9 – Discussion

The formation of clathrin-coated vesicles is characterized by the successive binding of various proteins. Studies in yeast and mammalian cells have led to significant advances in understanding the spatiotemporal events that take place during clathrin-mediated endocytosis. The general mechanisms and proteins involved in vesicle formation appear to have been conserved across evolution. There are, however, sufficient differences between the two systems to question whether either the yeast or mammalian model can be generalized to all clathrin-mediated endocytosis. For this reason I set out to characterize the spatiotemporal properties of clathrin-mediated endocytosis in the unicellular eukaryote *Dictyostelium discoideum*.

9.1 The AP-2 complex in *Dictyostelium*

The adaptor complex AP-2 acts as a central player in the process of clathrin-mediated endocytosis by binding to clathrin, many other accessory proteins and to cargo (McMahon and Boucrot, 2011). The results presented in this thesis show that an AP-2 complex exists in *Dictyostelium* that localizes to internalizing clathrin-coated pits on the plasma membrane. This AP-2 complex in *Dictyostelium* is homologous to the one present in yeast and mammals in its subunit composition. Furthermore, I was able to develop a tool, the GFP tagged α subunit of AP-2, to specifically visualize and follow the AP-2 complex in living cells. Interestingly, *Dictyostelium* only has one gene that has equal homology to the mammalian β1 of AP-1 and β2 of AP-2. My data confirm the gene *Ap1B1* functions as the β subunit of the AP-2 complex in *Dictyostelium* as previously reported (Sosa et al., 2012). Since the AP-1 complex has been shown to localize to the

Golgi (Lefkir et al., 2003), and I have shown that AP-2 functions at the plasma membrane, my data suggest that membrane specificity of the AP complexes is not conferred by the β subunit. This is consistent with studies of mammalian AP complexes that showed β subunits primarily function in clathrin binding rather than membrane specificity (Page and Robinson, 1995; Shih et al., 1995). Phylogenetic studies have shown that a β-subunit common to AP-1 and AP-2 was present in the last eukaryotic common ancestor (Dacks et al., 2008). Similar to *Dictyostelium*, β subunits are also shared between AP-1 and AP-2 in *Drosophila* and *C.elegans* (Boehm and Bonifacino, 2002). The presence of separate β subunits in animals and yeast is believed to be the result of gene duplications in these lineages and resulting parallel evolution (Dacks et al., 2008).

Co-immunoprecipitation experiments with GFP-Ap2A1 revealed that in *Dictyostelium,* the binding partners of the AP-2 complex are also conserved. Although these binding partners were not validated in this thesis, these data suggest that the endocytic interaction network is also conserved in *Dictyostelium* and AP-2 may act as a central organizer for endocytosis, as suggested for mammalian cells (Praefcke et al., 2004). Proteins of interest include one of the *Dictyostelium* homologs of dynamin (dymA), esp15, chcA and clc. A subunit of the COPII coat (sec23) and other intracellular trafficking proteins were also identified (sec61g, Vps13B). These proteins would not normally be expected to bind AP-2 and their interactions may be due to the presence of the AP-1/AP-2 shared β subunit. The identification of the SNARE recycling protein nsfA is also of interest, especially as AP-2 has been implicated in sorting of the v-SNARE VAMP7 in *Dictyostelium*.

9.2 Clathrin-mediated endocytosis exists in *Dictyostelium*

The previous results demonstrated biochemical interactions between clathrin and AP-2 in *Dictyostelium* recapitulate the interactions present in mammalian cells during clathrin-mediated endocytosis. To probe the involvement of these proteins during clathrin-mediated endocytosis, I used a few different modalities of live cell imaging.

In *Dictyostelium,* clathrin and AP-2 showed similar behaviors and dynamics at the membrane and, when imaged simultaneously, they co-localized in puncta and disappeared from the TIR-FM field together. This signature is consistent with the behavior of AP-2 and clathrin puncta in mammalian cells (Rappoport et al., 2006). For both AP-2 and clathrin puncta there was a wide variety of durations on the plasma membrane, again a property consistent with mammalian clathrin-coated pits (Mattheyses et al., 2011). Two-color live cell imaging of AP-2 and clathrin puncta showed that they disappeared from the plasma membrane together, although the time resolution used in these experiments (image every 1sec) may not be enough to detect small differences. Quantitative analysis of the appearance of AP-2 and clathrin relative to each other was not performed but could be informative to the kinetics of formation of the clathrin-coated vesicles. In general no obvious trend was observed and AP-2 and clathrin seemed to appear and accumulate together.

The spatial selectivity of TIR-FM compared to wide-field illumination allows imaging of the internalization of clathrin-coated pits as they moved from the plasma membrane into the cell. When clathrin and AP2 puncta were imaged using this approach I saw that a minimum of 34.4% of disappearing puncta showed internalization behavior, with this proportion being possibly as high as 80%. Measurements using EPI-TIR in

mammalian cells show 79 to 89% of clathrin disappearing puncta correspond to genuine movements into the cell (Merrifield et al., 2002; Mattheyses et al., 2011). Unfortunately, I was unable to successfully carry out EPI-TIR measurements using dajumin-GFP cargo as a marker. This was due to the high cytoplasmic background seen in EPI for both the dajumin and clathrin channels. This meant that not all vesicle behaviors could be measured, such as the distinction between abortive pits and productive endocytic vesicles that rapidly uncoat after scission. The data presented, however, demonstrated that puncta of AP-2 and clathrin accumulate at the plasma membrane and subsequently disappear from the TIR-FM field corresponding to productive endocytic events.

9.3 Clathrin-mediated endocytosis has differential requirements for clathrin and AP-2

Deletions in clathrin and AP-2 genes in *Dictyostelium* were used to study the requirements for these proteins in clathrin-coated vesicle formation. These results showed that AP-2 can form membrane puncta in the absence of clathrin, thus clathrin is not required for the plasma membrane localization of AP-2. This is similar to observations of AP-2 puncta in mammalian cells treated with RNAi to clathrin (Hinrichsen et al., 2003). Although AP-2 membrane localization was intact, in *chcA*- cells puncta appeared more diffuse and sometimes all localized to one side of the cell. This is very similar to the localization of AP180 in *chcA*- cells (Stavrou and O'Halloran, 2006) and suggests clathrin is not essential for membrane binding of adaptors but may play a role in concentrating them into puncta. Live-cell imaging allowed analysis of the dynamics of AP-2 in clathrin knockouts. Although puncta were present, loss of *chcA*- led to the appearance of two new

AP-2 populations. One population consisted of very short lived puncta, indicating that clathrin plays a role in stabilizing AP-2 at the membrane. These puncta may represent early clathrin-coated pits that begin to form but are not able to progress to vesicle formation. This has been observed anecdotally in mammalian cells where RNAi to clathrin caused AP-2 to only form very transient membrane puncta (Henne et al., 2010). The second population observed consisted of abnormally long-lived puncta, these AP-2 were often present for the whole timelapse and never disappeared. It is possible that these puncta corresponded to AP-2 that bound to the membrane and formed a stable interaction but were never internalized due to the lack of coat proteins. The fact that clathrin appears to be required for normal puncta formation suggests that the progressive nature of clathrin-coated vesicle formation has been conserved throughout evolution. The existence of these two populations does however indicate there might be differential requirements for clathrin in pit formation and thus heterogeneity in the mechanism of coated-pit formation in *Dictyostelium*.

The effect of removal of subunits of the AP-2 complex on coated-vesicle formation was also tested. Loss of AP-2 subunits did not appear to affect clathrin dynamics indicating redundancy between adaptors and arguing against a central role for AP-2 as an organizer of coated-pit formation in *Dictyostelium*. It should however be noted that, at least in AP2 μ2 subunit knockouts, a partial AP-2 complex was formed. In the absence of the AP2 μ2 subunit, GFP-Ap2A1 was stable and able to localize to plasma membrane puncta which represented partial AP-2 complexes as shown by co-immunoprecipitation and mass spectrometry experiments. This partial complex may be still be functional and therefore explain the lack of aberrant phenotypes in these cells.

Additionally, GFP-Ap2A1 was still able to bind to eps15 and nsfA in the μ2 knockout indicating that the interaction network was not disrupted in these cells. This also suggests that the AP-2 complex can assemble and target to the plasma membrane without the μ2 subunit, consistent with findings for AP-1 in *Dictyostelium* (Lefkir et al., 2003).

Phylogenetic analysis has shown that all large subunits of AP complexes (γ, α, δ, ε, β1/2 β3, β4), β-COP and γ-COP are descendants of a single ancestral gene. Likewise is true for the small subunits (μ1-4, σ1-4) δ-COP and ζ-COP (Schledzewski et al., 1999). One ancestral large and one ancestral small subunit are hypothesized to create a primitive adaptor which led to the current set of adaptors by coordinated gene duplications. The heterotetrameric AP-2 complex therefore may actually consist of two heterodimeric sub-complexes made from one large and one small subunit (α with σ2, and β1/2 with μ2) (Boehm and Bonifacino, 2001). This may explain the lack of phenotypes observed in this thesis when AP-2 subunits were knocked out in *Dictyostelium*. It is possible that the AP complexes are more dynamic than previously thought with subunits functioning independently or exchanging freely. Interestingly, I also detected the γ subunit of AP-1 in our co-immunoprecipitations. Since AP-1 and AP-2 use the same β subunit it is possible I detected the γ subunit via indirect interactions. The appearance of a short lived population of AP-2 puncta in the μ2 and α knockouts indicated that the individual subunits may play a role in stabilizing the binding of the AP-2 complex to the membrane. The presence of partial complexes does not appear to be likely in mammalian cells where loss of one subunit of the AP-2 complex destabilizes that other subunits (Motley et al., 2003).

9.4 Physiological functions of clathrin-mediated endocytosis in *Dictyostelium*

A major impediment to examining the physiological role of clathrin-mediated endocytosis in *Dictyostelium* was the lack of a cargo that is internalized in clathrin-coated vesicles. I found that the contractile vacuole marker dajumin-GFP (Gabriel et al., 1999) is also present at the plasma membrane where it co-localizes with clathrin and AP-2 puncta and internalizes in clathrin-coated vesicles. I therefore have identified the first cargo marker that can be used for studying endocytosis in *Dictyostelium*.

Attempts to label dajumin on its extracellular domain revealed that it is cleaved from its membrane bound anchor. These results agreed with previously published data showing the existence of a C-terminal fragment of dajumin both when full-length dajumin was tagged with GFP (Gabriel et al., 1999), and when the C-terminus of dajumin was fused with the contact site A protein (CsA-dajumin) (Barth et al., 1994). Immunofluorescence staining of cells with antibodies to CsA was used to show that the CsA-dajumin fusion protein predominantly localized to the plasma membrane. However, in the same study dajumin-GFP was predominantly seen to localize to the contractile vacuole, causing the authors to conclude that addition of the GFP tag to dajumin rerouted it to the contractile vacuole (Gabriel et al., 1999). My results using double-labeled dajumin suggested that dajumin is cleaved before it reaches the contractile vacuole and explain why in the immunofluorescence experiments (which only detect the full-length protein) CsA-dajumin was seen only on the plasma membrane (Gabriel et al., 1999). Since dajumin-GFP allows visualization of both full-length and the C-terminal fragment its contractile vacuole localization can be observed. Without antibodies to dajumin it is not possible to determine the localization of the endogenous protein but my results

suggest that GFP does not affect its trafficking as previously suggested (Gabriel et al., 1999). Full-length dajumin-GFP appears to be synthesized in the endoplasmic reticulum and thus is likely delivered to the cell surface as part of the secretory pathway. Protein cleavage may occur either at the endoplasmic reticulum or at the plasma membrane. The purpose of this cleavage, as well as the function of the dajumin protein in the cell, is unknown.

A biotinylation assay was used to confirm the plasma membrane localization and internalization of dajumin-GFP and demonstrated that internalization is blocked in *chcA*- cells. In this assay dajumin was internalized within 15 minutes in line with the time-course of internalization by clathrin-mediated endocytosis (Marks et al., 1996). This assay did show full-length dajumin on the cell surface that was internalized in agreement with previous immunofluorescence data using the CsA-dajumin protein (Gabriel et al., 1999). In contrary, my imaging experiments with extracellular tagged dajumin did not detect full-length dajumin on the cell surface but it is possible that the imaging techniques used here were not sensitive enough.

While the biotinylation assay does not distinguish between different endocytic pathways, the imaging results and use of *chcA*- knockout cells show that dajumin-GFP is endocytosed via clathrin-coated vesicles and, similar to previous reports, I never detected co-localization of dajumin-GFP with markers of fluid-phase endocytosis (Gabriel et al., 1999). These observations suggest that dajumin-GFP is predominantly internalized by clathrin-mediated endocytosis and not by other endocytic pathways such as macropinocytosis.

Since clathrin mutants are not lethal in unicellular organisms (O'Halloran and Anderson, 1992; Payne and Schekman, 1985; Lemmon and Jones, 1987) it has been suggested that clathrin-mediated endocytosis acts as a non-specialized endocytic portal in these lower eukaryotes (McMahon and Boucrot, 2011). This thesis, however, shows that in *Dictyostelium* a specific transmembrane cargo, dajumin-GFP, is internalized via clathrin-mediated endocytosis. Just as clathrin is required for internalization of many cargos in mammalian cells, internalization of dajumin-GFP is fully dependent on clathrin. Interestingly its uptake is not dependent on AP-2, a property normally associated with clathrin-mediated endocytosis in mammalian cells. As discussed above, it is however possible that AP-2 function is not removed in AP-2 subunit knockouts. Endocytosis independent of AP-2 function is also seen in yeast (Huang et al., 1999; Yeung et al., 1999) and such has led to suggestions of dependence on AP-2 as an evolved property. I suggest these results could also be explained by the different stabilities, and thus functions, of AP-2 hemi-complexes in different organisms.

It is, of course, still possible that in *Dictyostelium* AP-2 is not essential to form clathrin-coated vesicles and that there is redundancy between adaptors. Selection of dajumin-GFP as cargo may be dependent on molecules, such as AP180, that has already been shown to play a role in retrieving Vamp7B from contractile vacuoles limiting their homotypic fusion (Wen et al., 2009).

Clathrin, in addition to localizing to plasma membrane puncta of dajumin-GFP and AP-2, clathrin is also localized to the bladders and tubules of the contractile vacuole. Clathrin puncta on contractile vacuole bladders are known to contain AP-2, AP180 and epsin but not Hip1r (Wen et al., 2009), indicating they may be functionally distinct from

plasma membrane puncta. The results from three-dimensional observations of clathrin puncta on contractile vacuoles showed they can be localized anywhere on the contractile vacuole, but were often seen at the junctions between tubules and bladders. These junctions presumably have inverse membrane curvature to that normally found on clathrin-coated vesicles, therefore the function of clathrin at these locations is not clear.

Attempts at identifying other endocytic cargo in *Dictyostelium* using a biochemical purification approach were unsuccessful. Possible cargos were however identified from their co-immunoprecipitation with AP-2. These include calmodulin (*calA*) and calcium-dependent cell adhesion molecule-1 (*cadA*) both of which are membrane associated proteins that localize to the contractile vacuole (Sesaki et al., 1997). Additionally the transmembrane subunit of the vacuolar H+ ATPase (VatM), along with some of its peripheral subunits, was identified. The vacuolar H+ ATPase is localized in the membrane of contractile vacuoles and endosomes and is responsible for the transport of protons into the lumen of these organelles (Clarke et al., 2002). The identification of these contractile vacuole proteins indicates that AP-2 and clathrin-coated vesicles may be responsible for sorting of a variety of contractile vacuole proteins. When mRFP-clc was imaged with GFP tagged VatM, co-localization in disappearing plasma membrane puncta was not observed (data not shown). Since AP-2 and clathrin localize to the contractile vacuole bladders as well as the plasma membrane, it is possible this is where they interact with VatM and suggests AP-2 and clathrin-coated vesicles may play multiple roles at the contractile vacuole.

9.5 Clathrin-mediated endocytosis as a mechanism for protein sorting

A role for clathrin and AP-1 in contractile vacuole biogenesis is well documented (O'Halloran and Anderson, 1992; Wang et al., 2003; Lefkir et al., 2003; Sosa et al., 2012). In AP-1 μ1 knockouts the contractile vacuole protein Rh50 is mislocalized to punctate structures inside the cell (Lefkir et al., 2003), indicating at least some contractile vacuole components are trafficked in a clathrin-coated vesicle dependent mechanism. The results in this thesis demonstrate that clathrin also regulates internalization of contractile vacuole proteins from the cell membrane. This is in agreement with the results for Rh50 showing that a fusion protein with the cytoplasmic tail of Rh50, and the transmembrane domain of dajumin, traffics via the plasma membrane en route to the contractile vacuole (Mercanti et al., 2006a). It would be interesting to see if this protein is also internalized via clathrin-mediated endocytosis.

Dajumin-GFP localization to the plasma membrane in *chcA*- and β1/2 knockout cells was previously reported (Sosa et al., 2012), and these studies suggested that AP-2 only functions in sorting of dajumin-GFP in the context of an AP-1 knockout. In agreement I saw no defect in dajumin-GFP internalization in AP-2 knockouts suggesting it is not involved in the clathrin-mediated endocytosis of this cargo in wild-type cells. However, as mentioned above, AP-2 may still function in the α and μ2 knockouts that were used. It is possible that AP-2 functions are removed in β1/2 knockouts and the matching phenotype to *chcA*- cells is due to blockage of an AP-2 dependent step upstream of an AP-1 sorting step, both of which would be blocked in *chcA*- cells. This hypothesis could be tested by using combinations of double knockouts in AP-1 and AP-2 subunits.

In this thesis I found that dajumin-GFP traffics though the plasma membrane even in wild-type cells, indicating that dajumin-GFP plasma membrane accumulation in *chcA*- cells is due to a block in its internalization via clathrin-mediated endocytosis. The data shows a role for clathrin-mediated endocytosis in retrieval of contractile vacuole proteins and is thus important for the biogenesis and/or maintenance of this organelle. It is possible trafficking via the plasma membrane may also be important for the cleavage of dajumin and its function (which is unknown).

The contractile vacuole membrane is thought to fuse with the plasma membrane and create a transient pore to allow release of its contents. This is akin to a kiss-and-run mechanism and not thought to involve any membrane mixing (Heuser, 2006). A full release of dajumin-GFP into the plasma membrane was not obvious upon contractile vacuole emptying (Gabriel et al., 1999). This suggests that the clathrin-mediated endocytosis of dajumin-GFP observed here is either part of the trafficking of the protein to the contractile vacuole, or is used to retrieve any dajumin-GFP that may have leaked into the membrane upon pore formation. Both of these hypotheses are compatible with each other and the observed kiss-and-run fusion of contractile vacuoles.

It is possible that clathrin-mediated endocytosis arose as a mechanism of protein sorting and has evolved to serve other specialized functions in higher eukaryotes. Indeed there are a variety of examples of proteins present on intracellular organelles that are transported via the plasma membrane in mammalian cells (TGN38, CI-MPR) (Maxfield and McGraw, 2004). As already mentioned, the last eukaryotic common ancestor is presumed have possessed a somewhat complex endomembrane system based on the presence of AP1-4 and COPI genes. Secondary and tertiary structural comparisons of the

clathrin/AP, COPI and COPII adaptor complexes indicate that the large subunits of these complexes consist of alpha solenoids with beta propeller domain. This architecture is also seen in the scaffolding proteins of the nuclear pore complex leading to the idea of an early protocoatomer protein that was present in the earliest eukaryote. This protocoatomer protein may have had membrane binding and curving abilities. Gene duplication and specialization allowed more specific vesicular transport and thus introduced a more complex endomembrane system. This process would have continued after the separation of the major eukaryotic groups where mammalian cells could have co-opted clathrin-mediated endocytosis to regulate cell surface signaling processes. Further identification of cargos internalized by clathrin-mediated endocytosis in *Dictyostelium* will help in addressing whether it performs only a sorting function in this organism.

The results presented in this thesis offer the first direct demonstration that clathrin is utilized for endocytosis of membrane cargo in *Dictyostelium* in a process distinct from macropinocytosis and phagocytosis. This pathway can be distinguished by a new class of endosomes that contain AP-2, clathrin and dajumin. Furthermore, analysis of this pathway at a high spatial and temporal resolution shows the high degree of similarity in the kinetics of internalization of individual clathrin-coated vesicles between *Dictyostelium* and mammalian cells. These similarities support the conclusion that the formation of clathrin-coated vesicles is homologous between *Dictyostelium* and mammals and that *Dictyostelium* is a useful model to study clathrin-mediated endocytosis *in vivo*. Upon starvation, *Dictyostelium* cells progress through a developmental cycle where they form a multicellular fruiting body. Since it is possible to visualize the

transition from a unicellular state to multicellularity, *Dictyostelium* is uniquely positioned to study the dynamics of clathrin-mediated endocytosis during multicellular development.

CHAPTER 10 - Materials and Methods

10.1 Cell growth

AX2 cells were cultured axenically in HL5 medium at 22°C. Knockout cells lines used were *Ap2A1-*, *apm2-, clc-* and *chcA-* and were provided by the Dicty Stock Center (www.dictybase.org). Expression constructs were introduced into cells by electroporation. Briefly $5x10^6$ cells were washed twice in cold H-50 buffer (20mM HEPES, 50mM KCl, 10mM NaCl, 1mM $MgSO_4$, 5mM $NaHCO_3$, 1.3mM NaH_2PO_4, pH7.0) and resuspended in 100µl of H-50. Cells were mixed with 10µg of plasmid DNA and electroporated twice at 0.85 kV and 25µF with 5 seconds between pulses. Cuvettes were incubated on ice for 5 minutes and cells were transferred to HL5. Selection was started the next day in HL5 medium containing 20µg/ml Geneticin, 10µg/ml BlasticidinS or 35µg/ml Hygromycin. A list of expression constructs and strains can be found in Appendix VI.

10.2 Biotinylation assay

10.2.1 Biotinylation of cell surface

AX2 cells were grown in HL5 on 15cm dishes, 2 dishes were used per sample (~$9x10^7$ cells). Growth media was removed and cells washed 3 times in ice-cold Sörensen's Buffer containing sorbitol (SBS; 14.7mM KH_2PO_4, 2mM Na_2HPO_4, 120mM sorbitol, pH 7.8). Sulfo-NHS-SS-biotin was dissolved in SBS (0.67mg/ml) and 4ml was added to each dish for 20 minutes at 4°C, control dishes were incubated in SBS only. Unreacted sulfo-NHS-SS-biotin was quenched by adding ice-cold SBS containing 100mM glycine. Cells were washed once more in ice-cold SBS and lysed at 4°C by

adding 2ml of RIPA buffer containing protease inhibitors to each dish. Lysate was collected from the dishes using cell scrapers. Samples were either stored at -20°C or used immediately for avidin pull downs.

10.2.2 Neutravidin pull down

Total protein concentration in lysates was assayed using the BioRad DC Protein Assay, lysates were diluted with RIPA buffer so equal amounts of total protein were used for each sample. Biotinylated proteins were isolated from lysates by adding 200µl of High Capacity NeutrAvidin Agarose Resin (Pierce) to lysates and mixed for 1hr at 4°C. Beads were collected by centrifugation at 2,000g and washed with 1ml of wash buffer (50mM Tris-Cl, 150mM NaCl, 1% Triton X-100, pH8.0) buffer followed by two washes with 1ml of wash buffer containing 0.5M NaCl. Beads were then washed with 1ml of 50mM Tris-Cl, pH8.0 and proteins were eluted from the beads by adding 30µl of 6X SDS sample buffer followed by boiling for 10 minutes. Beads were collected at 15,000g and supernatants were loaded onto 4-20% Tris-glycine gels, gels were stained with Coomassie Blue. Proteins in excised gel pieces were digested using in-gel trypsin digestion and the proteolytic fragments were analyzed by LC-MS/MS. Proteins were identified using the Mascot protein identification system applying the *D.discoideum* database. Trypsin digestion, mass spectrometry and database searches were performed by the Proteomics Resource Center at Rockefeller University.

10.2.3 Biotinylation microscope assay

AX2 cells were grown on glass bottom MatTek dishes in HL5, approximately 2 hours before the experiment cells were incubated with imaging media (Low Fluorescence Axenic Media, www.dictybase.org). Biotinylation was performed as described in section 10.2.1. After the final wash, cells were fixed in 4% paraformaldehyde in PBS for 30 minutes at room temperature (RT) followed by two washes in PBS. Cells were then permeablized with 0.1% Triton X-100 for 2 minutes followed by two washes in PBS. Cells were incubated with streptavidin-AlexaFluor568 at 4μg/ml in PBS for 1hr at RT followed by two washes in PBS. Cells were covered with PBS and imaged using conventional wide-field microscopy (see 10.8.3; EPI1).

10.3 Plasmid construction

See Appendix VII for primer sequences

10.3.1 Ap2A1 cloning

A cDNA library was generated from AX2 cells using Superscript III CellsDirect cDNA synthesis kit. DNA corresponding to the coding region of *Ap2A1* was PCR amplified from the cDNA library using primers Ap2A1-F and Ap2A1-R, which added a BamHI and EcoRI site respectively. The *Ap2A1* gene was inserted into the BamHI and EcoRI site of vector 339-3 [provided by Dr. A. Müller-Taubenberger (Fischer et al., 2004)] to generate mRFPmars-Ap2A1 (mRFP-Ap2A1). To generate GFP-Ap2A1 the mRFP sequence was removed by digestion with HindIII and BamHI and replaced with the GFP sequence from pTX-GFP-clc [provided by Dr. T. O'Halloran (Wang et al., 2006)]. GFP-Ap2A1 or mRFP-Ap2A1 was PCR amplified with primers that added a 5'-

BgllII and 3'-SpeI site and inserted into these sites on plasmids pDM304, pDM326 and/or pDM358 (Veltman et al., 2009) to allow selection with other resistance markers.

10.3.2 Clc cloning

To generate mRFPmars-clc (mRFP-clc) the clc sequence was removed from pTX-GFP-clc by digestion with SmaI and BamHI and inserted into the BamHI and EcoRV site of vector 339-3. mRFP-clc was PCR amplified from this plasmid using primers mRFP-clc-F and mRFP-clc-R, which added a BglII and SpeI site respectively. The mRFP-clc fragment was inserted into the BglII and SpeI site of vector pDM304 for expression. To generate clc-mRFPmars (clc-mRFP), first the mRFP sequence was PCR amplified from 339-3 using primers mRFP-F and mRFP-R, which added a SpeI and XbaI site respectively. The mRFP sequence was then inserted into the SpeI site of pDM304 or pDM326 to generate pDM304-mRFP(C) and pDM326-mRFP(C). The clc sequence was then amplified from mRFP-clc using primers clc-F and clc-R, which added a BglII and SpeI site respectively. The clc sequence was then inserted into the BglII and SpeI site of pDM304-mRFP(C) and pDM326-mRFP(C) to generate clc-mRFP.

10.3.3 Dajumin cloning

The plasmid encoding dajumin-GFP was provided by Dr. A. Müller-Taubenberger (Gabriel et al., 1999). The dajumin sequence was PCR amplified with primers daj-F and daj-R that added a 5'-BgllII and 3'-SpeI site and inserted into these sites on plasmid pDM326-mGFP(C) to generate dajumin-mGFP.

Site directed mutagenesis was used to add the sequence encoding a KpnI and NheI site between the amino acids of interest in the dajumin sequence. This generates a GT and AS linker at the beginning and end of the inserted GFP sequence. The pHluorin or sfGFP was amplified with primers pH-F and pH-R or sfGFP-F and sfGFP-R, which added a KpnI and NheI site respectively. The pHluorin or sfGFP sequence was then inserted into the introduced KpnI and NheI sites in the dajumin sequence to generate pH^{S247}-dajumin, $sfGFP^{S247}$-dajumin, pH^{L403}-dajumin, and $sfGFP^{L403}$-dajumin. These sequences were then inserted into the BglII and SpeI site of pDM326 for expression.

To generate pH-$dajC^{A470\text{-}T544}$ the sequence corresponding to A470-T544 of dajumin was cut from the dajumin sequence with PstI and SpeI and inserted onto the C-terminus of pHluorin. The sequence encoding the dajumin signal sequence was digested using KpnI and NotI and inserted onto the N-terminus of the pHluorin sequence. This sequence was inserted into the BglII and SpeI site of pDM326 for expression. To generate pH-$dajC^{A470\text{-}T544}$mRFP the same strategy was used except the stop codon of dajumin was removed. The sequence was then inserted into pDM326-mRFP(C) for expression.

To generate $pH^{L403}dajC^{A470\text{-}T544}$ and $pH^{L403}dajC^{A470\text{-}T544}$mRFP the sequence encoding pH^{L403}-dajumin was digested with ApaI and BglII and inserted on the same sites on pH-$dajC^{A470\text{-}T544}$ and pH-$dajC^{A470\text{-}T544}$mRFP.

10.4 Western blots

Cells were lysed on ice with RIPA buffer containing protease inhibitors and mixed with SDS sample buffer, 16μg of protein was run on a 4-20% Tris-glycine gel.

For western blots with concentrated media, 4mls of media was collected after 24 hours of cell growth and spun at 7000g for 5mins at 4°C to remove any cells and debris. The supernatant was applied to an Amicon filter with a 10kDa cut off. Filters were spun at 2000g for 30mins at 4°C to concentrated media to 500-100µl, 16µl was mixed with SDS sample buffer and run on 4-20% Tris-glycine gels.

After gel running, proteins were transferred to nitrocellulose membranes. Membranes were blocked with 5% non-fat milk in TBS-T and probed with anti-GFP antibody (Novus NB600-303 at 1:2000 or Clontech JL-8 at 1:5000) followed by anti-rabbit-HRP (Sigma A0545) at 1:50000 or anti-mouse-HRP (Sigma A9917) at 1:5000. HRP was visualized using Supersignal West Pico Chemiluminescent Substrate (Pierce) or ECL Plus (GE).

10.5 Growth curves

Cells ($1x10^5$ cells) were seeded on 10cm dishes and were counted with a hemocytometer every 24 hours for 5 days by washing cells from the dish.

10.6 Development on non-nutrient agar plates

Growth phase cells were collected at 1000g for 2min and washed twice with KK2 (16mM KH_2PO_4, 4mM K_2HPO_4, pH6.5). Cells ($2x10^8$) were resuspended in a small volume (~1ml) of KK2 and spread on a 10cm 1% Bacto Agar-KK2 plate. After cells had attached to the plate (~20 minutes), excess liquid was removed and plates incubated at 22°C in a dark, humid chamber. At various times plates were removed and photographed using a dissection microscope.

10.7 Co-immunoprecipitation assay

Growth phase cells ($9x10^7$) were collected at 600g for 2min and lysed on ice in 10ml of lysis buffer (10mM Tris-Cl pH7.5, 150mM NaCl, 0.5mM EDTA, 0.5% NP-40) for 30min with pipetting every 10min. The lysate was cleared by centrifugation at 20,000g for 10min at 4°C and the supernatant was collected. 60µl of GFP-Trap-A beads (ChromoTek) were washed in dilution buffer (10mM Tris-Cl pH7.5, 150mM NaCl, 0.5mM EDTA) according to the manufacturers instructions and then added to the cell lysate and mixed for 5 hours at 4°C. Beads were collected by centrifugation at 2,000g and washed with 1ml of dilution buffer followed by a wash with 1ml of dilution buffer containing 0.5M NaCl. Proteins were eluted from the beads by adding 50µl of 2X SDS sample buffer followed by boiling for 10min. Beads were collected at 2,700g and supernatants were loaded onto 4-20% Tris-glycine gels. Gels were stained with Coomassie Blue and bands were excised from the gel and analyzed by LC-MS/MS followed by a database search using MASCOT (Proteomics Resource Center, Rockefeller University).

10.8 Microscopy

Growth phase cells were washed off growth dishes and allowed to adhere to MatTek dishes for approximately 1 hour; growth media was then replaced by imaging media (Low Fluorescence Axenic Media, www.dictybase.org) for several hours before imaging.

10.8.1 Spinning disk confocal microscopy

Confocal microscopy was performed at the Rockefeller University Bio-Imaging Resource Center (BIRC). A Zeiss Axiovert 200 microscope with a Perkin-Elmer Ultraview spinning disk confocal head and a 100x 1.45NA objective was used. For imaging GFP, the laser excitation used was 491nm with an ET500LP emission filter. For imaging mRFP, the laser excitation used was 561nm with an ET605/70 emission filter. The dichroics used were a 491LP (GFP) or a 440/491/561/640 polychroic (GFP and mRFP). The microscope has an Andor iXon 512x512 EMCCD camera and images were captured at 0.13μm/pixel with Metamorph software.

10.8.2 Total internal reflection fluorescence microscopy

Two similar microscopes were used in these experiments. The first microscope (TIR1) was an Olympus IX70 with a home-built TIRF illuminator. The laser was directed to the objective by a pair of galvanometers and a custom side-facing dichroic mirror. A 60x 1.45NA objective combined with an additional 1.5x magnifier was used. The laser excitation was 488nm to excite GFP-Ap2A1 and GFP-clc or 514nm to excite dajumin-GFP and 594nm to excite mRFP. The dichroics used were a 488LP (GFP) and a 442/514/594 polychroic or a 405/488/594 polychroic (GFP and mRFP). The galvanometers were controlled via Metamorph. The microscope has a Hamamatsu Orca-ER CCD camera and images were acquired at 0.07μm/pixel using Metamorph software.

The second microscope (TIR2) was an Olympus IX70 equipped with a prototype TIRF combiner and a 60x 1.45NA objective combined with an additional 1.5x magnifier. The laser excitation used in experiments was 488nm to excite GFP and 568nm to excite

mRFP. The dichroics used were 488LP (GFP) and a 488/568 polychroic (GFP and mRFP). The microscope has a Hamamatsu Orca-ER CCD camera or a Hamamatsu EM-CCD Digital camera C9100 and images were acquired at 0.07μm/pixel using Metamorph software.

For all TIR-FM imaging an exposure time of 500ms was used and images were taken every 1 second for timelapse imaging or continuously for streaming. On both microscopes for dual color imaging fluorescence emission was collected simultaneously and split into two images using a Cairn OptosplitIII emission splitter. Filters used for GFP were an HQ515/30, an HQ525/50 or an HQ550/50, filters used for mRFP were an HQ580LP or an ET632/60 combined with a 585LP dichroic mirror to split the emission. All dichroics and filters were from Chroma Technologies.

10.8.3 EPI-TIR assay

Images were acquired on TIR1 by changing the angle of incidence of the laser with the galvanometers so that either TIR illumination or wide-field illumination (EPI) was achieved. A 500ms exposure was used for both EPI and TIR with a delay of ~200ms between EPI and TIR acquisitions. One set of images was acquired every 1.5 seconds.

10.8.4 Wide-field microscopy

Wide-field microscopy was performed on two different microscopes. The first microscope (Deltavision) was at the Rockefeller University BIRC. A Deltavision Image Restoration Microscope was used which was comprised of an Olympus IX-70 microscope with a 100x 1.4 NA objective. Samples were excited with a xenon lamp and a

490/20 excitation filter, a GFP/mCherry polychroic was used with a 528/38 emission filter. The microscope has a Photometrics CoolSnap QE CCD camera and images were captured at 0.068μm/pixel using softWoRx software. Exposure times were 50-200ms and Z-slices were taken with steps of 200nm. The softWoRx software was used to deconvolve the images using measured PSFs.

The second microscope (EPI1) was an Olympus IX-81 microscope with a 100x 1.35NA objective. Samples were excited with a xenon lamp and a 470/40 excitation filter, a GFP dichroic mirror was used with a 520/40 emission filter. The microscope has a Hamamatsu Orca-ER CCD camera and the images were acquired at 0.0633 μm/pixel using Metamorph. The exposure time was 100ms and Z-slices were taken with steps of 500nm. The software Huygens was used to deconvolve the images using calculated PSFs.

10.9 Image analysis

10.9.1 Behavior of GFP-clc or GFP-Ap2A1 puncta

Cells were imaged by streaming acquisition and individual puncta were tracked manually for 7.5 seconds and their behavior over this period described. Puncta that disappeared due to cell movement were not included in the analysis.

10.9.2 Duration of GFP-clc or GFP-Ap2A1 on the surface

Cells were imaged by timelapse acquisition and individual puncta were tracked manually or automatically. For manual tracking the frame of appearance in TIR or disappearance from TIR of individual puncta was used to determine the duration as ‘time of disappearance from TIR’ – ‘time of appearance from TIR’.

For automatic tracking individual puncta were tracked using the 'spots' function in the software Imaris. Criteria for determining spots was manually adjusted for each cell. For tracking, the Brownian motion algorithm was used with a maximum distance of 5 and a gap of 0. The time of appearance in TIR or disappearance from TIR of individual puncta was determined and the duration was calculated as 'time of disappearance from TIR' – 'time of appearance from TIR'.

Statistical Analysis: A two-sample Kolmogorov-Smirnov (KS) test was used to ask whether the distributions of durations for the different cell lines are drawn from the same distribution. The null hypothesis is that the durations are drawn from the same distribution. A non-parametric test was used as the distributions of durations did not correspond to a normal distribution. The test was implemented in Origin 8.5 software.

10.9.3 Number of long lived puncta

Puncta present in the last frame of the timelapse were tracked and their frame of appearance was determined. Their duration was determined as 'time of last frame' – 'time of appearance in TIR'. The number of puncta with durations over 350 seconds were calculated as a percentage of all the puncta tracked.

10.9.4 Co-localization analysis

For dual color imaging, red and green fluorescence emission channels were split and aligned using the Cairn Image Splitter Analyzer plugin for ImageJ (Rasband, W.S., ImageJ, U. S. National Institutes of Health, Bethesda, Maryland, USA, http://imagej.nih.gov/ij/, 1997-2011). Since the Hamamatsu camera has a signal of 200

when there is no input, this background value of 200 was subtracted from all images followed by using the rolling ball background subtract function with a radius of 50-100 and no smoothing. Single frames from the beginning of timelapse images were used for co-localization analysis. Manual thresholding was used to outline the puncta for either channel. The position of the maximum intensity pixel within each outline was overlaid onto the outlines of the other channel. A maximum was counted as co-localized if it fell within an outline on the other channel. Percentage overlap was calculated as (number of co-localized maxima/total maxima) x 100. For pixel shift analysis the outline image was shifted 20 pixels to the left or right in one pixel increments. The overlap analysis was then performed at each position. Percentage overlap values were calculated for each position then normalized to the unshifted value. These procedures were implemented via custom macros in ImageJ.

10.9.5 Analysis of individual puncta

Puncta were selected for analysis if a fluorescence signal was present in both channels and the puncta disappeared from the TIR field during the timelapse. For GFP-Ap2A1 and mRFP-clc, puncta were circled in the GFP-Ap2A1 channel and the positions were transferred to the clathrin channel. For dajumin-GFP and mRFP-clc, puncta were circled in the mRFP-clc channel and positions transferred to the dajumin channel. Puncta were tracked using a combination of MATLAB and the ImageJ plugin SpotTracker 2D as described in (Mattheyses et al., 2011). The average fluorescence intensity of the puncta was measured for both channels and the values normalized to the maximum intensity in each channel for each puncta. The time of initiation of departure was determined for each

channel as the point at which the fluorescence intensity of a puncta started to decline irreversibly. Time between AP-2 and clathrin disappearance or between dajumin and clathrin disappearance was calculated as 'initiation of departure for mRFP-clc' – 'initiation of departure for GFP-Ap2A1 or dajumin-GFP'.

10.9.6 Analysis of EPI-TIR puncta

The same puncta tracking was performed as above (10.9.5); puncta centroids were calculated from the GFP-Ap2A1 TIR channel and applied to all other channels. The average fluorescence intensity of the puncta was measured for all channels and the values normalized to the maximum intensity in each channel for each puncta, I then applied a rolling average to the data using a seven-frame window. The time of initiation of appearance was determined for each channel as the point in which fluorescence intensity of a puncta started to increase irreversibly. The time of disappearance was determined as the point at which the fluorescence intensity decline plateaus. Kymographs were created using a maximum intensity projection of the 4 pixels either side of the center of the spot for every time point. Classification of puncta into various categories was done manually by assessing both the fluorescence intensity measurements and kymographs for each punctum.

10.9.7 Analysis of clathrin localization on contractile vacuoles

Spinning disk images of mRFP-clc and dajumin-GFP were overlaid and the localization of clathrin puncta associated with the contractile vacuole in each frame was assigned manually to one of three locations: on bladders, at bladder/tubule junction or

behind the emptying bladder. If any puncta were seen in any of these locations that frame was scored as positive.

For analysis of clathrin localization with contractile vacuole cycle, the dajumin-GFP channel was used to determine the state of the contractile vacuole. Three states were described: filling, filled and emptying. Filling was characterized by vacuoles that had just emptied and were starting to increase in size again, these vacuole have a distinctive crescent shape. Vacuoles were classed as filled if they appeared not to increase in size and were round in shape. Emptying vacuoles are distinguished by fusion with the membrane followed by rapid flattening against it, emptying was normally seen over a few frames only. Observation of clathrin anywhere on the vacuole was scored as positive localization and the percentage of frames that had clathrin localized to a contractile vacuole were calculated for each state of filling. Determination of filled state and clathrin localization was performed manually.

10.9.8 Three-dimensional rendering

Deconvolved stacks of dajumin-GFP and mRFP-clc were acquired on the Deltavision microscope. The software Imaris was used to create three-dimensional reconstructions of the cells from these z-stacks. Images were reconstructed using the volume rendering function and the isosurface function. In the isosurface function the software uses a specified gray value range in the data to create an artificial solid object. In the volume function the data is weighed based in closeness to the viewer to give a 3D impression. For both functions the gray value ranges were specified manually.

10.9.9 Three-dimensional co-localization analysis

Analysis was performed using Imaris to create three-dimensional objects for both the clathrin and dajumin signals. A mask was created from the images of the individual planes using Metamorph. A top hat circular filter of 10 pixel diameter was applied to the image followed by thresholding to include only the top 2% of pixels based on intensity. Any regions smaller than 8 pixels in area were discarded and the remaining areas used to define the edges of the 3D objects in Imaris. The total number of objects and the total number of voxels was recorded for each channel. Imaris was then used to filter out any objects that did not overlap with the other channel and the measurements were made again. These were used to calculate the percentage of objects, and percentage of voxels, that overlapped with each other.

10.10 Biotin internalization assay

The assay was performed as in (Barth et al., 1994) but will be briefly described here. Growth phase cells ($5x10^6$ cells per time point) were washed twice in ice-cold Sörensen's Buffer (SB; 14.7mM KH_2PO_4, 2mM Na_2HPO_4, pH 8.0). Cells were resuspended in ice-cold SB containing 1mg/ml sulfo-NHS-SS-biotin at $1.5x10^7$ cells/ml and shaken on ice at 150rpm for 30min. After labeling, the cells were washed twice in ice-cold SB containing ammonium chloride (SBA; SB, pH7.2, 40mM NH_4Cl). For internalization, cells were resuspended in SBA at $5x10^6$ cells/ml and shaken at 150rpm at RT for various times, internalization controls were kept on ice. After the internalization step, cells were collected and resuspended at a density of $1x10^7$ cells/ml in ice-cold reducing solution (50mM glutathione, 75mM NaCl, 75mM NaOH, 1% BSA) and shaken

on ice at 150rpm for 30min, reduction controls were incubated in SBA. After reduction, cells were washed twice in ice-cold SBA and lysed in 50-100µl of RIPA buffer containing protease inhibitors. Total protein concentration was assayed using the BioRad DC Protein Assay and lysates were diluted so equal amounts of total protein were used for each sample.

Co-immunoprecipitation was performed as described above (10.7) except 10-20µl of GFP-Trap-A beads were used and mixing was performed for 2 hours at 4°C. Samples were eluted from the bead in 30-60µl of non-reducing sample buffer. For detecting GFP, western blots were performed as described above (10.4); 5-25µl of the sample was run on a 4-20% Tris-glycine gel followed by transfer to nitrocellulose membranes. For detection of biotin, 20µl of the sample was run on a 4-20% Tris-glycine gel followed by transfer to nitrocellulose membranes. Membranes were blocked for 1 hour with 2% BSA Fraction V in sodium borate buffer (150mM NaCl, 50mM $Na_2B_4O_7$, pH 10.0) and then probed for 1 hour with Pierce High Sensitivity Streptavidin-HRP (1:8,000) in 4% BSA Fraction V in sodium borate buffer containing 0.02% Triton-X100. Membranes were washed three times with sodium borate buffer containing 0.01% Triton-X100, followed by three washes with sodium borate buffer containing 0.1% Triton-X100. HRP was visualized using ECL Plus.

10.11 VatM immunofluorescence

Cells were washed off growth dishes and allowed to adhere to 25mm #1.5 glass coverslips for 1 hour. Cells were incubated in imaging media for several hours and then fixed as described in (Fok et al., 1993) but without the agar overlay. After fixation the

cells were immunostained as in (Clarke et al., 1987) with the N4 antibody (Fok et al., 1993) at a 1:50 dilution followed by a goat anti-mouse AF488 secondary antibody at a 1:400 dilution. Cells were imaged by wide-field microscopy with EPI1.

10.12 FM4-64 staining

Cells were washed off growth dishes and allowed to adhere to MatTek dishes for 1 hour. Cells were incubated in imaging media for several hours and FM4-64 dye was added at 1μg/ml for 20min. Cells were imaged with the Deltavision microscope described above with DIC illumination or with a xenon lamp and a 555/28 excitation filter, a DAPI/FITC/Rhod/Cy5 polychroic mirror, and a 685/40 emission filter. Exposure times were 150-250ms.

APPENDIX I – p143-149

Proteins identified by cell surface biotinylation

Name	Gene	DDB G_ID	Score	Number of Peptides	Mass
Cytoskeleton					
actin	act10	DDB_G0289811	1860	119	41948
alpha actinin 1	abpA	DDB_G0268632	830	47	97754
14-3-3	fttB	DDB_G0269138	600	26	28857
Regulatory myosin light chain	mlcR	DDB_G0276077	371	16	18368
severin	sevA	DDB_G0289327	218	8	40130
elongation factor 1 alpha	efaA1	DDB_G0269134	213	24	49936
profilin II	proB	DDB_G0286187	159	15	12893
actin related protein 2/3 complex, subunit 1	arcA	DDB_G0277825	130	3	41439
actin related protein 3	arpC	DDB_G0283755	128	9	47068
profilin I	proA	DDB_G0287125	126	9	13113
myosin heavy chain A	mhcA	DDB_G0286355	113	12	115442
cortexillin II	ctxB	DDB_G0276893	96	4	50600
actin related protein 2/3 complex, subunit 2	arcB	DDB_G0282813	92	7	32968
actin binding protein	abpB	DDB_G0279081	79	6	33617
actin capping protein subunit alpha	acpB	DDB_G0272104	75	2	31419
fimbrin	fimA	DDB_G0277855	73	3	67503
alpha tubulin	tubA	DDB_G0287689	68	9	51613
actin related protein 2/3 complex, subunit 3	arcC	DDB_G0292804	68	4	19706
actin capping protein subunit beta	acpA	DDB_G0267374	67	3	31017
beta tubulin	tubB	DDB_G0269196	54	5	51816
NCK-Associated protein	napA	DDB_G0274519	50	4	134083

Metabolism					
putative fatty acid synthase	pks16	DDB_G0275069	588	31	292720
hypoxanthine phosphoribosyltransferase	hprT	DDB_G0285193	250	10	20580
glutamate-ammonia ligase	glnA3	DDB_G0279591	238	16	83077
glyceraldehyde-3-phosphate dehydrogenase (GAPDH)	gpdA	DDB_G0275153	225	6	36757
S-adenosyl-L-homocysteine hydrolase	sahA	DDB_G0267418	166	18	47877
isocitrate dehydrogenase	idhC	DDB_G0272208	143	6	46797
ATP citrate synthase	acly	DDB_G0278345	140	13	67905
serine-pyruvate transaminase	agxt	DDB_G0289923	124	6	45309
esterase/lipase/thioesterase domain-containing protein	cinB	DDB_G0291121	116	5	36372
3-phosphoglycerate dehydrogenase	serA	DDB_G0281071	112	6	45234
pyruvate kinase	pyk	DDB_G0283247	105	5	55477
NAD-dependent epimerase/dehydratase family protein		DDB_G0276473	95	2	40421
UMP-synthetase	pyr56	DDB_G0280041	94	4	52788
aldehyde dehydrogenase		DDB_G0276821	92	4	55783
O-methyltransferase family 3 protein	omt6	DDB_G0275501	84	4	25952
glutamate dehydrogenase 2	glud2	DDB_G0280319	77	10	117584
phosphoribosylamine-glycine ligase	purD	DDB_G0290121	73	6	88677
GMP synthetase	guaA	DDB_G0281551	72	9	80083
glycogen phosphorylase 1	glpV	DDB_G0281383	71	7	97797
putative acteyltransferase		DDB_G0275913	67	4	20940
putative ATP citrate synthase		DDB_G0278341	63	6	50520
pyruvate dehydrogenase E1 beta subunit	pdhB	DDB_G0292994	58	2	42474
1,4-alpha-glucan branching enzyme	glgB	DDB_G0274105	55	2	89116
aconitase	aco1	DDB_G0279159	53	4	98499
aldehyde dehydrogenase		DDB_G0290537	53	6	55109

aldehyde dehydrogenase	hydA	DDB_G0290479	53	6	54877
pyruvate dehydrogenase E1 alpha subunit	pdhA	DDB_G0276417	51	7	39214
S-adenosylmethionine synthetase		DDB_G0291179	50	3	42079
Mitochondrial proteins					
ATP synthase beta chain, mitochondrial	atp5b	DDB_G0269916	634	28	71029
citrate synthase, mitochondrial		DDB_G0275311	446	16	51473
ADP/ATP translocase	ancA	DDB_G0267454	259	12	33619
Stress-70 protein, mitochondrial	mhsp70	DDB_G0293298	148	12	71603
aconitase, mitochondrial	aco2	DDB_G0278779	143	14	83889
mitochondrial processing peptidase alpha subunit	mppA1	DDB_G0290997	120	7	47831
succinate dehydrogenase	sdhA	DDB_G0280535	111	4	69157
putative mitochondrial transferase caf17		DDB_G0285011	99	5	46177
ATP synthase alpha subunit, mitochondrial	atp1	DDB_G0294012	76	9	57543
2-oxoglutarate dehydrogenase, E1 subunit	ogdh	DDB_G0288127	70	4	114681
EF-hand domain-containing protein	mcfO	DDB_G0283329	67	6	85879
electron transfer flavoprotein alpha subunit	etfa	DDB_G0290927	67	2	37784
porin	porA	DDB_G0271848	58	1	30140
NAD-dependent glutamate dehydrogenase	glud1	DDB_G0287469	55	5	55464
TU translation elongation factor, mitochondrial	tufM	DDB_G0289593	54	2	46111
mitochondrial glycoprotein family member		DDB_G0288137	51	2	36700
Oxidoreductase activity					
peroxiredoxin 5	prdx5	DDB_G0285741	225	26	18521
peroxiredoxin 4	prdx4	DDB_G0274859	182	10	23234
amine oxidase		DDB_G0291301	139	14	121339
phosphogluconate dehydrogenase	gnd	DDB_G0277885	134	7	54370
Proteasome and proteases					
cathepsin D	ctsD	DDB_G0279411	114	4	41494

cell division cycle protein 48	cdcD	DDB_G0288065	113	9	89242
puromycin-sensitive aminopeptidase-like protein	psaB	DDB_G0270670	90	7	98123
leukotriene A4 hydrolase	lkhA	DDB_G0269148	90	5	68825
Protein biosynthesis					
elongation factor 1 gamma	efa1G	DDB_G0282979	404	12	47258
elongation factor 2	efbA	DDB_G0288373	374	39	93512
elongation factor 1b	efa1B	DDB_G0284035	209	13	24220
40S ribosomal protein SA	rpsA	DDB_G0270316	198	9	27329
40S ribosomal protein S7	rps7	DDB_G0289025	175	13	22190
S60 ribosomal protein L10	rpl10	DDB_G0288273	163	10	24871
60S ribosomal protein L6	rpl6	DDB_G0292460	160	6	25811
40S ribosomal protein S5	rps5	DDB_G0286075	160	9	21428
60S ribosomal protein L4	rpl4	DDB_G0277803	159	11	40278
60S ribosomal protein L9	rpl9	DDB_G0278959	140	12	21376
60S ribosomal acidic phosphoprotiein P2	rplP2	DDB_G0283393	137	8	10559
40S ribosomal protein S15	rps15	DDB_G0285561	132	4	16395
seryl-tRNA synthetase	serS	DDB_G0272660	123	3	52058
tyrosine-tRNA ligase	tyrS	DDB_G0276721	103	6	44279
40S ribosomal protein S23	rps23	DDB_G0272250	102	2	15730
40S ribosomal protein S3	rps3	DDB_G0293000	98	10	24546
eukaryotic translation initiation factor 5A	eif5a	DDB_G0284861	97	3	18498
S60 ribosomal protein L27a	rpl27a	DDB_G0292388	95	4	16569
S60 ribosomal protein L27	rpl27	DDB_G0271298	91	4	16431
eukaryotic translation initiation factor 4A	ifdA	DDB_G0269146	88	3	44544
S60 ribosomal protein L14	rpl14	DDB_G0277975	80	7	17377
40S ribosomal protein S18	rps18	DDB_G0276415	78	10	18081
elongation factor Ts	tsfm	DDB_G0286399	75	5	39848

S60 ribosomal protein L12	rpl12	DDB_G0288295	74	4	17941
S60 ribosomal protein L11	rpl11	DDB_G0279189	72	2	8928
40S ribosomal protein S3a	rps3a	DDB_G0277345	69	4	30466
S60 ribosomal protein L7	rpl7	DDB_G0276441	68	9	28015
S60 ribosomal protein L38	rpl38	DDB_G0268302	66	3	8724
alanyl-tRNA synthetase	alaS	DDB_G0277823	62	8	106785
leucyl-tRNA synthetase	leuS	DDB_G0285451	62	7	120366
glutamate-tRNA ligase	gluS	DDB_G0287467	62	8	86073
S60 ribosomal protein L13	rpl13	DDB_G0291870	61	8	23719
S60 ribosomal protein L15	rpl15-2	DDB_G0272893	61	4	24483
S60 ribosomal protein L17	rpl17	DDB_G0285277	61	7	20344
60S ribosomal protein L5	rpl5	DDB_G0278539	60	3	32898
S60 ribosomal protein L8	rpl8	DDB_G0274113	59	3	27674
S60 ribosomal protein L15	rpl15-1	DDB_G0273983	59	5	31077
60S ribosomal protein L7a	rpl7a	DDB_G0277629	57	7	33854
40S ribosomal protein S4	rps4	DDB_G0272825	56	7	30131
ribosomal protein S2	rps2	DDB_G0293742	56	5	28814
S60 ribosomal protein L10a	rpl10a	DDB_G0276871	56	11	24495
eukaryotic translation initiation factor 3 subunit E	eif3E	DDB_G0293052	55	4	60573
60S ribosomal acidic phosphoprotiein P0	rplP0	DDB_G0286501	51	2	33003
Protein folding					
t-complex polypeptide 1	tcp1	DDB_G0269190	110	3	59808
chaperonin containing TCP1 theta subunit	cct8	DDB_G0276233	77	7	58872
Protein modification					
protein phosphatase 2C-related protein		DDB_G0284243	76	5	44621
ubiquitin activating enzyme E1	uae1	DDB_G0270272	59	11	114471

Pseudogene					
pseudogene similar to abpA		DDB_G0268632	816	46	97995
actin pseudogene	act24_ps	DDB_G0289505	163	13	42453
40S ribosomal protein S28 pseudogene	rps28_ps	DDB_G0285597	85	2	8163
Signalling					
G protein beta subunit	gpbB	DDB_G0275045	137	10	36550
Ran	ranA	DDB_G0291235	74	5	24202
RacC	racC	DDB_G0293526	70	4	21962
ogb-like ATPase	ola1	DDB_G0268758	68	3	44548
RasG	rasG	DDB_G0293434	58	3	21548
Ran binding protein 1 domain-containing protein	ranbp1	DDB_G0287391	55	4	22578
Stress response					
heat shock protein 90 family	hspD	DDB_G0267400	297	13	80060
heat shock protein Hsc70-2	hspE-2	DDB_G0273249	171	11	70089
heat shock protein Hsp70 family protein		DDB_G0276445	79	8	72664
Vacuolar H+ ATPase					
vacuolar H+ ATPase B subunit	vatB	DDB_G0277401	278	16	55013
vacuolar H+-ATPase E subunit	vatE	DDB_G0275701	244	22	26840
vacuolar H+-ATPase A subunit	vatA	DDB_G0287127	98	11	68671
Vesicular Transport					
clathrin heavy chain	chcA	DDB_G0277221	181	10	194902
Rab14	rab14	DDB_G0281337	87	3	23292
vacuolar sorting protein 35	vps35	DDB_G0293218	75	7	89705
gamma-COP	copG	DDB_G0289371	68	5	102358
cyclase associated protein	cap	DDB_G0288769	56	3	49896
GTP binding protein Sar1A	sarA	DDB_G0272296	54	7	20398

Rab1C	rab1C	DDB_G0269174	51	3	22557
Calcium binding					
calcium-binding protein	cbp2	DDB_G0267456	140	4	19841
DNA replication					
proliferating cell nuclear antigen	pcna	DDB_G0287607	177	6	28525
Membrane binding					
annexin VII	nxnA	DDB_G0269160	73	6	46790
mRNA					
polyA-binding protein, cytoplasmic 1	pabpc1A	DDB_G0293558	71	5	62969
Transmembrane proteins					
conditioned medium factor receptor	cmfB	DDB_G0289157	116	8	56860
Unknown					
unknown		DDB_G0293724	307	24	80963
unknown		DDB_G0290465	88	11	81150
unknown		DDB_G0281913	50	6	56712
unknown		DDB_G0288519	83	1	52067
proteasome component region PCI (PINT) domain-containing protein		DDB_G0287005	68	2	46777
alpha/beta hydrolase fold-3 domain-containing protein		DDB_G0287609	513	18	38857
alpha/beta hydrolase fold-3 domain-containing protein		DDB_G0290975	499	17	38943
putative SAM dependent methyltransferase		DDB_G0267734	146	13	33419
trimeric LpxA-like domain containing protein		DDB_G0288155	51	3	26744
unknown	lmcB	DDB_G0280533	209	7	17838

APPENDIX II – p150-153

Proteins identified in GFP-Ap2A1 (AX2) co-immunoprecipitation (duplicates)

Name	Gene	DDB_G ID	Score	Percent coverage	Number of unique peptides (total # of peptides)	MW (kDa)	
AP complex							
ap1b1	ap1b1	DDB_G0279141	2254	36.31	30 (75)	106.5	
			3549	40.76	35 (103)		
ap2a1	ap2a1	DDB_G0273439	5947	37.21	32 (191)	110.6	
			15464	47.02	46 (429)		
ap2s1	ap2s1	DDB_G0289721	939	ND	(95)	17.0	
			750	43.66	7 (36)		
apm2	apm2	DDB_G0277139	366	20.27	9 (16)	49.8	
			2453	31.21	13 (71)		
Vesicular Transport							
EPS15 homology (EH) domain-containing protein		DDB_G0287325	175	7.19	5 (6)	131.3	
			4728	40.89	34 (118)		
Vacuolar H+ ATPase							
vacuolar H+ ATPase M subunit	vatM	DDB_G0291858	155	7.24	4 (6)	93.2	
			77	3.93	2 (3)		
ABC Transporter							
ABC transporter-related protein	abcE1	DDB_G0290483	47	2.16	1 (1)	67.4	
			36	2.16	1 (1)		
ABC transporter-related protein	abcF2	DDB_G0284047	44	3.04	1 (1)	66.8	
			290	9.61	4 (9)		

Apoptosis							
apoptosis inducing factor	aif	DDB_G0288247	53 940	3.01 34.40	1 (1) 10 (20)	59.6	
Cytoskeleton							
alpha actinin 1	abpA	DDB_G0268632	33 355	2.42 8.01	1 (1) 4 (7)	97.3	B
cofilin	cofA	DDB_G0277833	35 106	10.22 6.79	1 (1) 1 (2)	28.9	
cofilin	cofB	DDB_G0291970	108 106	10.64 10.95	5 (7) 1 (2)	15.2	
DNA Binding							
myb domain-containing protein		DDB_G0280705	32 45	0.25 0.25	1 (1) 1 (2)	271.7	
Metabolism							
ATP citrate synthase	acly	DDB_G0278345	100 166	11.46 8.36	4 (6) 3 (4)	67.3	B
allantoicase	allC	DDB_G0280267	31 173	2.71 11.65	1 (1) 4 (7)	41.8	
putative ATP citrate synthase		DDB_G0278341	73 369	5.56 12.00	2 (2) 4 (7)	50.2	B
group IV decarboxylase	odc	DDB_G0281109	34 315	7.16 10.41	2 (2) 3 (5)	51.7	
bifunctional UMP-synthetase	pyr56	DDB_G0280041	85 522	4.60 17.36	2 (3) 5 (10)	52.5	B

Mitochondrial Protein							
ATP synthase alpha subunit, mitochondrial	atp1	DDB_G0294012	53	3.28	1 (1)	57.2	
			51	2.12	1 (1)		B
cytochrome c1	cyc1	DDB_G0292594	112	19.64	3 (3)	30.5	
			164	7.64	2 (3)		
Oxidoreductase Activity							
glucose/ribitol dehydrogenase family protein		DDB_G0284277	41	5.88	1 (1)	32.3	
			97	4.15	1 (2)		
Proteasome and proteases							
peptidase D	pepD	DDB_G0269382	49	2.99	1 (1)	56.4	
			279	10.98	4 (6)		
20S proteasome subunit C2	psmA1	DDB_G0282363	59	5.65	1 (1)	28.0	
			76	10.48	2 (2)		
Protein Biosynthesis							
prolyl-tRNA synthetase	proS	DDB_G0284197	34	2.92	1 (1)	62.4	
			224	8.03	3 (5)		
40S ribosomal protein S6	rps6	DDB_G0280823	136	13.98	2 (2)	26.1	
			405	19.92	4 (8)		
Protein Folding							
t-complex polypeptide 1	tcp1	DDB_G0269190	51	2.92	1 (1)	59.4	
			248	11.68	3 (5)		B
RNA binding							
major vault protein-alpha	mvpA	DDB_G0269156	85	6.52	3 (5)	94.1	
			616	14.83	9 (16)		

Unknown							
hypothetical protein		DDB_G0275519	62	ND	(9)	34.3	
			79	14.71	2 (2)		
class II aldolase/adducin		DDB_G0284915	25	4.33	1 (1)	26.5	
			36	4.76	1 (1)		
unknown		DDB_G0288519	36	3.18	1 (2)	51.6	
			267	18.86	4 (7)		B
hypothetical protein		DDB_G0289571	73	3.50	2 (2)	104.2	
			827	20.04	12 (20)		
hypothetical protein		DDB_G0290857	48	2.70	1 (1)	57.5	
			289	11.75	4 (6)		

APPENDIX III – p154-156

Proteins identified in GFP-Ap2A1 (AX2) co-immunoprecipitation (single hits)

Name	Gene	DDB_G ID	Score	Percent coverage	Number of unique peptides (total # of peptides)	MW (kDa)
Vesicular Transport						
N-ethylmaleimide-sensitive fusion protein	nsfA	DDB_G0276153	238.81	8.54	5 (8)	82.1
clathrin heavy chain	chcA	DDB_G0277221	101.96	1.59	2 (2)	193.5
sec23 (COPII coat)	sec23	DDB_G0281985	88.34	2.40	1 (1)	84.6
Dynamin like protien	dymA	DDB_G0277849	82.78	4.76	1 (1)	35.0
clathrin light chain	clc	DDB_G0277403	66.86	5.15	1 (2)	22.1
sec61 gamma subunit	sec61g	DDB_G0287777	64.62	23.19	1 (2)	7.6
vacuolar protein sorting-associated protein	vps13B	DDB_G0274917	54	ND	(38)	696377
Rab GTPase						
Rab2 1(RabB)	rab21	DDB_G0286553	235.08	19.81	3 (6)	23.5
Rab2b	rab2B	DDB_G0272138	211.39	12.87	2 (4)	22.7
Rab8a	rab8A	DDB_G0280043	131.85	12.98	1 (4)	23.2
Rab5a	rab5A	DDB_G0271984	80.80	6.97	1 (2)	22.3
RabR	rabR	DDB_G0271980	69.58	5.86	1 (1)	34.8
RabG2	rabG2	DDB_G0290783	69.54	8.75	1 (2)	17.7

Rab32a (RabE)	rab32A	DDB_G0283603	48.80	6.85	1 (1)	24.7
Transmembrane Protein						
phosphatidylinositol glycan class V	pigV	DDB_G0280891	63	ND	(4)	72541
calnexin	cnxA	DDB_G0271144	43.13	2.43	1 (1)	60.4
Vacuolar H+ ATPase						
vacuolar ATP synthase subunit D		DDB_G0274331	192.23	15.18	2 (4)	28.6
vacuolar H -ATPase A subunit	vatA	DDB_G0287127	146.22	10.03	3 (4)	68.2
vacuolar H+ ATPase E subunit	vatE	DDB_G0275701	100.33	4.29	1 (2)	26.6
Membrane associated						
calcium-dependent cell adhesion molecule-1	cadA	DDB_G0285793	144.41	8.38	1 (2)	21.4
calmodulin	calA	DDB_G0279407	76.13	21.05	1 (1)	17.1
WD repeat domain phosphoinositide-interacting protein 3	wdr45l	DDB_G0282581	63.51	4.00	1 (1)	39.3
annexin VII	nxnA	DDB_G0269160	52.55	2.39	1 (1)	46.6
Cytoskeleton						
arp 2/3 complex, subunit 3	arcC	DDB_G0292804	97.05	9.77	1 (1)	19.5
arp 2/3 complex, subunit 4	arcD	DDB_G0269102	95.25	11.24	2 (3)	19.6
arp 2/3 complex, subunit 1	arcA	DDB_G0277825	92.21	5.69	1 (2)	41.0
G-protein						
G-protein subunit alpha 1	gpaA	DDB_G0283349	118.07	8.43	2 (3)	40.2
Ras GTPase						
RasC	rasC	DDB_G0281385	243.95	12.17	1 (4)	21.5

Rho GTPase						
racH	racH	DDB_G0269240	181.35	10.50	1 (2)	22.2
RacC	racC	DDB_G0293526	98.51	9.90	1 (2)	21.7

APPENDIX IV – p157-158

Proteins identified in GFP-clc (clc-) co-immunoprecipitation

Name	Gene	DDB_G ID	Score	Number of peptides	MW (Da)		
Vesicular transport							
clathrin heavy chain	chcA	DDB_G0277221	19029	883	194902	B	*
clathrin light chain	clc	DDB_G0277403	1463	83	22124		*
Transmembrane protein							
putative protein serine/threonine kinase, UPR	ireA	DDB_G0267650	58	10	113074		
Ras GTPase							
RasC	rasC	DDB_G0281385	59	4	21539		*
Stress response							
heat shock protein Hsp70 family protein	hspH	DDB_G0290187	52	10	86410		
Developmental Gene							
armadillo-like helical domain-containing protein	DG1098	DDB_G0293192	50	15	235137		
DNA binding							
8-oxoguanine DNA-glycosylase	ogg1	DDB_G0292618	53	7	51123		
myb domain-containing protein		DDB_G0280705	142	29	272430		*
UV-damaged DNA binding protein1	repE	DDB_G0286013	51	6	128260		
replication factor C subunit	rfc1	DDB_G0285961	57	12	153944		
Metabolism							
glyceraldehyde-3-phosphate dehydrogenase	gpdA	DDB_G0275153	103	3	36757	B	
Mitochondrial protein							
ATP synthase alpha subunit, mitochondrial	atp1	DDB_G0294012	51	2	57543	B	*

Protein folding							
t-complex polypeptide 1	tcp1	DDB_G0269190	53	10	59825	B	*
Protein modification							
ubiquitin	ubqH	DDB_G0279721	416	36	42808		
ubiquitin/ribosomal protein S27a fusion protein	ubqC	DDB_G0276765	539	38	17666		
ubiquitin	ubqA	DDB_G0282295	539	40	42855		
Unknown							
hypothetical protein		DDB_G0285813	77	7	73950		
Unknown		DDB_G0274915	72	7	183089		
hypothetical protein		DDB_G0279567	72	3	32111		
hypothetical protein		DDB_G0290977	71	5	60402		
hypothetical protein		DDB_G0278199	51	12	81908		
hypothetical protein		DDB_G0292032	50	13	174809		
hypothetical protein		DDB_G0270056	50	14	163081		
hypothetical protein		DDB_G0279143	162	12	75439		
hypothetical protein		DDB_G0293674	293	39	70246		
hypothetical protein		DDB_G0277997	84	20	379442		
hypothetical protein		DDB_G0269594	76	24	99537		
hypothetical protein		DDB_G0280509	66	20	104843		
hypothetical protein		DDB_G0274963	66	16	147388		
hypothetical protein		DDB_G0270130	107	14	69633		
hypothetical protein		DDB_G0275861	51	12	284484		

APPENDIX V – p159-161

Proteins identified in GFP-Ap2A1 (apm2-) co-immunoprecipitation

Name	Gene	DDB_G ID	Score	Number of peptides	MW (kDa)		
AP complex							
ap2a1	ap2a1-1	DDB_G0273439	9015	376	111.371		*
ap2s1	ap2s1	DDB_G0289721	136	15	17.176		*
ap1b1	ap1b1	DDB_G0279141	116	17	107.568		*
ap1g1	ap1g1	DDB_G0281957	76	8	100.36		
Vesicular Transport							
EPS15 homology (EH) domain-containing protein		DDB_G0287325	2491	92	131.372		*
N-ethylmaleimide-sensitive fusion protein	nsfA	DDB_G0276153	70	8	82.589		*
Rab GTPase							
Rab5a	rab5A	DDB_G0271984	67	2	22.476		*
Cytoskeleton							
actin binding protein	abpD	DDB_G0287291	56	17	204.646		
DNA binding							
histone H2B domain-containing protein	H2Bv3	DDB_G0286509	113	18	17.089		
histone H3	H3a	DDB_G0267402	66	7	15.75		
myb domain-containing protein		DDB_G0280705	59	19	272.43		*
structural maintenance of chromosome protein	smc4	DDB_G0286403	52	23	161.911		
Metabolism							
putative fatty acid synthase	pks17	DDB_G0275077	321	41	293.074		
group IV decarboxylase	odc	DDB_G0281109	213	4	52.232		*
Putative NADH dehydrogenase		DDB_G0272476	97	3	15.528		

SNO glutamine amidotransferase family protein	pdx2	DDB_G0288305	78	5	28.018		
adenosine deaminase	ada	DDB_G0287371	64	6	88.487		
ATP citrate synthase	acly	DDB_G0278345	56	7	67.905	B	*
sulfotransferase	kil1	DDB_G0267630	52	2	55.876		
Mitochondrial protein							
mitochondrial substrate carrier family protein	mcfG	DDB_G0293556	50	4	32.491		
Peroxisome							
Peroxisomal biogenesis factor 5	pex5	DDB_G0286033	332	17	74.71		
Proteasome and proteases							
cell division cycle protein 48	cdcD	DDB_G0288065	348	38	89.242	B	
26S proteasome regulatory subunit S1	psmD1	DDB_G0287953	55	10	108.554		
Protein biosynthesis							
S60 ribosomal protein L10a	rpl10a	DDB_G0276871	105	5	24.495	B	
40S ribosomal protein S7	rps7	DDB_G0289025	100	5	22.19	B	
ribosomal protein 1024	rps9	DDB_G0289877	98	7	21.191		
40S ribosomal protein S23	rps23	DDB_G0272250	84	2	15.73	B	
S60 ribosomal protein L27a	rpl27a	DDB_G0292388	71	6	16.569	B	
S60 ribosomal protein L10E	rpl10	DDB_G0288273	65	5	24.871	B	
60S ribosomal protein L7	nubp2	DDB_G0277157	65	9	28.015		
S60 ribosomal protein L7	rpl7	DDB_G0276441	65	4	28.085	B	
S60 ribosomal protein L18	rpl18	DDB_G0279997	57	4	20.682		
lysine-tRNA ligase	lysS	DDB_G0281437	50	5	62.476		
Protein modification							
ubiquitin	ubqC	DDB_G0276765	676	47	17.535		
Signalling							
nuclear Dbf2-related kinase	ndrC	DDB_G0284839	56	7	150.067		
protein phosphatase 4 catalytic subunit	ppp4c	DDB_G0272116	52	2	35.467		

SH2 domain-containing kinase	shkA	DDB_G0283267	51	4	60.094		
Stress response							
heat shock protein Hsp70 family protein		DDB_G0285709	183	35	57.787		
heat shock protein Ddj1	ddj1	DDB_G0280037	129	10	46.195		
Unknown							
hypothetical protein		DDB_G0288519	383	17	52.067	B	*
hypothetical protein		DDB_G0293674	332	22	70.246		
hypothetical protein		DDB_G0289571	301	33	105.137		*
hypothetical protein		DDB_G0281783	210	10	89.452		
hypothetical protein		DDB_G0286289	132	11	73.1		
hypothetical protein		DDB_G0278507	60	8	70.825		
hypothetical protein		DDB_G0290107	60	2	69.479		
hypothetical protein		DDB_G0291406	54	16	478.82		
hypothetical protein		DDB_G0285807	54	4	28.751		
hypothetical protein		DDB_G0283381	53	13	209.822		

APPENDIX VI – p162-163

List of strains

Strain Name	Expression Plasmid
AX2/[A15]:GFP:Ap2A1	339-3 (Bsn)
Ap2A1-/[A15]:GFP:Ap2A1	339-3 (Bsn)
apm2-/[A15]:GFP:Ap2A1	pDM304 (G418)
clc-/[A15]:GFP:Ap2A1	pDM304 (G418)
chcA-/[A15]:GFP:Ap2A1	pDM304 (G418)
AX2/[A15]:mRFP:clc	pDM304 (G418)
Ap2A1-/[A15]: mRFP:clc	pDM304 (G418)
apm2-/[A15]: mRFP:clc	pDM304 (G418)
clc-/[A15]: mRFP:clc	pDM304 (G418)
chcA-/[A15]: mRFP:clc	pDM304 (G418)
AX2/[A15]:GFP:Ap2A1 [A15]:mRFP:clc	339-3 (Bsn); pDM304 (G418)
AX2/[A15]:GFP:Ap2A1 [A15]:clc:mRFP	339-3 (Bsn); pDM304 (G418)
AX2/[A15]:dajumin:GFP [A15]:mRFP:clc	pDEXRH (G418); pDM326 (Bsn)
AX2/[A15]:dajumin:GFP [A15]:mRFP:Ap2A1	pDEXRH (G418); pDM358 (Hgr)
Ap2A1-/[A15]: dajumin:GFP	pDM326 (Bsn)
apm2-/[A15]: dajumin:GFP	pDEXRH (G418)
clc-/[A15]: dajumin:GFP	pDEXRH (G418)
chcA-/[A15]: dajumin:GFP	pDEXRH (G418)
AX2/[A15]: pH^{S247}-dajumin	pDM326 (Bsn)
AX2/[A15]: $sfGFP^{S247}$-dajumin	pDM326 (Bsn)

AX2/[A15]: pH^{L403}-dajumin	pDM326 (Bsn)
AX2/[A15]: $sfGFP^{L403}$-dajumin	pDM326 (Bsn)
AX2/[A15]: pH-dajumin$^{A470\text{-}T544}$	pDM326 (Bsn)
AX2/[A15]: pH-dajumin$^{A470\text{-}T544}$mRFP	pDM326 (Bsn)
AX2/[A15]: pH^{L403}dajumin$^{A470\text{-}T544}$	pDM326 (Bsn)
AX2/[A15]: pH^{L403}dajumin$^{A470\text{-}T544}$mRFP	pDM326 (Bsn)

Strain shows the genetic background and the promoter used to drive expression. Plasmids used for expression are listed along with the antibiotic resistance used for selection. Bsn = blasticidin, G418 = geneticin, Hgr = hygromycin.

APPENDIX VII – List of primers

Primer Name	Sequence (5'-3')
Ap2A1-F	GCGGATCCATGAGTATGAATGTTACAAATCCAAATATTGC
Ap2A1-R	GCGAATTCTTATTGTAAATGAGAGATTAATAAATTTTTAATTG
GFP-Ap2A1-F	GCAGATCTAAAAAATGCATCATCATCATCATCATCATCATG
GFP-Ap2A1-R	GCACTAGTTTATTGTAAATGAGAGATTAATAAATTTTTAATTG
mRFP-Ap2A1-F	AATAAAAATCAGATCTAAAATGGCATCATCAGAAGATGTTATTAAAGA
mRFP-Ap2A1-R	TATTTATTTAACTAGTTTATTGTAAATGAGAGATTAATAAATTTTTAATTG
mRFP-clc-F	GCAGATCTAAAATGGCATCATCAGAAGATGTTATTAAAGA
mRFP-clc-R	GCACTAGTTTAAACAATTGGTTGATTTTTTAAACGAATTAA
mRFP-F	GCACTAGTAGTGCATCATCAGAAGATGTTATTAAAGAA
mRFP-R	TCTAGATTATGCACCTGTTGAATGTCTACCTT
clc-F	GCAGATCTAAAAAATGTCAGATCCATTTGGTGAAGAAAATG
clc-R	ACTAGTAACAATTGGTTGATTTTTTAAACGAATTAAAATTTC
daj-F	GCAGATCTAAAAAATGAAGAATTTTATTCTATTAGTTTTTTTATTTTTTATTAGTTTC
daj-R	ACTAGTTGTGGTGATTTCATCCAACATTTGGAATGGTAC
daj-S247	TGTTCTTTCAATACTTTTAATTATAGAATTTGGTTGAAAATGTTTGCTAGCGGTACCACTTGAACTTTGTCCATTTTTAT
daj-L403	TGTTGTATTGGTGGTTTTTGGTGATGAGCTAGCGGTACCTAAAGTATGGTATGATTTACTTAATTC
pH-F/sfGFP-F	GGTACCATGAGTAAAGGAGAAGAACTTTTCAC
pH-R	GCTAGCTTTGTATAGTTCATCCATGCCATGTG
sfGFP-R	GCTAGCTTTGTAGAGCTCATCCATGCCATGT

References

Aghamohammadzadeh, S., and K.R. Ayscough. 2009. Differential requirements for actin during yeast and mammalian endocytosis. *Nat Cell Biol*. 11:1039–1042.

Aguado-Velasco, C., and M.S. Bretscher. 1999. Circulation of the plasma membrane in Dictyostelium. *Mol Biol Cell*. 10:4419–4427.

Allen, C.L., D. Goulding, and M.C. Field. 2003. Clathrin-mediated endocytosis is essential in Trypanosoma brucei. *EMBO J*. 22:4991–5002.

Anderson, R.G., M.S. Brown, and J.L. Goldstein. 1977. Role of the coated endocytic vesicle in the uptake of receptor-bound low density lipoprotein in human fibroblasts. *Cell*. 10:351–364.

Anderson, R.G., M.S. Brown, U. Beisiegel, and J.L. Goldstein. 1982. Surface distribution and recycling of the low density lipoprotein receptor as visualized with antireceptor antibodies. *J Cell Biol*. 93:523–531.

Aubry, L., G. Klein, J.L. Martiel, and M. Satre. 1993. Kinetics of endosomal pH evolution in Dictyostelium discoideum amoebae. Study by fluorescence spectroscopy. *J Cell Sci*. 105 (Pt 3):861–866.

Axelrod, D. 2001. Total internal reflection fluorescence microscopy in cell biology. *Traffic*. 2:764–774.

Ayscough, K.R., J. Stryker, N. Pokala, M. Sanders, P. Crews, and D.G. Drubin. 1997. High rates of actin filament turnover in budding yeast and roles for actin in establishment and maintenance of cell polarity revealed using the actin inhibitor latrunculin-A. *J Cell Biol*. 137:399–416.

Bacon, R.A., C.J. Cohen, D.A. Lewin, and I. Mellman. 1994. Dictyostelium discoideum mutants with temperature-sensitive defects in endocytosis. *J Cell Biol*. 127:387–399.

Bakthavatsalam, D., and R.H. Gomer. 2010. The secreted proteome profile of developing Dictyostelium discoideum cells. *Proteomics*. 10:2556–2559.

Barth, A., A. Müller-Taubenberger, P. Taranto, and G. Gerisch. 1994. Replacement of the phospholipid-anchor in the contact site A glycoprotein of D. discoideum by a transmembrane region does not impede cell adhesion but reduces residence time on the cell surface. *J Cell Biol*. 124:205–215.

Bazinet, C., A.L. Katzen, M. Morgan, A.P. Mahowald, and S.K. Lemmon. 1993. The Drosophila clathrin heavy chain gene: clathrin function is essential in a multicellular organism. *Genetics*. 134:1119–1134.

Behnia, R., and S. Munro. 2005. Organelle identity and the signposts for membrane traffic. *Nature*. 438:597–604.

Benmerah, A., J. Gagnon, B. Bègue, B. Mégarbané, A. Dautry-Varsat, and N. Cerf-Bensussan. 1995. The tyrosine kinase substrate eps15 is constitutively associated with the plasma membrane adaptor AP-2. *J Cell Biol*. 131:1831–1838.

Bennett, N., F. Letourneur, M. Ragno, and M. Louwagie. 2008. Sorting of the v-SNARE VAMP7 in Dictyostelium discoideum: a role for more than one Adaptor Protein (AP) complex. *Exp Cell Res*. 314:2822–2833.

Boehm, M., and J.S. Bonifacino. 2001. Adaptins: the final recount. *Mol Biol Cell*. 12:2907–2920.

Boehm, M., and J.S. Bonifacino. 2002. Genetic analyses of adaptin function from yeast to mammals. *Gene*. 286:175–186.

Bonifacino, J.S., and B.S. Glick. 2004. The mechanisms of vesicle budding and fusion. *Cell*. 116:153–166.

Boucrot, E., S. Saffarian, R. Zhang, and T. Kirchhausen. 2010. Roles of AP-2 in clathrin-mediated endocytosis. *PLoS ONE*. 5:e10597.

Brady, R.J., C.K. Damer, J.E. Heuser, and T.J. O'Halloran. 2010. Regulation of Hip1r by epsin controls the temporal and spatial coupling of actin filaments to clathrin-coated pits. *J Cell Sci*. 123:3652–3661.

Brady, R.J., Y. Wen, and T.J. O'Halloran. 2008. The ENTH and C-terminal domains of Dictyostelium epsin cooperate to regulate the dynamic interaction with clathrin-coated pits. *J Cell Sci*. 121:3433–3444.

Carpenter, G., and S. Cohen. 1976. 125I-labeled human epidermal growth factor. Binding, internalization, and degradation in human fibroblasts. *J Cell Biol*. 71:159–171.

Carroll, S.Y., P.C. Stirling, H.E.M. Stimpson, E. Giesselmann, M.J. Schmitt, and D.G. Drubin. 2009. A Yeast Killer Toxin Screen Provides Insights into A/B Toxin Entry, Trafficking, and Killing Mechanisms. *Dev Cell*. 17:552–560.

Chang-Ileto, B., S.G. Frere, R.B. Chan, S.V. Voronov, A. Roux, and G. Di Paolo. 2011. Synaptojanin 1-mediated PI(4,5)P2 hydrolysis is modulated by membrane curvature and facilitates membrane fission. *Dev Cell*. 20:206–218.

Chen, C.-Y., and F.M. Brodsky. 2005. Huntingtin-interacting protein 1 (Hip1) and Hip1-related protein (Hip1R) bind the conserved sequence of clathrin light chains and thereby influence clathrin assembly in vitro and actin distribution in vivo. *J Biol Chem*. 280:6109–6117.

Clarke, M., J. Köhler, Q. Arana, T. Liu, J. Heuser, and G. Gerisch. 2002. Dynamics of the vacuolar H(+)-ATPase in the contractile vacuole complex and the endosomal pathway of Dictyostelium cells. *J Cell Sci*. 115:2893–2905.

Clarke, M., S.C. Kayman, and K. Riley. 1987. Density-dependent induction of discoidin-I synthesis in exponentially growing cells of Dictyostelium discoideum. *Differentiation*. 34:79–87.

Collins, B.M., A.J. McCoy, H.M. Kent, P.R. Evans, and D.J. Owen. 2002. Molecular architecture and functional model of the endocytic AP2 complex. *Cell*. 109:523–535.

Cremona, O., G. Di Paolo, M.R. Wenk, A. Lüthi, W.T. Kim, K. Takei, L. Daniell, Y. Nemoto, S.B. Shears, R.A. Flavell, D.A. McCormick, and P. De Camilli. 1999. Essential role of phosphoinositide metabolism in synaptic vesicle recycling. *Cell*. 99:179–188.

Dacks, J.B., P.P. Poon, and M.C. Field. 2008. Phylogeny of endocytic components yields insight into the process of nonendosymbiotic organelle evolution. *Proc Natl Acad Sci USA*. 105:588–593.

Damer, C.K., and T.J. O'Halloran. 2000. Spatially regulated recruitment of clathrin to the plasma membrane during capping and cell translocation. *Mol Biol Cell*. 11:2151–2159.

Damke, H., T. Baba, D.E. Warnock, and S.L. Schmid. 1994. Induction of mutant dynamin specifically blocks endocytic coated vesicle formation. *J Cell Biol*. 127:915–934.

Dautry-Varsat, A., A. Ciechanover, and H.F. Lodish. 1983. pH and the recycling of transferrin during receptor-mediated endocytosis. *Proc Natl Acad Sci USA*. 80:2258–2262.

Deborde, S., E. Perret, D. Gravotta, A. Deora, S. Salvarezza, R. Schreiner, and E. Rodriguez-Boulan. 2008. Clathrin is a key regulator of basolateral polarity. *Nature*. 452:719–723.

De Lozanne, A., and J.A. Spudich. 1987. Disruption of the Dictyostelium myosin heavy chain gene by homologous recombination. *Science*. 236:1086–1091.

Doherty, G.J., and H.T. McMahon. 2009. Mechanisms of Endocytosis. *Annu Rev Biochem*. 78:857–902.

Dormann, D., and C.J. Weijer. 2006. Visualizing signaling and cell movement during the multicellular stages of dictyostelium development. *Methods Mol Biol*. 346:297–309.

Doyon, J.B., B. Zeitler, J. Cheng, A.T. Cheng, J.M. Cherone, Y. Santiago, A.H. Lee, T.D. Vo, Y. Doyon, J.C. Miller, D.E. Paschon, L. Zhang, E.J. Rebar, P.D. Gregory, F.D. Urnov, and D.G. Drubin. 2011. Rapid and efficient clathrin-mediated endocytosis revealed in genome-edited mammalian cells. *Nat Cell Biol*. 13:331–337.

Ehrlich, M., W. Boll, A. Van Oijen, R. Hariharan, K. Chandran, M.L. Nibert, and T. Kirchhausen. 2004. Endocytosis by random initiation and stabilization of clathrin-coated pits. *Cell*. 118:591–605.

Eichinger, L., J.A. Pachebat, G. Glöckner, M.-A. Rajandream, R. Sucgang, M. Berriman, J. Song, R. Olsen, K. Szafranski, Q. Xu, B. Tunggal, S. Kummerfeld, M. Madera, B.A. Konfortov, F. Rivero, A.T. Bankier, R. Lehmann, N. Hamlin, R. Davies, P. Gaudet, P. Fey, K. Pilcher, G. Chen, D. Saunders, E. Sodergren, P. Davis, A. Kerhornou, X. Nie, N. Hall, C. Anjard, L. Hemphill, N. Bason, P. Farbrother, B. Desany, E. Just, T. Morio, R. Rost, C. Churcher, J. Cooper, S. Haydock, N. van Driessche, A. Cronin, I. Goodhead, D. Muzny, T. Mourier, A. Pain, M. Lu, D. Harper, R. Lindsay, H. Hauser, K. James, M. Quiles, M. Madan Babu, T. Saito, C. Buchrieser, A. Wardroper, M. Felder, M. Thangavelu, D. Johnson, A. Knights, H. Loulseged, K. Mungall, K. Oliver, C. Price, M.A. Quail, H. Urushihara, J. Hernandez, E. Rabbinowitsch, D. Steffen, M. Sanders, J. Ma, Y. Kohara, S. Sharp, M. Simmonds, S. Spiegler, A. Tivey, S. Sugano, B. White, D. Walker, J. Woodward, T. Winckler, Y. Tanaka, G. Shaulsky, M. Schleicher, G. Weinstock, A. Rosenthal, E.C. Cox, R.L. Chisholm, R. Gibbs, W.F. Loomis, M. Platzer, R.R. Kay, J. Williams, P.H. Dear, A.A. Noegel, B. Barrell, and A. Kuspa. 2005. The genome of the social amoeba Dictyostelium discoideum. *Nature*. 435:43–57.

Farsad, K., N. Ringstad, K. Takei, S.R. Floyd, K. Rose, and P. De Camilli. 2001. Generation of high curvature membranes mediated by direct endophilin bilayer interactions. *J Cell Biol*. 155:193–200.

Ferguson, S.M., G. Brasnjo, M. Hayashi, M. Wölfel, C. Collesi, S. Giovedi, A. Raimondi, L.-W. Gong, P. Ariel, S. Paradise, E. O'toole, R. Flavell, O. Cremona, G. Miesenböck, T.A. Ryan, and P. De Camilli. 2007. A selective activity-dependent requirement for dynamin 1 in synaptic vesicle endocytosis. *Science*. 316:570–574.

Ferguson, S.M., S. Ferguson, A. Raimondi, S. Paradise, H. Shen, K. Mesaki, A. Ferguson, O. Destaing, G. Ko, J. Takasaki, O. Cremona, E. O' Toole, and P. De Camilli. 2009. Coordinated actions of actin and BAR proteins upstream of dynamin at endocytic clathrin-coated pits. *Dev Cell*. 17:811–822.

Ferguson, S.S. 2001. Evolving concepts in G protein-coupled receptor endocytosis: the role in receptor desensitization and signaling. *Pharmacol. Rev.* 53:1–24.

Field, M.C., and J.B. Dacks. 2009. First and last ancestors: reconstructing evolution of the endomembrane system with ESCRTs, vesicle coat proteins, and nuclear pore complexes. *Curr. Opin. Cell Biol.* 21:4–13.

Fischer, M., I. Haase, E. Simmeth, G. Gerisch, and A. Müller-Taubenberger. 2004. A brilliant monomeric red fluorescent protein to visualize cytoskeleton dynamics in Dictyostelium. *FEBS Lett*. 577:227–232.

Fok, A.K., M. Clarke, L. Ma, and R.D. Allen. 1993. Vacuolar H(+)-ATPase of Dictyostelium discoideum. A monoclonal antibody study. *J Cell Sci*. 106 (Pt 4):1103–1113.

Ford, M.G.J., I.G. Mills, B.J. Peter, Y. Vallis, G.J.K. Praefcke, P.R. Evans, and H.T. McMahon. 2002. Curvature of clathrin-coated pits driven by epsin. *Nature*. 419:361–366.

Fotin, A., Y. Cheng, N. Grigorieff, T. Walz, S.C. Harrison, and T. Kirchhausen. 2004. Structure of an auxilin-bound clathrin coat and its implications for the mechanism of uncoating. *Nature*. 432:649–653.

Fujimoto, L.M., R. Roth, J.E. Heuser, and S.L. Schmid. 2000. Actin assembly plays a variable, but not obligatory role in receptor-mediated endocytosis in mammalian cells. *Traffic*. 1:161–171.

Gabriel, D., U. Hacker, J. Köhler, A. Müller-Taubenberger, J.M. Schwartz, M. Westphal, and G. Gerisch. 1999. The contractile vacuole network of Dictyostelium as a distinct organelle: its dynamics visualized by a GFP marker protein. *J Cell Sci*. 112 (Pt 22):3995–4005.

Gaidarov, I., F. Santini, R.A. Warren, and J.H. Keen. 1999. Spatial control of coated-pit dynamics in living cells. *Nat Cell Biol*. 1:1–7.

Gammie, A.E., L.J. Kurihara, R.B. Vallee, and M.D. Rose. 1995. DNM1, a dynamin-related gene, participates in endosomal trafficking in yeast. *J Cell Biol*. 130:553–566.

Gassama-Diagne, A., and B. Payrastre. 2009. Phosphoinositide signaling pathways: promising role as builders of epithelial cell polarity. *Int Rev Cell Mol Biol*. 273:313–343.

Gassama-Diagne, A., W. Yu, M. ter Beest, F. Martin-Belmonte, A. Kierbel, J. Engel, and K. Mostov. 2006. Phosphatidylinositol-3,4,5-trisphosphate regulates the formation of the basolateral plasma membrane in epithelial cells. *Nat Cell Biol*. 8:963–970.

Gerisch, G., J. Heuser, and M. Clarke. 2002. Tubular-vesicular transformation in the contractile vacuole system of Dictyostelium. *Cell Biol. Int.* 26:845–852.

González-Gaitán, M., and H. Jäckle. 1997. Role of Drosophila alpha-adaptin in presynaptic vesicle recycling. *Cell*. 88:767–776.

Gotthardt, D., V. Blancheteau, A. Bosserhoff, T. Ruppert, M. Delorenzi, and T. Soldati. 2006. Proteomics fingerprinting of phagosome maturation and evidence for the role of a Galpha during uptake. *Mol. Cell Proteomics*. 5:2228–2243.

Greene, B., S.H. Liu, A. Wilde, and F.M. Brodsky. 2000. Complete reconstitution of clathrin basket formation with recombinant protein fragments: adaptor control of clathrin self-assembly. *Traffic*. 1:69–75.

Greener, T., B. Grant, Y. Zhang, X. Wu, L.E. Greene, D. Hirsh, and E. Eisenberg. 2001. Caenorhabditis elegans auxilin: a J-domain protein essential for clathrin-mediated endocytosis in vivo. *Nat Cell Biol*. 3:215–219.

Haar, ter, E., A. Musacchio, S.C. Harrison, and T. Kirchhausen. 1998. Atomic structure of clathrin: a beta propeller terminal domain joins an alpha zigzag linker. *Cell*. 95:563–573.

Haar, ter, E., S.C. Harrison, and T. Kirchhausen. 2000. Peptide-in-groove interactions link target proteins to the beta-propeller of clathrin. *Proc Natl Acad Sci USA*. 97:1096–1100.

Hacker, U., R. Albrecht, and M. Maniak. 1997. Fluid-phase uptake by macropinocytosis in Dictyostelium. *J Cell Sci*. 110 (Pt 2):105–112.

Haigler, H., J.F. Ash, S.J. Singer, and S. Cohen. 1978. Visualization by fluorescence of the binding and internalization of epidermal growth factor in human carcinoma cells A-431. *Proc Natl Acad Sci USA*. 75:3317–3321.

Hawryluk, M.J., P.A. Keyel, S.K. Mishra, S.C. Watkins, J.E. Heuser, and L.M. Traub. 2006. Epsin 1 is a polyubiquitin-selective clathrin-associated sorting protein. *Traffic*. 7:262–281.

Henne, W.M., E. Boucrot, M. Meinecke, E. Evergren, Y. Vallis, R. Mittal, and H.T. McMahon. 2010. FCHo proteins are nucleators of clathrin-mediated endocytosis. *Science*. 328:1281–1284.

Henne, W.M., H.M. Kent, M.G.J. Ford, B.G. Hegde, O. Daumke, P.J.G. Butler, R. Mittal, R. Langen, P.R. Evans, and H.T. McMahon. 2007. Structure and analysis of FCHo2 F-BAR domain: a dimerizing and membrane recruitment module that effects membrane curvature. *Structure*. 15:839–852.

Heuser, J. 1980. Three-dimensional visualization of coated vesicle formation in fibroblasts. *J Cell Biol*. 84:560–583.

Heuser, J. 2006. Evidence for recycling of contractile vacuole membrane during osmoregulation in Dictyostelium amoebae--a tribute to Günther Gerisch. *Eur J Cell Biol*. 85:859–871.

Heuser, J., and T. Kirchhausen. 1985. Deep-etch views of clathrin assemblies. *J Ultrastruct Res*. 92:1–27.

Heuser, J., Q. Zhu, and M. Clarke. 1993. Proton pumps populate the contractile vacuoles of Dictyostelium amoebae. *J Cell Biol*. 121:1311–1327.

Hinrichsen, L., A. Meyerholz, S. Groos, and E.J. Ungewickell. 2006. Bending a membrane: how clathrin affects budding. *Proc Natl Acad Sci USA*. 103:8715–8720.

Hinrichsen, L., J. Harborth, L. Andrees, K. Weber, and E.J. Ungewickell. 2003. Effect of clathrin heavy chain- and alpha-adaptin-specific small inhibitory RNAs on endocytic accessory proteins and receptor trafficking in HeLa cells. *J Biol Chem*. 278:45160–45170.

Hinshaw, J.E., and S.L. Schmid. 1995. Dynamin self-assembles into rings suggesting a mechanism for coated vesicle budding. *Nature*. 374:190–192.

Hirst, J., L.D. Barlow, G.C. Francisco, D.A. Sahlender, M.N.J. Seaman, J.B. Dacks, and M.S. Robinson. 2011. The fifth adaptor protein complex. *PLoS Biol.* 9:e1001170.

Hsu, V.W., S.Y. Lee, and J.-S. Yang. 2009. The evolving understanding of COPI vesicle formation. *Nat Rev Mol Cell Biol*. 10:360–364.

Huang, F., A. Khvorova, W. Marshall, and A. Sorkin. 2004. Analysis of clathrin-mediated endocytosis of epidermal growth factor receptor by RNA interference. *J Biol Chem*. 279:16657–16661.

Huang, K.M., K. D'Hondt, H. Riezman, and S.K. Lemmon. 1999. Clathrin functions in the absence of heterotetrameric adaptors and AP180-related proteins in yeast. *EMBO J*. 18:3897–3908.

Idrissi, F.-Z., H. Grötsch, I.M. Fernández-Golbano, C. Presciatto-Baschong, H. Riezman, and M.-I. Geli. 2008. Distinct acto/myosin-I structures associate with endocytic profiles at the plasma membrane. *J Cell Biol*. 180:1219–1232.

Ingalls, H.M., C.M. Goodloe-Holland, and E.J. Luna. 1986. Junctional plasma membrane domains isolated from aggregating Dictyostelium discoideum amebae. *Proc Natl Acad Sci USA*. 83:4779–4783.

Inoue, T., T. Hayashi, K. Takechi, and K. Agata. 2007. Clathrin-mediated endocytic signals are required for the regeneration of, as well as homeostasis in, the planarian CNS. *Development*. 134:1679–1689.

Jackson, L.P., B.T. Kelly, A.J. McCoy, T. Gaffry, L.C. James, B.M. Collins, S. Höning, P.R. Evans, and D.J. Owen. 2010. A large-scale conformational change couples membrane recruitment to cargo binding in the AP2 clathrin adaptor complex. *Cell*. 141:1220–1229.

Jaiswal, J.K., V.M. Rivera, and S.M. Simon. 2009. Exocytosis of post-Golgi vesicles is regulated by components of the endocytic machinery. *Cell*. 137:1308–1319.

Journet, A., G. Klein, S. Brugière, Y. Vandenbrouck, A. Chapel, S. Kieffer, C. Bruley, C. Masselon, and L. Aubry. 2012. Investigating the macropinocytic proteome of Dictyostelium amoebae by high-resolution mass spectrometry. *Proteomics*. 12:241–245.

Kaksonen, M., C.P. Toret, and D.G. Drubin. 2005. A Modular Design for the Clathrin- and Actin-Mediated Endocytosis Machinery. *Cell*. 123:305–320.

Kaksonen, M., Y. Sun, and D.G. Drubin. 2003. A pathway for association of receptors, adaptors, and actin during endocytic internalization. *Cell*. 115:475–487.

Kayman, S.C. 1983. Relationship between axenic growth of Dictyostelium discoideum strains and their track morphology on substrates coated with gold particles. *J Cell Biol*. 97:1001–1010.

Keyel, P.A., S.C. Watkins, and L.M. Traub. 2004. Endocytic adaptor molecules reveal an endosomal population of clathrin by total internal reflection fluorescence microscopy. *J Biol Chem*. 279:13190–13204.

Kirchhausen, T. 2000. CLATHRIN. *Annu Rev Biochem*. 69:699–727.

Kirchhausen, T., and S.C. Harrison. 1981. Protein organization in clathrin trimers. *Cell*. 23:755–761.

Koenig, J.H., and K. Ikeda. 1989. Disappearance and reformation of synaptic vesicle membrane upon transmitter release observed under reversible blockage of membrane retrieval. *J. Neurosci.* 9:3844–3860.

Koh, T.-W., P. Verstreken, and H.J. Bellen. 2004. Dap160/intersectin acts as a stabilizing scaffold required for synaptic development and vesicle endocytosis. *Neuron*. 43:193–205.

Koh, T.-W., V.I. Korolchuk, Y.P. Wairkar, W. Jiao, E. Evergren, H. Pan, Y. Zhou, K.J.T. Venken, O. Shupliakov, I.M. Robinson, C.J. O'Kane, and H.J. Bellen. 2007. Eps15 and Dap160 control synaptic vesicle membrane retrieval and synapse development. *J Cell Biol*. 178:309–322.

Kumari, S., S. Mg, and S. Mayor. 2010. Endocytosis unplugged: multiple ways to enter the cell. *Cell Res.* 20:256–275.

Kübler, E., and H. Riezman. 1993. Actin and fimbrin are required for the internalization step of endocytosis in yeast. *EMBO J*. 12:2855–2862.

Lefkir, Y., B. de Chassey, A. Dubois, A. Bogdanovic, R.J. Brady, O. Destaing, F. Bruckert, T.J. O'Halloran, P. Cosson, and F. Letourneur. 2003. The AP-1 clathrin-adaptor is required for lysosomal enzymes sorting and biogenesis of the contractile vacuole complex in Dictyostelium cells. *Mol Biol Cell*. 14:1835–1851.

Legendre-Guillemin, V., M. Metzler, J.-F. Lemaire, J. Philie, L. Gan, M.R. Hayden, and P.S. McPherson. 2005. Huntingtin interacting protein 1 (HIP1) regulates clathrin assembly through direct binding to the regulatory region of the clathrin light chain. *J Biol Chem*. 280:6101–6108.

Lemmon, S.K., and E.W. Jones. 1987. Clathrin requirement for normal growth of yeast. *Science*. 238:504–509.

Liu, J., Y. Sun, D.G. Drubin, and G.F. Oster. 2009. The mechanochemistry of endocytosis. *PLoS Biol.* 7:e1000204.

Lu, H., and D. Bilder. 2005. Endocytic control of epithelial polarity and proliferation in Drosophila. *Nat Cell Biol*. 7:1232–1239.

Macia, E., M. Ehrlich, R. Massol, E. Boucrot, C. Brunner, and T. Kirchhausen. 2006. Dynasore, a cell-permeable inhibitor of dynamin. *Dev Cell*. 10:839–850.

Marks, M.S., L. Woodruff, H. Ohno, and J.S. Bonifacino. 1996. Protein targeting by tyrosine- and di-leucine-based signals: evidence for distinct saturable components. *J Cell Biol*. 135:341–354.

Mattheyses, A.L., C.E. Atkinson, and S.M. Simon. 2011. Imaging single endocytic events reveals diversity in clathrin, dynamin and vesicle dynamics. *Traffic*. 12:1394–1406.

Mattheyses, A.L., S.M. Simon, and J.Z. Rappoport. 2010. Imaging with total internal reflection fluorescence microscopy for the cell biologist. *J Cell Sci*. 123:3621–3628.

Maurer, M.E., and J.A. Cooper. 2006. The adaptor protein Dab2 sorts LDL receptors into coated pits independently of AP-2 and ARH. *J Cell Sci*. 119:4235–4246.

Maxfield, F.R., and T.E. McGraw. 2004. Endocytic recycling. *Nat Rev Mol Cell Biol*. 5:121–132.

Mayor, S., and R.E. Pagano. 2007. Pathways of clathrin-independent endocytosis. *Nat Rev Mol Cell Biol*. 8:603–612.

McMahon, H.T., and E. Boucrot. 2011. Molecular mechanism and physiological functions of clathrin-mediated endocytosis. *Nat Rev Mol Cell Biol*. 12:517–533.

Mercanti, V., C. Blanc, Y. Lefkir, P. Cosson, and F. Letourneur. 2006a. Acidic clusters target transmembrane proteins to the contractile vacuole in Dictyostelium cells. *J Cell Sci*. 119:837–845.

Mercanti, V., S.J. Charette, N. Bennett, J.-J. Ryckewaert, F. Letourneur, and P. Cosson. 2006b. Selective membrane exclusion in phagocytic and macropinocytic cups. *J Cell Sci*. 119:4079–4087.

Merrifield, C.J., D. Perrais, and D. Zenisek. 2005. Coupling between clathrin-coated-pit invagination, cortactin recruitment, and membrane scission observed in live cells. *Cell*. 121:593–606.

Merrifield, C.J., M.E. Feldman, L. Wan, and W. Almers. 2002. Imaging actin and dynamin recruitment during invagination of single clathrin-coated pits. *Nat Cell Biol*. 4:691–698.

Miesenböck, G., D.A. De Angelis, and J.E. Rothman. 1998. Visualizing secretion and synaptic transmission with pH-sensitive green fluorescent proteins. *Nature*. 394:192–195.

Motley, A., N.A. Bright, M.N.J. Seaman, and M.S. Robinson. 2003. Clathrin-mediated endocytosis in AP-2-depleted cells. *J Cell Biol*. 162:909–918.

Musacchio, A., C.J. Smith, A.M. Roseman, S.C. Harrison, T. Kirchhausen, and B.M. Pearse. 1999. Functional organization of clathrin in coats: combining electron cryomicroscopy and X-ray crystallography. *Mol. Cell*. 3:761–770.

Müller-Taubenberger, A. 2006. Application of fluorescent protein tags as reporters in live-cell imaging studies. *Methods Mol Biol*. 346:229–246.

Nesterov, A., R.E. Carter, T. Sorkina, G.N. Gill, and A. Sorkin. 1999. Inhibition of the receptor-binding function of clathrin adaptor protein AP-2 by dominant-negative mutant mu2 subunit and its effects on endocytosis. *EMBO J*. 18:2489–2499.

Neuhaus, E.M., and T. Soldati. 2000. A myosin I is involved in membrane recycling from early endosomes. *J Cell Biol*. 150:1013–1026.

Neuhaus, E.M., H. Horstmann, W. Almers, M. Maniak, and T. Soldati. 1998. Ethane-freezing/methanol-fixation of cell monolayers: a procedure for improved preservation of structure and antigenicity for light and electron microscopies. *J Struct Biol*. 121:326–342.

Neuhaus, E.M., W. Almers, and T. Soldati. 2002. Morphology and dynamics of the endocytic pathway in Dictyostelium discoideum. *Mol Biol Cell*. 13:1390–1407.

Niswonger, M.L., and T.J. O'Halloran. 1997a. Clathrin heavy chain is required for spore cell but not stalk cell differentiation in Dictyostelium discoideum. *Development*. 124:443–451.

Niswonger, M.L., and T.J. O'Halloran. 1997b. A novel role for clathrin in cytokinesis. *Proc Natl Acad Sci USA*. 94:8575–8578.

Nolta, K.V., J.M. Rodriguez-Paris, and T.L. Steck. 1994. Analysis of successive endocytic compartments isolated from Dictyostelium discoideum by magnetic fractionation. *Biochim Biophys Acta*. 1224:237–246.

Nothwehr, S.F., E. Conibear, and T.H. Stevens. 1995. Golgi and vacuolar membrane proteins reach the vacuole in vps1 mutant yeast cells via the plasma membrane. *J Cell Biol*. 129:35–46.

Novak, K.D., M.D. Peterson, M.C. Reedy, and M.A. Titus. 1995. Dictyostelium myosin I double mutants exhibit conditional defects in pinocytosis. *J Cell Biol*. 131:1205–1221.

O'Halloran, T.J., and R.G. Anderson. 1992. Clathrin heavy chain is required for pinocytosis, the presence of large vacuoles, and development in Dictyostelium. *J Cell Biol*. 118:1371–1377.

Ohno, H., J. Stewart, M.C. Fournier, H. Bosshart, I. Rhee, S. Miyatake, T. Saito, A. Gallusser, T. Kirchhausen, and J.S. Bonifacino. 1995. Interaction of tyrosine-based sorting signals with clathrin-associated proteins. *Science*. 269:1872–1875.

Olusanya, O., P.D. Andrews, J.R. Swedlow, and E. Smythe. 2001. Phosphorylation of threonine 156 of the mu2 subunit of the AP2 complex is essential for endocytosis in vitro and in vivo. *Curr Biol*. 11:896–900.

Owen, D.J., B.M. Collins, and P.R. Evans. 2004. Adaptors for clathrin coats: structure

and function. *Annu. Rev. Cell Dev. Biol.* 20:153–191.

Padh, H., J. Ha, M. Lavasa, and T.L. Steck. 1993. A post-lysosomal compartment in Dictyostelium discoideum. *J Biol Chem*. 268:6742–6747.

Page, L.J., and M.S. Robinson. 1995. Targeting signals and subunit interactions in coated vesicle adaptor complexes. *J Cell Biol*. 131:619–630.

Palade, G. 1975. Intracellular aspects of the process of protein synthesis. *Science*. 189:347–358.

Payne, G.S., and R. Schekman. 1985. A test of clathrin function in protein secretion and cell growth. *Science*. 230:1009–1014.

Pearse, B.M. 1976. Clathrin: a unique protein associated with intracellular transfer of membrane by coated vesicles. *Proc Natl Acad Sci USA*. 73:1255–1259.

Pearse, B.M. 1982. Coated vesicles from human placenta carry ferritin, transferrin, and immunoglobulin G. *Proc Natl Acad Sci USA*. 79:451–455.

Pechstein, A., J. Bacetic, A. Vahedi-Faridi, K. Gromova, A. Sundborger, N. Tomlin, G. Krainer, O. Vorontsova, J.G. Schäfer, S.G. Owe, M.A. Cousin, W. Saenger, O. Shupliakov, and V. Haucke. 2010. Regulation of synaptic vesicle recycling by complex formation between intersectin 1 and the clathrin adaptor complex AP2. *Proc Natl Acad Sci USA*. 107:4206–4211.

Praefcke, G.J.K., M.G.J. Ford, E.M. Schmid, L.E. Olesen, J.L. Gallop, S.-Y. Peak-Chew, Y. Vallis, M.M. Babu, I.G. Mills, and H.T. McMahon. 2004. Evolving nature of the AP2 alpha-appendage hub during clathrin-coated vesicle endocytosis. *EMBO J*. 23:4371–4383.

Pylypenko, O., R. Lundmark, E. Rasmuson, S.R. Carlsson, and A. Rak. 2007. The PX-BAR membrane-remodeling unit of sorting nexin 9. *EMBO J*. 26:4788–4800.

Qualmann, B., D. Koch, and M.M. Kessels. 2011. Let's go bananas: revisiting the endocytic BAR code. *EMBO J*. 30:3501–3515.

Rappoport, J.Z., A. Benmerah, and S.M. Simon. 2005. Analysis of the AP-2 adaptor complex and cargo during clathrin-mediated endocytosis. *Traffic*. 6:539–547.

Rappoport, J.Z., and S.M. Simon. 2003. Real-time analysis of clathrin-mediated endocytosis during cell migration. *J Cell Sci*. 116:847–855.

Rappoport, J.Z., and S.M. Simon. 2009. Endocytic trafficking of activated EGFR is AP-2 dependent and occurs through preformed clathrin spots. *J Cell Sci*. 122:1301–1305.

Rappoport, J.Z., B.W. Taha, S. Lemeer, A. Benmerah, and S.M. Simon. 2003. The AP-2 complex is excluded from the dynamic population of plasma membrane-associated

clathrin. *J Biol Chem*. 278:47357–47360.

Rappoport, J.Z., S. Kemal, A. Benmerah, and S.M. Simon. 2006. Dynamics of clathrin and adaptor proteins during endocytosis. *Am. J. Physiol., Cell Physiol.* 291:C1072–81.

Reider, A., S.L. Barker, S.K. Mishra, Y.J. Im, L. Maldonado-Báez, J.H. Hurley, L.M. Traub, and B. Wendland. 2009. Syp1 is a conserved endocytic adaptor that contains domains involved in cargo selection and membrane tubulation. *EMBO J*. 28:3103–3116.

Repass, S.L., R.J. Brady, and T.J. O'Halloran. 2007. Dictyostelium Hip1r contributes to spore shape and requires epsin for phosphorylation and localization. *J Cell Sci*. 120:3977–3988.

Ricotta, D., S.D. Conner, S.L. Schmid, K. von Figura, and S. Höning. 2002. Phosphorylation of the AP2 mu subunit by AAK1 mediates high affinity binding to membrane protein sorting signals. *J Cell Biol*. 156:791–795.

Roth, T.F., and K.R. Porter. 1964. Yolk protein uptake in the oocyte of the mosquito *Aedes aegypti*. L. *J Cell Biol*. 20:313–332.

Ruscetti, T., J.A. Cardelli, M.L. Niswonger, and T.J. O'Halloran. 1994. Clathrin heavy chain functions in sorting and secretion of lysosomal enzymes in Dictyostelium discoideum. *J Cell Biol*. 126:343–352.

Saffarian, S., E. Cocucci, and T. Kirchhausen. 2009. Distinct dynamics of endocytic clathrin-coated pits and coated plaques. *PLoS Biol.* 7:e1000191.

Schaap, P. 2011. Evolutionary crossroads in developmental biology: Dictyostelium discoideum. *Development*. 138:387–396.

Scheele, U., C. Kalthoff, and E. Ungewickell. 2001. Multiple interactions of auxilin 1 with clathrin and the AP-2 adaptor complex. *J Biol Chem*. 276:36131–36138.

Schledzewski, K., H. Brinkmann, and R.R. Mendel. 1999. Phylogenetic analysis of components of the eukaryotic vesicle transport system reveals a common origin of adaptor protein complexes 1, 2, and 3 and the F subcomplex of the coatomer COPI. *J. Mol. Evol.* 48:770–778.

Schlessinger, J., Y. Shechter, M.C. Willingham, and I. Pastan. 1978. Direct visualization of binding, aggregation, and internalization of insulin and epidermal growth factor on living fibroblastic cells. *Proc Natl Acad Sci USA*. 75:2659–2663.

Schlossman, D.M., S.L. Schmid, W.A. Braell, and J.E. Rothman. 1984. An enzyme that removes clathrin coats: purification of an uncoating ATPase. *J Cell Biol*. 99:723–733.

Sesaki, H., E.F. Wong, and C.H. Siu. 1997. The cell adhesion molecule DdCAD-1 in Dictyostelium is targeted to the cell surface by a nonclassical transport pathway involving contractile vacuoles. *J Cell Biol*. 138:939–951.

Shevchuk, O., C. Batzilla, S. Hägele, H. Kusch, S. Engelmann, M. Hecker, A. Haas, K. Heuner, G. Glöckner, and M. Steinert. 2009. Proteomic analysis of Legionella-containing phagosomes isolated from Dictyostelium. *Int. J. Med. Microbiol.* 299:489–508.

Shih, W., A. Gallusser, and T. Kirchhausen. 1995. A clathrin-binding site in the hinge of the beta 2 chain of mammalian AP-2 complexes. *J Biol Chem*. 270:31083–31090.

Shivas, J.M., H.A. Morrison, D. Bilder, and A.R. Skop. 2010. Polarity and endocytosis: reciprocal regulation. *Trends Cell Biol*. 20:445–452.

Smaczynska-de Rooij, I.I., E.G. Allwood, S. Aghamohammadzadeh, E.H. Hettema, M.W. Goldberg, and K.R. Ayscough. 2010. A role for the dynamin-like protein Vps1 during endocytosis in yeast. *J Cell Sci*. 123:3496–3506.

Sorkin, A., and M. von Zastrow. 2009. Endocytosis and signalling: intertwining molecular networks. *Nat Rev Mol Cell Biol*. 10:609–622.

Sosa, R.T., M.M. Weber, Y. Wen, and T.J. O'Halloran. 2012. A single Beta adaptin contributes to AP1 and AP2 complexes and clathrin function in Dictyostelium. *Traffic*. 13:305–316.

Stavrou, I., and T.J. O'Halloran. 2006. The monomeric clathrin assembly protein, AP180, regulates contractile vacuole size in Dictyostelium discoideum. *Mol Biol Cell*. 17:5381–5389.

Stimpson, H.E.M., C.P. Toret, A.T. Cheng, B.S. Pauly, and D.G. Drubin. 2009. Early-arriving Syp1p and Ede1p function in endocytic site placement and formation in budding yeast. *Mol Biol Cell*. 20:4640–4651.

Sun, Y., S. Carroll, M. Kaksonen, J.Y. Toshima, and D.G. Drubin. 2007. PtdIns(4,5)P2 turnover is required for multiple stages during clathrin- and actin-dependent endocytic internalization. *J Cell Biol*. 177:355–367.

Swanson, J.A., D.L. Taylor, and J.T. Bonner. 1981. Coated vesicles in Dictyostelium discoideum. *J Ultrastruct Res*. 75:243–249.

Sweitzer, S.M., and J.E. Hinshaw. 1998. Dynamin undergoes a GTP-dependent conformational change causing vesiculation. *Cell*. 93:1021–1029.

Takei, K., P.S. McPherson, S.L. Schmid, and P. De Camilli. 1995. Tubular membrane invaginations coated by dynamin rings are induced by GTP-gamma S in nerve terminals. *Nature*. 374:186–190.

Takei, K., V.I. Slepnev, V. Haucke, and P. De Camilli. 1999. Functional partnership between amphiphysin and dynamin in clathrin-mediated endocytosis. *Nat Cell Biol*. 1:33–39.

Taylor, M.J., D. Perrais, and C.J. Merrifield. 2011. A high precision survey of the

molecular dynamics of mammalian clathrin-mediated endocytosis. *PLoS Biol.* 9:e1000604.

Thilo, L., and G. Vogel. 1980. Kinetics of membrane internalization and recycling during pinocytosis in Dictyostelium discoideum. *Proc Natl Acad Sci USA*. 77:1015–1019.

Ungewickell, E., and D. Branton. 1981. Assembly units of clathrin coats. *Nature*. 289:420–422.

Ungewickell, E., H. Ungewickell, S.E. Holstein, R. Lindner, K. Prasad, W. Barouch, B. Martin, L.E. Greene, and E. Eisenberg. 1995. Role of auxilin in uncoating clathrin-coated vesicles. *Nature*. 378:632–635.

Urwyler, S., Y. Nyfeler, C. Ragaz, H. Lee, L.N. Mueller, R. Aebersold, and H. Hilbi. 2009. Proteome analysis of Legionella vacuoles purified by magnetic immunoseparation reveals secretory and endosomal GTPases. *Traffic*. 10:76–87.

van Delft, S., C. Schumacher, W. Hage, A.J. Verkleij, and P.M. van Bergen en Henegouwen. 1997. Association and colocalization of Eps15 with adaptor protein-2 and clathrin. *J Cell Biol*. 136:811–821.

van der Bliek, A.M., T.E. Redelmeier, H. Damke, E.J. Tisdale, E.M. Meyerowitz, and S.L. Schmid. 1993. Mutations in human dynamin block an intermediate stage in coated vesicle formation. *J Cell Biol*. 122:553–563.

Veltman, D.M., G. Akar, L. Bosgraaf, and P.J.M. Van Haastert. 2009. A new set of small, extrachromosomal expression vectors for Dictyostelium discoideum. *Plasmid*. 61:110–118.

Verstreken, P., O. Kjaerulff, T.E. Lloyd, R. Atkinson, Y. Zhou, I.A. Meinertzhagen, and H.J. Bellen. 2002. Endophilin mutations block clathrin-mediated endocytosis but not neurotransmitter release. *Cell*. 109:101–112.

Vigers, G.P., R.A. Crowther, and B.M. Pearse. 1986. Three-dimensional structure of clathrin cages in ice. *EMBO J*. 5:529–534.

Wang, J., V.C. Virta, K. Riddelle-Spencer, and T.J. O'Halloran. 2003. Compromise of clathrin function and membrane association by clathrin light chain deletion. *Traffic*. 4:891–901.

Wang, J., Y. Wang, and T.J. O'Halloran. 2006. Clathrin light chain: importance of the conserved carboxy terminal domain to function in living cells. *Traffic*. 7:824–832.

Wen, Y., I. Stavrou, K. Bersuker, R.J. Brady, A. De Lozanne, and T.J. O'Halloran. 2009. AP180-mediated trafficking of Vamp7B limits homotypic fusion of Dictyostelium contractile vacuoles. *Mol Biol Cell*. 20:4278–4288.

Wessels, D., J. Reynolds, O. Johnson, E. Voss, R. Burns, K. Daniels, E. Garrard, T.J.

O'Halloran, and D.R. Soll. 2000. Clathrin plays a novel role in the regulation of cell polarity, pseudopod formation, uropod stability and motility in Dictyostelium. *J Cell Sci*. 113 (Pt 1):21–36.

Williams, J.G. 2010. Dictyostelium finds new roles to model. *Genetics*. 185:717–726.

Ybe, J.A., B. Greene, S.H. Liu, U. Pley, P. Parham, and F.M. Brodsky. 1998. Clathrin self-assembly is regulated by three light-chain residues controlling the formation of critical salt bridges. *EMBO J*. 17:1297–1303.

Ybe, J.A., F.M. Brodsky, K. Hofmann, K. Lin, S.H. Liu, L. Chen, T.N. Earnest, R.J. Fletterick, and P.K. Hwang. 1999. Clathrin self-assembly is mediated by a tandemly repeated superhelix. *Nature*. 399:371–375.

Yeung, B.G., H.L. Phan, and G.S. Payne. 1999. Adaptor complex-independent clathrin function in yeast. *Mol Biol Cell*. 10:3643–3659.

Yu, A., J.-F. Rual, K. Tamai, Y. Harada, M. Vidal, X. He, and T. Kirchhausen. 2007. Association of Dishevelled with the clathrin AP-2 adaptor is required for Frizzled endocytosis and planar cell polarity signaling. *Dev Cell*. 12:129–141.

Zastrow, von, M., and B.K. Kobilka. 1992. Ligand-regulated internalization and recycling of human beta 2-adrenergic receptors between the plasma membrane and endosomes containing transferrin receptors. *J Biol Chem*. 267:3530–3538.

Zhu, Q., T. Liu, and M. Clarke. 1993. Calmodulin and the contractile vacuole complex in mitotic cells of Dictyostelium discoideum. 104 (Pt 4):1119–1127.